Computational and Physical Modelling of the Flow and Sediment Transport in a New Vortex-type Stormwater Retention Pond

A Thesis Submitted to the

College of Graduate and Postdoctoral Studies

in Partial Fulfillment of the Requirements

for the degree of

Doctor of Philosophy

in the Department of Civil, Geological, and Environmental Engineering

University of Saskatchewan

Saskatoon

By

Mina Sadat Ahadi

Permission to Use

In presenting this thesis in partial fulfilment of the requirements for a Postgraduate degree from the University of Saskatchewan, I agree that the Libraries of this University may make it freely available for inspection. I further agree that permission for copying of this thesis in any manner, in whole or in part, for scholarly purposes may be granted by the professor or professors who supervised my thesis work or, in their absence, by the Head of the Department or the Dean of the College in which my thesis work was done. It is understood that any copying or publication or use of this thesis or parts thereof for financial gain shall not be allowed without my written permission. It is also understood that due recognition shall be given to me and to the University of Saskatchewan in any scholarly use which may be made of any material in my thesis.

Requests for permission to copy or to make other uses of materials in this thesis/dissertation in whole or part should be addressed to:

Head of the Civil, Geological, and Environmental Engineering Department

57 Campus Drive

University of Saskatchewan

Saskatoon, Saskatchewan S7N 5A9 Canada

OR

Dean

College of Graduate and Postdoctoral Studies

University of Saskatchewan

116 Thorvaldson Building, 110 Science Place

Saskatoon, Saskatchewan S7N 5C9 Canada

Abstract

Given the current water quality requirements for a stormwater retention pond, the civil and environmental engineering community requires accurate and efficient methods to explore the sediment removal of retention ponds. This research studied the use of Computational Fluid Dynamics (CFD) for modeling sediment retention ponds with comparison of the fluid flow results to in-house experimental data. This study provided insight on the pond design using single- and two-phase modeling approaches. This research highlighted the potential of using an Eulerian-Eulerian two-fluid model (TFM) approach, without the empirical ad hoc relations often used to determine the sediment concentration profile, for modeling flow and sediment in a new vortex-type pond design. This manuscript-based thesis documented four different studies.

The first study summarized the fundamental concepts involved in the overall design of stormwater retention ponds. A comprehensive and in-depth description of different computational methods used in the literature for modeling stormwater retention ponds was given. Previous applications of CFD to modeling stormwater retention ponds was critically reviewed. The present position of multiphase modeling in the simulation of storage ponds was addressed, and possible directions for future development were outlined.

The second study explored the potential of single-phase CFD modeling in a new vortex-type stormwater retention pond. The flow pattern in a 1:13.3 scale model of the vortex-type retention pond was characterized and some problematic recirculation zones were identified. The mean and fluctuating velocity fields in the pond were explored using computational and experimental methods. For the CFD modeling, the 3D Reynolds averaged Navier-Stokes (RANS) equations together with a $k - \varepsilon$ turbulence model were solved using ANSYS Fluent 19.2. In general, the predictions and measurements were in good agreement.

In the third study, an Eulerian-Eulerian TFM using constitutive equations based on granular kinetic theory, coupled with a low-Reynolds-number turbulence model, was used to predict the liquid and sediment transport in an equilibrium channel for fully-developed, steady, dilute flow. The particle-wall boundary

condition was also investigated. The model predictions of the liquid and sediment velocity profiles, sediment concentration, turbulence statistics and fluctuating particle velocity field were documented against experimental data from the literature.

In the last study, the TFM was implemented to assess pond performance and to provide insight on the sediment transport in the vortex-type stormwater retention pond for the case of steady, dilute flow with no sediment deposition. The model predictions of the liquid and sediment velocity profiles, and sediment concentration were documented. The study demonstrated the spatial distribution of sediment in the pond: the recirculation zones documented in the single-phase CFD study were characterized by relatively high concentrations of sediment.

Overall, the current study demonstrated the application of single-phase CFD in detecting problematic regions such as low velocity zones and stagnation regions in a new pond design by providing a map of the flow patterns. This study also showed the application of two-phase CFD in the simulation of fluid and dilute sediment transport in the same pond as a step towards more comprehensive simulations, which in turn supports the goal of achieving higher water quality. No sediment deposition was included, which is the next step in applying the TFM formulation to retention pond studies.

Acknowledgements

First and foremost, I wish to thank my supervisor Professor Bergstrom for his unwavering support and belief in me. Throughout my PhD journey, I was guided by a wise and kind human with immense knowledge and plentiful experience. His vision, passion, and sincerity have deeply inspired me.

Then, I would like to thank members of my advisory committee: Dr. Bugg, Dr. Lindenschmidt, Dr. Kells, and Dr. Hawkes for their insightful comments and suggestions which motivated me to widen my research in various perspectives. I thank all the University Faculty, employees and technicians, especially Dale Pavier, who have contributed their expertise behind the scenes, and professionals in the field that have generously shared their knowledge.

I finish with my family: the source of my energy from back home, Iran. My deep and sincere gratitude to my mother who taught me to be a strong woman, my father who raised me to always be in the search for truth, and my brother and sister who are my motivation to live my life to the fullest and make a difference along the way. I dedicate this milestone to my wonderful family.

Contents

List of Tables

List of Figures

Nomenclature

C	Tracer concentration
C_D	Drag coefficient
C_μ	Empirical constant in the eddy viscosity equation
$C_{1\varepsilon}$	Empirical constant in the eddy viscosity equation
$C_{2\varepsilon}$	Empirical constant in the eddy viscosity equation
d	Particle diameter
d_{cr}	Shields critical particle diameter
D	Pipe diameter
D_i	Diffusivity coefficient
$\mathcal{D}_s$	Diffusion of granular energy
D_{16}	Sediment grain size for which 16% of the particles are smaller than that size
D_{50}	Sediment grain size for which 50% of the particles are smaller than that size
D_{84}	Sediment grain size for which 84% of the particles are smaller than that size
E	Residence time distribution
e_{ss}	Particle-particle restitution coefficient
e_w	Wall restitution coefficient
g_i	Gravity vector in i-direction
$g_{0,ss}$	Radial distribution function
h	Flow depth at the pond
k	Kinetic energy
$\mathrm{K}_{x,ls}$	Interphase momentum exchange coefficients in x-components
$\mathrm{K}_{y,ls}$	Interphase momentum exchange coefficients in y-components
K_{Θ_s}	Diffusion coefficient for granular energy
M	Total inflow tracer mass
P	Mean pressure

$\mathcal{P}_s$	Generation of granular energy by the sediment stress tensor
Q	Volume Flow rate
q_s	Flux of granular temperature at the wall
r	Radius (horizontal distance from the center of the pond)
R_h	Hydraulic radius of the channel
$R_{x,ls}$	x-component of interaction forces between the liquid and sediment phases
$R_{y,ls}$	y-component of interaction forces between the liquid and sediment phases
Re	Reynolds number
Re_τ	Reynolds number based on friction velocity
Re_p	Reynolds number of the particle
S	Specific gravity
t	Time
t_n	Nominal residence time
TI	Turbulence intensity
u	x-component of velocity
u_*	Shear velocity
u'	Stream-wise velocity fluctuation
u_i	Velocity component in i-direction
u_j	Velocity component in the j-direction
U	Magnitude of local mean Stream-wise velocity
U_i	Mean velocity component in i-direction
$\vec{U}_{s,\mathrm{II}}$	Particle slip velocity parallel to the wall
v	y-component of velocity
v'	Transverse velocity fluctuation
V	Velocity
x_i	Spatial coordinate in i-direction

x_j	Spatial coordinate in j-direction
z	Distance from the pond bed

Greek symbols

α	Volume fraction
$\alpha_{s,max}$	Maximum solid volume fraction (packing limit)
γ_{Θ_s}	Collisional dissipation of energy
δ_{ij}	Kronecker delta
ε	Dissipation
Θ_s	Granular temperature
κ	Von Karman constant
λ_s	Sediment phase bulk viscosity
μ	Viscosity
$\mu_{s,col}$	Collisional component of the sediment shear viscosity
$\mu_{s,kin}$	Kinetic component of the sediment shear viscosity
ν	Kinematic viscosity
v_r	Radial velocity
v_t	Eddy viscosity
v_z	Vertical velocity
v_θ	Azimuthal velocity
ρ	Density
σ_k	Empirical constant in the eddy viscosity equation
τ_b	Shear stress on the on bed
$\tau_{xy,s}$	Shear stress at the wall
φ	Specularity coefficient
$\emptyset_{ls}$	Energy exchange between liquid and sediment phases
ω	Turbulence frequency

Subscripts and superscripts

l Liquid phase

s Solid phase

List of Abbreviations

ACM	Adaptive Collision Model
ADV	Acoustic Doppler Velocimeter
CFD	Computational Fluid Dynamics
DEM	Discrete Element Methods
DNS	Direct Numerical Simulation
LDV	Laser Doppler Velocimetry
LES	Large Eddy Simulation
PIV	Particle Image Velocimetry
PTV	Particle Tracking Velocimetry
RANS	Reynolds Averaged Navier-Stokes
RSM	Reynolds Stress Model
SNR	Signal to Noise Ratio
SST	Shear Stress Transport
TKE	Turbulent Kinetic Energy
TFM	Two-Fluid Model
VOF	Volume of Fluid
2D	Two-dimensional
3D	Three-dimensional

Chapter One

1. INTRODUCTORY REMARKS AND OBJECTIVES

1.1 Introduction

1.1.1 Background

Excessive sediment discharged into rivers degrades water quality, reduces the lifetime and stability of downstream structures, and disturbs aquatic life. For many years, stormwater retention ponds have been used to prevent flooding by using storage. However, they are also recognized as stormwater quality treatment facilities through sedimentation. Stormwater retention ponds collect the stormwater and keep it in a permanent pool controlled by the outlet. The sediment in the runoff has time to settle, and the treated water is released into the river at a rate that prevents flooding and erosion. Even though improvements have been achieved in the design of stormwater ponds based on sediment removal efficiency, many stormwater retention ponds still do not meet the sediment removal criteria specified in their local guidelines. In addition, there is little information on the current operational status and function of retention ponds (Al-Rubaei et al. 2017).

Computational Fluid Dynamics (CFD) is a numerical technique to solve the governing transport equations that describe the fluid flow and sediment transport in a pond. It can provide comprehensive information (both spatial and temporal) about the flow characteristics and sediment transport dynamics at any location within the pond before it is built. CFD is also useful in testing the effect of retrofitting elements on the performance of existing ponds. At the present time, pond analysis typically ignores the sediment phase, solves the conservation equations for the liquid phase, and uses an advection-diffusion equation for a tracer material to investigate sediment retention times. By ignoring the influence of sediment particles on each other and on the liquid flow field, the single-phase description is strictly limited to flow regions with low concentrations of sediments. However, stormwater retention ponds function at relatively high sediment concentrations, especially in the region near the bed where deposition and resuspension occur. Therefore, a single-phase description is incapable of bringing in important physics of the sediment transport in

stormwater retention ponds. Instead, authentic multiphase CFD models are required to explore the sediment removal capability of stormwater ponds.

Multiphase CFD models can be categorized as either a particle tracking or a two-fluid model (TFM). In both models the Navier-Stokes conservation equations are solved for the continuous liquid phase in the Eulerian frame, but the sediment phase is treated differently in each model. In particle tracking models, the particle trajectories are computed individually based on the Newton's second law of motion. In the TFMs, the particle phase is assumed to be a continuum like the liquid phase so that two separate sets of mass and momentum conservation equations discretized on fixed control volumes are solved for each phase. The TFM has significant potential as a numerical methodology for predicting sediment transport. However, it has not been applied to stormwater retention ponds to date. The TFM can be especially favorable for simulation of large-scale ponds where the number of particles required for particle-tracking becomes excessive, and the effect of turbulence becomes challenging to model.

1.1.2 Motivation and Challenges

A new vortex-type stormwater retention pond was proposed in a conceptual study by Albers and Amell (2010). It demonstrated more resistance to the formation of dead zones and short-circuiting currents than traditional stormwater ponds. The pond structure consists of a circular pool with sloped walls. An inlet pipe enters the pond at an angle of 30° with the tangent line to the pond circumference. A permanent pool is maintained by an elevated, closed-top, perforated outlet pipe located at the center of the pond. This central outlet is surrounded by an annular trapezoidal berm. An opening along the top of the inner wall of the berm directs the treated water from the main pool towards the outlet. Periodic dredging of settled sediment in retention ponds is necessary and is a costly part of pond maintenance. It is more cost efficient if the pond design causes the sediment to settle closer to the outer walls where it is more accessible for maintenance purposes. The hydrodynamics of the pond creates flow patterns that in turn modify the local sediment transport.

This research was initially focused on further development of the new vortex-type pond technology using three-dimensional (3D) computational modeling to assess its effectiveness at improving water quality through sediment capture. The initial and motivating question for this PhD study was the following:

"Could this new vortex-type pond technology provide better stormwater treatment by allowing the deposition of sediment particles closer to the outer wall of the pond?"

Accordingly, the following general goals were defined to answer this question:

1) *To explore the flow pattern in the pond to see if the fluid velocity was uniform throughout the pond and ensure that no recirculation zones were present*; and

2) *To investigate the fluid flow and sediment dynamics to evaluate the spatial distribution of sediment concentration to determine if the pond promoted the deposition of sediment near the outer wall of the channel.*

Based on a comprehensive and in-depth study of different computational methods used in the literature for CFD modeling of sediment transport in stormwater retention ponds (provided in Chapter 2), the objectives of the current PhD thesis are defined in the next section. CFD modeling provides the opportunity to better understand, evaluate, and design stormwater retention ponds. CFD models have advanced from single-phase models to multiphase models. The single-phase models assess a pond based on a prediction of the flow pattern, while multiphase models simulate both the liquid and sediment transport, as well as their interaction. The multiphase models provide specific information, e.g. spatial sediment concentration, that a single-phase study cannot.

Given the challenges associated with a full CFD study of both the hydrodynamic flow field and sediment distribution in a pond, some limitations were required on the scope of the present study. It should be noted that in this research, only one turbulence model, the two-equation $k - \varepsilon$ model, was considered. Furthermore, in terms of sediment transport, only steady and dilute flows without sediment deposition and

resuspension were explored. Within this scope, the study retained the vortex-type pond geometry as the test case for CFD modeling. Although it used computational models to fully explore the flow field in the pond, the study stopped short of an attempt to predict the sediment deposition.

1.2 Objectives of the thesis

Considering the context given above, the present thesis research has four incremental objectives:

(1) **To provide a database for validation of the velocity field in a vortex-type pond by three-dimensional mean and fluctuating velocity measurements**: 3D velocity measurements were conducted in a scale laboratory model of the pond to obtain a more detailed picture of the flow dynamics, and to provide a comprehensive database for the validation of CFD predictions. Taking comprehensive flow measurements (e.g. mean and fluctuating velocity components) is a necessary step towards understanding the pond dynamics.

(2) **To model the flow in a vortex-type pond using a single-phase CFD simulation, and to assess the predictions against the corresponding mean and fluctuating velocity measurements:** To simulate the vortex-type pond, the three-dimensional Reynolds Averaged Navier-Stokes (RANS) equations together with a $k - \varepsilon$ turbulence model are solved using ANSYS Fluent 19.2. The computational predictions provide enhanced knowledge of the velocity field and flow pattern in this new pond design.

(3) **To implement an Eulerian-Eulerian TFM and then to assess the model performance in fully developed open channel flow against flow and sediment measurements taken from the literature:** To apply the TFM to the vortex-type pond with multiple levels of complexity, a step-by-step modeling is required. Before applying the model to the vortex-type pond, different aspects of the TFM should be evaluated in a simpler flow for which experimental data are available. A fully-developed open channel flow, for which the sediment measurements are available, is modeled using the TFM. The numerical predictions are compared to measurements of the velocity and sediment concentration in the channel.

(4) **To investigate the Eulerian-Eulerian TFM performance for steady flow and dilute sediment transport in the vortex-type pond:** No one has previously modeled sediment transport in a stormwater retention pond using the TFM. Therefore, the TFM implemented in ANSYS Fluent 19.2 is applied to the vortex-type stormwater retention pond and the predictions for the sediment transport are explored.

As described above, this thesis research makes two complementary contributions. It provides specific insight on the flow features of the new vortex-type pond. It also demonstrates the use of multiphase CFD modeling to predict the fluid flow and sediment distribution in a retention pond for the case of steady and dilute flow.

1.3 Structure of the thesis

This thesis adopts a manuscript-based format. In all studies reported in this thesis, the author set up and performed the simulations, post-processed and analyzed the results, and prepared the first draft of each manuscript. She then worked with the co-authors to discuss the results presented in each manuscript, and finalize the content and form of the manuscripts.

This manuscript-based thesis includes six chapters. The four chapters corresponding to the published manuscripts each have an individual abstract, introduction, methodology, results and discussion, conclusion, and references. The first chapter (the current one) is a general introduction to the thesis, describing the motivation and objectives, and giving an outline of the thesis structure. The second chapter critically reviews a total of 90 journal papers and conference proceedings to give a comprehensive description of computational methods used in the literature for CFD modeling of sediment transport in stormwater retention ponds. This work was published in the Journal of Environmental Engineering in 2020 (Ahadi et al. 2020). In the third chapter, flow in the vortex-type stormwater retention pond is characterized using both experimental and computational results. The measurements provide a comprehensive data base for CFD validation of the mean and fluctuating velocity fields in the stormwater retention pond. The

computational predictions provide enhanced insight as to the flow pattern. The measurements and CFD results together are used to obtain a detailed picture of the flow dynamics in the vortex-type pond. In the fourth chapter, the capability of the TFM for predicting sediment transport in a dilute flow is assessed using a fully-developed open channel flow for which experimental measurements are available in the literature. This flow regime is similar to the flow in the fully developed region of the pond downstream of the jet area. The TFM methology elements, e.g. effect of particles on the turbulence field, and particle-particle and particle-wall boundary conditions, are further explored. In the fifth chapter, the TFM implemented for open channel flow in Chapter 4, is applied to the vortex-type stormwater retention pond to simulate the sediment dynamics. Finally, the conclusions and recommendations for future work are presented in the sixth chapter. Chapter 6 also includes a comprehensive set of references, in addition to those given in the individual chapters.

1.4 Copyright and author permissions

Chapters 2 through 4 of this thesis consist of manuscripts that are published or are currently under review, while Chapter 5 represents the content of a conference paper. The appropriate manuscript citations are provided below in order to maintain consistency with copyright and author rights for each publisher. For all manuscripts, the student is the first author as per the College of Graduate and Postdoctoral Studies research guidelines for manuscript style theses.

Chapter 2: Ahadi, M., Bergstrom, D., & Mazurek, K.A. (2020) Computational Fluid Dynamics Modeling of the Flow and Sediment Transport in Stormwater Retention Ponds: A Review, Journal of Environmental Engineering, 146(2).

Chapter 3: Ahadi, M., Bergstrom, D., Mazurek, K.A. (2021) Flow Pattern Investigation of a Scale Model Vortex-type Stormwater Retention Pond: Experimental and Computational, Journal of Hydraulic Engineering, under review.

Chapter 4: Ahadi, M., Bergstrom, D., & Mazurek, K.A. (2019) Application of the Two-Fluid Model to Prediction of Sediment Transport in Turbulent Open Channel Flow, Physics and Chemistry of the Earth, Parts A/B/C, 113, 73-82.

Chapter 5: Ahadi, M., and Bergstrom, D. (2021) Two-fluid modeling of sediment transport in a vortex-type stormwater retention pond, Canadian Water Resources Association (CWRA) National Conference 2021.

Chapter Two

2. COMPUTATIONAL FLUID DYNAMICS MODELING OF THE FLOW AND SEDIMENT TRANSPORT IN STORMWATER RETENTION PONDS: A REVIEW

A similar version of this chapter has been published as:

- Ahadi, M., Bergstrom, D., & Mazurek, K.A. (2020) Computational Fluid Dynamics Modeling of the Flow and Sediment Transport in Stormwater Retention Ponds: A Review, Journal of Environmental Engineering, 146(2).

Preamble

Reviewing a total of about 90 journal papers and conference proceedings, this paper briefly introduces the fundamental concepts associated with the overall design of stormwater retention ponds. Then, it gives a comprehensive description of different computational methods used in the literature for modeling stormwater retention ponds. The paper critically reviews the application of Computational Fluid Dynamics (CFD) to modeling the stormwater retention ponds. Given the current water quality requirements for a stormwater retention pond, this information would be of significant value to the civil and environmental engineering community. This study also aims to help new researchers in the field understand the opportunity of CFD to fill current research gaps, e.g. the effects of flow-sediment and sediment-sediment interactions.

CFD modeling provides the opportunity to better understand, assess, and design stormwater retention ponds. CFD models have advanced from single-phase models that assess a pond based on the flow pattern prediction, to multiphase models that simulate both the liquid and sediment transport, as well as their interaction. The single-phase description is strictly limited to flow regions with low concentrations of sediments, since the influence of sediment particles on each other and on the flow field are neglected. However, stormwater retention ponds can function at high sediment concentrations, especially in the region near the bed where deposition and resuspension occur. In high concentration regions, particle collisions and frictional contact are the dominant mechanism of sediment transport and can no longer be neglected. The

paper represents a potentially beneficial two-phase CFD model which has not been applied to stormwater ponds, yet.

Abstract

This paper reviews the application of Computational Fluid Dynamics (CFD) to numerically model the two-phase flow of water and sediment in the complex environment of a stormwater retention pond. The review is intended to draw the attention of the hydraulic engineering community, specifically those involved in pond design, to recent advancements in computational modeling of sediment transport in ponds. It provides an up-to-date survey of current simulation capability, focusing on the potential of fully three-dimensional methods for solving sediment transport in complex pond flows. An additional goal of this paper is to alert new researchers engaged in stormwater retention pond design to the research opportunities presented by CFD.

Even though pond configurations have become more complex to improve their performance, many studies have continued to rely solely on single-phase models. At the present time, unsteady three-dimensional two-phase models are becoming available to study these problems. Of the multiphase models that might be considered, the particle tracking (Eulerian - Lagrangian) method and the two-fluid (Eulerian-Eulerian) method both are potentially applicable to modeling sediment transport in pond-type flows. To date, only the particle-tracking method has been applied to stormwater retention ponds. The two-fluid method is capable of simulating sediment transport in retention ponds. It would be advantageous for simulation of large-scale ponds, where the number of particles required for particle-tracking becomes excessive. Currently, fully three-dimensional CFD methods are being successfully used to model a variety of multiphase flows in mechanical and chemical engineering, as well as some specific applications in hydraulic engineering. Its application to predict sediment transport in a retention pond shows significant promise, especially when the effect of turbulence becomes challenging to model.

9

2.1 Introduction

Growing urbanization, along with the increasing presence of impermeable surfaces, has led to increasing problems with stormwater runoff from urban areas (Barbosa et al. 2012, Yan 2013). Urban stormwater runoff causes frequent downstream flooding (Aryal et al. 2010, Barbosa et al. 2012). It also degrades water quality in receiving streams (Khan et al. 2009, Spencer et al. 2011, Yan 2013. Gu et al. 2017). Urban runoff has been observed to contain sediment, nutrients, pesticides, garbage, emission deposits from vehicles, metals, and bacteria (Kantrowitz and Woodham 1995).

Sediment is a concern in receiving waters because of the potential negative impacts on the aquatic ecosystem, e.g. fish (Kjelland et al. 2015). In the U.S., 40% of assessed river miles were found to be threatened by excessive sediment (USEPA 1998). Water quality criteria are periodically published by states governments, e.g. the North Carolina Department of Environment, Health, and Natural Resources (1995) required an 85% reduction in suspended solids for retention ponds. In Canada, after finding that stormwater discharged into the Bow River from the city of Calgary contributed about 10 times more total suspended solids to the river than its sewage treatment facilities (City of Calgary 2011), the municipal government instituted a policy that their stormwater retention ponds must provide a minimum of 85% removal of total suspended solids for particle sizes equal to 50 μm or larger (City of Calgary 2011). In the province of Ontario, stormwater management facilities are required to meet the water quality objectives of the average removal of 80, 70 and 60% of suspended solids in the total runoff volume for "enhanced," "normal" and "basic" protection levels, respectively (Ontario Ministry of the Environment 2003). Currently, some Canadian cities are required to report to their regulators the total pollutant loadings produced from their drainage areas (City of Edmonton 2008). These municipalities further anticipate that in the future they will also be required to control the pollution produced within their boundaries (City of Edmonton 2008).

Stormwater retention ponds, or wet ponds, are a commonly-used solution for controlling the damaging impacts of stormwater runoff (Yousef et al. 1994, Khan et al. 2009, Yan 2013., Gu et al. 2017).

They were initially developed to prevent flooding through storage, but have also demonstrated effectiveness at improving water quality and are known to capture sediment (Wu et al. 1996, Khan et al. 2009). Wet ponds are now widely used for the purpose of improving water quality (Wu et al. 1996, Comings et al. 2000, German and Svensson 2005, Gu et al. 2017). A retention pond consists of a permanent pool created by an outlet structure set at a higher elevation than the pond bed to control the release to receiving waters (Weiss et al. 2007, Yan 2013, Arnold et al. 1993). The permanent pool stores rainfall until it is displaced by runoff from the next storm event (Yan 2013, Gillis et al. 2015). The permanent pool typically has a depth between 0.5 - 2 m and a surface area between 100 - 10,000 m^2 depending on the watershed size it is intended to treat (Persson 2000). Sediment is removed by the pond through sedimentation.

Traditionally, stormwater retention pond design has used "rules of thumb" and experience from previous ponds, with minimal consideration of the hydraulic design of the pond (Khan et al. 2012). For example, current Canadian design standards for stormwater retention ponds tend to provide guidelines for the pond volume, maximum water levels, active storage detention times, minimum width-to-length ratios, and depths for permanent and active storage in the ponds. For example, according to the City of Saskatoon (2018), a wet pond should have a length-to-width ratio of 4:1 to 5:1 with a maximum depth of 1.8 m. The traditional method of designing stormwater ponds may lead to problems with short-circuiting and dead zones, which reduce a pond's effectiveness at removing contaminants by reducing the effective treatment volume of the pond (Shaw et al. 1997, Pettersson et al. 1998). Altering the flow pattern to eliminate dead zones is known to result in improved removal efficiencies for contaminants (Pettersson et al. 1998). For example, some studies have tried retrofitting modifications such as adding baffles (e.g., Van Buren 1994, Persson 2000, Thaxton et al. 2004, Gu et al. 2017).

The sediment removal efficiency of a pond is determined from sediment concentration samples collected at its inlet(s) and outlet(s), i.e. the percent of sediment mass entering the pond that is captured. It is typically calculated based on either a specified period called the load-based sediment removal efficiency,

or a storm event called the event-based sediment removal efficiency. Weiss et al. (2007) reported average load-based sediment removal efficiencies of 65% ± 32 % by retention ponds across the United States. Takaijudin et al. (2011) studied an individual stormwater retention pond located in Malaysia over three months and reported the load-based sediment removal efficiency ranging from 13% to 24%. The Centre for Watershed Protection (2007) studied 44 wet ponds for removal efficiencies of total suspended solids, based on the storm event method, and found an average removal of 80%. However, values for removal were as low as -33% and as high as 99 %. A negative value of the sediment removal efficiency indicates that sediment has been resuspended by the flow as it moves through the pond to the pond outflow. Wu et al. (1996) studied three urban retention ponds located in three different locations of a watershed in North Carolina. Event-based removal efficiencies ranged from 82 to 100 % for one pond, -7 to 87 % for the second, and 18 to 67 % for the third. Gillis (2017) found a removal rate of -67 % based on the annual load of sediment during an atorm event in 2014 for the Erindale Pond in Saskatoon, Saskatchewan. Binns et al. (2019) studied two wet ponds in the Toronto area and found a sediment removal efficiency of 70-90 % based on event mean concentration. Overall there is a wide variation in the sediment removal efficiencies measured in existing ponds, which suggests that current design approaches may be unable to ensure that future ponds meet more demanding sediment removal regulations.

Computational fluid dynamics (CFD) represents an important design tool for evaluating wet ponds (Adamsson 1999, Yan 2013). CFD is a numerical technique to solve the governing transport equations that describe the fluid flow and sediment transport in a pond. It can provide comprehensive information about the flow characteristics at any location within the pond before a pond is built (Jarman et al. 2008, Yan 2013). The predictive nature of CFD has significant advantages over field and lab studies for pond design, as well as for testing potential modifications to existing ponds (Yan 2013). Obtaining the comprehensive information (both spatial and temporal) provided by CFD would be extremely costly and time consuming by any other means, and in some situations, impossible (Adamsson 1999). However, in general CFD is not yet mature enough to be used without validation against field, lab, or highly resolved numerical simulation

data (Shilton 2000, Laurent et al. 2013). A variety of CFD models with different levels of complexity have been developed. The more sophisticated models increase both the cost of computation and data management, while simplified models may generate unreliable results (Papanicolaou et al. 2008).

Given the enhanced computational resources presently available, solving unsteady and fully 3D flows is now practical for a wide variety of applications, even though it involves the challenge of managing large data files. It is only in the last two decades that CFD has broadly engaged fully 3D and unsteady flows. Prior to that, prediction of 3D flows was simply too expensive for most industry applications in terms of the computer resources required (Rodi 2017). Instead, simpler but still effective models were developed.

One of the simpler models that has been widely and successfully used in stormwater pond applications is the two-dimensional (2D) depth-averaged model (also called shallow water equations) (Persson 2000; Binns et al. 2019). This model eliminates the variation of the velocity and pressure in the vertical direction by integration of the transport equations in that direction. The resultant depth-averaged velocity field only varies in the streamwise and transverse directions. The 2D depth-averaged models will remain useful, particularly for applications with a relatively large spatial extent or extending over a long period of time, e.g. for river morphology at the watershed scale. In many applications, the 2D depth-averaged model is capable of predicting the general hydraulic behavior with less computational cost than 3D models.

Other simplified model formulations exist. For example, in 3D models, the hydrostatic pressure assumption can be adopted to reduce the computational cost of predicting flows in which the vertical velocity component is much smaller than the horizontal velocity component (Pedlosky 1979, Lin and Falconer 1997). With this assumption, the momentum equation in the vertical direction is reduced to an expression for the hydrostatic pressure (Chen 2005). Also, often there is no need for a very fine vertical grid resolution with small time steps to model vertical mixing (Nakhaei et al. 2018). However, for applications with secondary flows, e.g. for curved channels (Leupi and Altinakar 2005), local scouring due

to the presence of hydraulic structures (Uchida and Fokuoka 2009), and irregular bed shapes (Fraga et al. 2012), the non-hydrostatic pressure effects may be significant, and this formulation is not appropriate (Chen 2005, Wang et al. 2014).

CFD modeling of stormwater retention ponds is complicated by such features as wind (Shaw et al. 1997), stratification (Song et al. 2013), vegetation (Li et al. 2007), unsteady inflows, complex geometry and multiple inlets with three- features. For complex pond flows, the physics of the sediment transport varies throughout the pond and depends on the local flow features. All of these issues combine to make modeling a retention pond a special, and in some ways a unique, challenge. For simulating the flow and sediment transport in a complex and inherently 3D stormwater retention pond, a fully 3D and unsteady methodology has advantages. There are relatively few successful implementations of complex hydrodynamic models in stormwater retention ponds (Troitsky et al. 2019). This paper critically reviews the methodologies available for 3D CFD modeling of flow and sediment transport in stormwater retention ponds. It also documents some of the previous computational studies of flows in retention ponds, including both single-phase and multiphase formulations. Finally, some recommendations for the future application of 3D CFD to pond modeling are presented.

2.2 Application of CFD to modeling liquid flow in stormwater retention ponds
2.2.1 Methodology
2.2.1.1 Turbulence

With respect to three-dimensional CFD modelling of the flow in a pond, the treatment of turbulence is a critical task. Turbulence often dominates the transport of mass and momentum in such a flow. The sediment settling process can be negatively impacted by the turbulence, since it has the potential to resuspend the sediment. On the other hand, turbulence facilitates the flocculation of particles, which enhances their settling. Hence, turbulence strongly affects the flow and sediment dynamics within the pond (Rodi 2017, Gu et al. 2017). Turbulent flow typically includes a wide range of length and time scales. If sufficient computational resources are available, a Direct Numerical Simulation (DNS) that resolves even

the smallest motions is the most accurate method for predicting a turbulent flow. However, currently DNS is a scientific tool and not feasible for most engineering and industrial applications (Moin and Mahesh 1998).

Large Eddy Simulation (LES) is a computationally less demanding alternative. LES computes the large-scale turbulent motions directly (similar to DNS) and it models the small-scale motions; therefore a coarser grid can be used (Aghaee and Hakimzade 2010, Khosronejad and Sotiropoulos 2014). Limits on the computational power available restricts the use of LES in large-scale hydraulic engineering problems, especially when a second phase, i.e. sediment, is present. LES is inherently a time-intensive solution method, because of the need for time-stepping using very small time increments. For the same reason, it also accumulates large data files, and can provide much more information than an engineer typically requires, e.g. instantaneous velocity fields.

The most common method for treating turbulence in engineering problems is the Reynolds Averaged Navier-Stokes (RANS) formulation, which relates the turbulence to the mean (or time-averaged) velocity field (Hanjalic and Launder 2011). After decomposing the velocities and pressure in the Navier-Stokes equations into mean and fluctuating components, and averaging, a new term , i.e. the Reynolds stress tensor, appears in the RANS equations that represents the turbulent transport. The RANS equations are used to determine the mean velocity and pressure fields; their prediction depends on the choice of the turbulence model. Different levels of approximation can be used to model the Reynolds stress tensor. The two-equation $k - \varepsilon$ and $k - \omega$ models, are the most widely used RANS models; they both relate the Reynolds stress to the mean velocity gradient via an eddy viscosity model. This requires an expression for the turbulent viscosity. For the $k - \varepsilon$ model, two extra transport equations are solved for the turbulence kinetic energy (k) and its dissipation rate (ε), which are then used to form the expression for the turbulent viscosity (Menter 1994). For the $k - \omega$ model, two transport equations are solved for the turbulence kinetic energy (k) and turbulence frequency (ω) which are used to calculate the turbulent viscosity (Menter 1994).

The $k - \omega$ shear stress transport (SST) model is an improved version of the $k - \omega$ model for predicting flow separation (Menter 1994). In a stormwater retention pond, examples of flow separation would typically relate to recirculation and dead zones. The SST model combines the desirable features of two popular turbulence model formulations by applying the $k - \omega$ model in the near-wall region and switching to the $k - \varepsilon$ model in the outer region of a wall-bounded flow (Menter 1994).

The eddy viscosity model formulation works well for simple shear flows such as flow in a pipe, but it is less appropriate for complex 3D flows that involve multiple strain-rates (Rodi 2017). The reasons for this deficiency are the assumption of an isotropic eddy viscosity model and the use of a simple linear relationship between the Reynolds stress and the mean velocity gradient. For more complex flows, a higher order model is required, e.g., a second moment closure that determines the components of the Reynolds stress tensor from their own transport equations (Launder 1989, Jaw and Chen 1998). For example, second moment closure models are able to predict the turbulence-driven secondary motions in duct and channel flows, which makes them superior to eddy viscosity models in terms of predictive realism. However, they are theoretically more difficult to implement and computationally more demanding, so that their application in general has been more limited than simpler models (Rodi 2017).

2.2.1.2 Boundary conditions

The boundaries confining the pond, i.e. bottom, side walls, and free surface, have to be defined in a CFD model. Regarding the bottom and walls, no-slip, free slip, or partial-slip conditions can be imposed. For near-wall regions, finer grids are required to capture the effect of wall and the associated sharp velocity gradients. In many RANS-type models the turbulence model formulation is modified to account for wall damping using a near-wall treatment. Wall functions are the most common near-wall treatment method. They assume a logarithmic velocity profile in the near-wall region and allow a coarser mesh to be used near the wall. However, if local flow separation is present, e.g. over baffles, the wall function treatment cannot be used (Chen and Patel 1988). In that case, a low-Reynolds number formulation can be used to predict the

turbulence all the way to the wall. Roughness can be implemented either by wall functions or special two-equation closures, e.g. a two-layer $k - \varepsilon$ model that uses a hydrodynamic roughness length to implement a rough-wall boundary condition (Durbin et al. 2001, Zaman and Bergstrom 2014).

It has been a common practice to model the free surface with no deformation (i.e, without waves) as a free-slip wall (Hsu et al. 2003, Bombardelli and Jha 2009, and Liang et al. 2017). A more realistic approach is to use the Volume of Fluid (VOF) method to track the deformation of the free surface. VOF allows a specific control volume to include both liquid and air, which in turn allows the variation of the liquid surface to be approximated (Hirt and Nichols 1981).

2.2.1.3 Residence time Distribution

There have been several research studies where CFD has been employed to study the flow pattern in a pond and to estimate the so-called residence time distribution (Persson 2000, Adamsson et al. 2005, Khan et al. 2009). The residence time is the length of time that water entering the pond resides within the pond. The residence time distribution is of interest because it can be used to characterize the flow behavior in the pond, e.g. identify the effect of dead zones in a pond (Walker 1998). In addition, the sediment retention of a pond is known to depend on the residence time distribution (Persson and Wittgren 2003, Birch et al. 2007). A long residence time generally is an indicator of low fluid velocities, which tend to enhance the sediment settlement and sediment removal efficiency (Persson 1999).

In experiments, the residence time distribution, E, can be determined using tracer testing. It indicates the mass fraction of tracer that has left the pond at a given time, t, after injection of the tracer at the inlet at time t = 0, and is given by (Levenspiel 2012):

$$E(t) = \frac{C(t)}{\int_0^\infty C(t)dt} = \frac{QC(t)}{M} \qquad [2.1]$$

where C, Q, and M are the outflow tracer concentration (kg/m³), flow rate (m³/s), and total inflow tracer mass (kg), respectively. The residence time distribution is often normalized using nominal residence time, t_n, i.e. the ratio of pond volume to the flow rate. The residence time distribution curve is plotted as the normalized residence time, i.e. $E(t)t_n$, against the dimensionless time, i.e. t/t_n.

To obtain the residence time distribution in a single-phase CFD model, first, the steady state velocity field is obtained. Then, a passive scalar concentration (or tracer) field is solved based on the velocity field using an unsteady advection-diffusion equation (Equation [2.2]) to predict the transport of a hypothetical slug of tracer in the pond.

$$\frac{\partial C}{\partial t} + \frac{\partial u_i C}{\partial x_i} = D_i \frac{\partial^2 C}{\partial x_i^2} \qquad [2.2]$$

where D_i is the diffusivity coefficient. The tracer concentration, C, is monitored at the outlet of the pond at time, t. Solving for C at the outlet at different times provides the information required to produce the residence time distribution using Equation [2.1].

2.2.1.4 Verification and Validation

Another important task in CFD modelling is verification and validation. The most important element of verification is grid independence, i.e. to determine the grid resolution required to reduce numerical approximation errors to an acceptable level. The design and construction of a quality grid is crucial to the success of a CFD analysis. The grid configuration has a significant impact on convergence, solution accuracy, and the computational cost. The grid density should be high enough to adequately resolve the relevant flow features. The grid adjacent to the wall should be fine enough to resolve any boundary layer regions. Ideally, for a single-phase simulation, model validation should compare the numerical results to measurements of both the mean velocity and turbulence fields. For a multiphase simulation, model validation should also include a comparison to measurements of the particle velocities and concentration.

2.2.2 Survey of single-phase studies

Table 2.1 lists 11 studies that represent the use of CFD over the last twenty years by the hydraulics engineering community for the study of retention ponds. These CFD studies considered such features such as pond shape, size, and vegetation. These studies simulated either prototype or scale model ponds. For model development and validation purposes, the scale models are easier to work with, since factors such as flow rate, wind, precipitation, and vegetation can be controlled in a laboratory. Furthermore, laboratory scale ponds are much smaller than prototype ponds, which makes simulations more feasible.

In a study to assess the flow behavior in an elliptical stormwater retention pond ($90 \times 60 \times 1.2$ m) located in Ontario, Canada, Shaw et al. (1997) used a single-phase 3D CFD model together with field measurements. The in-situ measurements were taken at three different base flow rates. The water level in the pond did not vary since the inflow and outflow are equal. The velocity measurements were conducted at three different depths for 16 sampling locations. The measurements were used for model calibration purposes. For the CFD model, the RANS equations with a $k - \varepsilon$ turbulence model were solved using PHOENICS software. The average wind speed and direction data were also recorded. The velocity predictions were modified to include the wind-induced flow based on using an empirical equation developed in a flume for still water by Baines and Knapp (1965). The authors identified three different zones in the pond, i.e. an advection zone characterized by high velocities, a circulation zone, and a dead zone characterized by low velocities. The overall flow pattern predicted by the CFD model was in agreement with the measured flow pattern.

The effect of pond shape, length-to-width ratio, vegetation, and retrofitting elements such as baffles, berms, and islands, are often tested by comparing the corresponding residence time distributions. Persson (2000) studied the residence time distribution of 13 different hypothetical scale model pond layouts with varied inlet and outlet locations, and retrofitting elements. The layouts all had a simple rectangular shape except for one which had an L-shape. To eliminate the scale effects, all of the test cases had equal

19

volume and depth. A 2D depth-averaged CFD commercial code called MIKE 21, developed by Danish

Hydraulic Institute (1996), was used. A 2D LES was applied to model the small scale turbulence motions.

Table 2.1 Summary of single-phase CFD studies of stormwater retention ponds

Author(s)	Prototype or scale model	Method	Turbulence model	Code	Verification	Validation
Shaw *et al.* (1997)	Prototype	3D RANS	$k - \varepsilon$	PHOENICS	No	No
Persson (2000)	Scale model	2D depth-averaged RANS	LES	MIKE 21	No	No
Adamsson *et al.* (2005)	Scale model	3D RANS	$k - \varepsilon$	ANSYS Fluent	No	Residence time distribution
Khan *et al.* (2009)	Scale model	3D RANS	$k - \varepsilon$	ANSYS CFX	No	No
Khan *et al.* (2012)	Scale model	3D RANS	$k - \varepsilon$ and $k - \omega$	ANSYS CFX	Yes	Residence time distribution and free surface velocity
He and Marsalek (2013)	Scale model	3D RANS +VOF	$k - \varepsilon$	ANSYS Fluent	No	No
Tsavdaris *et al.* (2015)	Prototype	3D RANS	$k - \varepsilon$	ANSYS Fluent	No	No
Farjood *et al.* (2016)	Scale model	3D RANS	$k - \omega$	ANSYS CFX	Yes	Residence time distribution
Sonnenwald *et al.* (2017)	Prototype	3D RANS	$k - \varepsilon$	ANSYS Fluent	No	No
Nakhaei *et al.* (2018)	Prototype	Unsteady 3D RANS	Simplified $k - \varepsilon$	ELCOM	No	Temperature
Binns *et al.* (2019)	Prototype	2D RANS	Not mentioned	RMA2 and SED2D	No	Mean concentration
Allafchi *et al.* (2019)	Prototype	Unsteady 3D RANS	$k - \varepsilon$	STAR CCM+	Yes	Mean bacteria concentration

Adamsson et al. (2005) used a single-phase 3D CFD model to produce residence time distributions in a rectangular retention pond ($13 \times 9 \times 1$ m) at three different discharges. The experimental pond was located in the hydraulic lab of Chalmers University of Technology, Sweden. The 3D RANS equations with a $k - \varepsilon$ turbulence model using standard wall functions were solved using ANSYS Fluent software. The wall boundary condition was set to no-slip and no consideration was given to surface roughness. The free surface was modeled as a free-slip wall. The computational domain was covered by 144,000 unstructured cells; the depth was resolved into 21 cell layers. The model was first run for steady state conditions to obtain the solution for the three velocity components. Then, the unsteady transport equation was solved to reproduce the tracer tests to find the residence time distribution. The computational residence time distributions were tested against measured residence time distributions. The authors were not able to match the results.

In a similar study, Khan et al. (2009) compared a number of computationally modeled residence time distributions corresponding to a trapezoidal stormwater retention pond, i.e. rectangular pond ($1.025 \times 0.375 \times 0.0575$ m) with side-sloped walls (2:1), retrofitted with different elements. The numerical model was developed in ANSYS CFX software as a 10:1 scale model of an existing pond in Auckland, New Zealand. The 3D RANS equations with a $k - \varepsilon$ turbulence model using standard wall functions were solved. The free surface was modeled as a free-slip wall and the wall boundary condition was set to no-slip with no consideration given to the surface roughness. Their study demonstrated how the residence time distribution of a trapezoidal pond can be affected by the use of various retrofitting elements (i.e. baffles, island, or subsurface berm) at different locations.

Later, Khan et al. (2012) performed surface velocity measurements in the same pond using Particle Tracking Velocimetry (PTV) and compared to the flow pattern at the surface predicted using ANSYS CFX. Three different grid refinements were tested; the grid including 42K cells was selected since the predicted velocity was less than 1% different from the solution on a finer mesh. Two turbulence models, namely the

$k - \varepsilon$ and $k - \omega$ SST models, using standard wall functions were tested; the differences between the velocity fields predicted by the two models was insignificant, i.e. less than 1%. The authors noted that their study was the first to compare the results from a CFD model of a stormwater retention pond to velocity measurements from a scale model. However, their study only considered the free surface velocity pattern by tracking the tracers floating on the surface; as such they only looked at the velocity and vorticity on the surface, and no measurements were taken through the depth of the pond. In complex flows, the velocity field will often vary over the depth of the pond, so that complete reliance on the surface flow can be misleading. The prediction of the free surface flow may also be compromised by the assumption of a free-slip wall as the boundary condition. Farjood et al. (2016), from the same research group, used the same code with the $k - \omega$ SST to investigate 27 different combinations of aspect ratios and wall slopes for the trapezoidal pond. After testing three different meshes, a grid containing 250K cells was selected. Their study showed that ponds with identical length-to-width ratios can perform differently because of different wall slopes. The finding was significant since the design of ponds often relied on the length-to-width ratio as the most significant and often only feature affecting the pond performance. Validation was based on the residence time distribution curves, and not the prediction of the velocity field.

He and Marsalek (2013) compared the computational flow pattern for a number of different flow rates in a scale model rectangular pond of size $1.025 \times 0.375 \times 0.0575$ m. The 3D modeling of the flow using the $k - \varepsilon$ turbulence model was performed in ANSYS Fluent. Unlike other studies, the authors did not apply a free-slip wall for the free surface boundary condition. Instead, they tracked the free surface using the VOF method.

Tsavdaris et al. (2015) investigated pond configurations by comparing residence time distributions. Large-scale elliptical configurations of vegetated ponds were modeled using ANSYS Fluent to solve the 3D RANS equations with a $k - \varepsilon$ turbulence model. A porosity added to the momentum equation as a sink term was used to simulate the effect of vegetation. In this study, the number of control volumes was

determined by the software version limitation of 512,000 which is a relatively low number for a large-scale pond (volume of 1400 m^3).

Sonnenwald et al. (2017) also studied the mixing effect of vegetation in a pond model and compared several vegetated pond configurations using residence time distributions. The ponds had a surface area of 500 m^2 and a depth of 1.5 m. ANSYS Fluent was used to solve the 3D RANS equations with a $k - \varepsilon$ turbulence model. A porosity term was added to the momentum equation to simulate the force vegetation exerts on the flow. Then, an advection-diffusion equation was solved where the diffusion coefficient was the turbulent viscosity. The primary usefulness of this study was the comparison of the effect of shape, length-to-width ratio, retrofitting elements, with and without vegetation, on the residence time distribution.

The internal thermal structure, i.e. stratification, within a pond can affect the hydraulic properties (Shilton 2005). Nakhaei et al. (2018) investigated the temperature variability in three prototype stormwater ponds in Alberta, Canada. The ponds had depths from 2.2 to 3.5 m, and the surface areas ranged from 18000 to 22000 m2. The Estuary and Lake Computer Model (ELCOM), developed at the Centre for Water Research at the University of Western Australia, was applied to solve the unsteady hydrostatic 3D RANS equations and the thermal energy equation (Hodges 2000). Two sets of temperature time series measurements were available. One set was used to calibrate the model by tuning coefficients, while the second set was used for validation.

Binns et al. (2019) studied two prototype retention ponds in Ontario, Canada. The ponds had irregular shapes and sizes of approximately $200 \times 25 \times 2$ m. The authors used a package developed by the United States Army Corps of Engineers, which included a 2D depth-averaged finite element model called RMA2 for hydrodynamic modeling, and a sediment transport model called SED2D, which solves the advection-diffusion equation for sediment based on the hydrodynamic results. The computational mesh size was as coarse as 1 to 5 m. The authors calibrated the SED2D model based on available field data from a single rain event by tuning the bed roughness coefficient to capture the measured flow and sediment

discharges at the outlet. Then, a variety of length-to-width ratios, retrofitting elements, and outlet locations were tested.

Allafchi et al. (2019) studied the distribution of bacteria in a 235,000 m^3 irregular-shaped stormwater pond in Alberta, Canada. The 3D unsteady RANS (URANS) equations, together with a $k - \varepsilon$ turbulence model and an advection-diffusion equation for the bacteria, were solved using the commercial CFD code STAR-CCM+. The effect of wind was implemented by specifying a velocity vector on the free surface. A grid independence study was used to determine that an unstructured grid with 1.5 million cells was sufficient. To enhance convergence, first a steady-state simulation with only an average wind speed was carried out, and the resultant velocity field was used as the initial condition for the main set of simulations. A storm event hydrograph was introduced at the inlet. The pond was simulated for a period beginning 1 hour before the start of the storm event and ending 24 hours after the event. The CFD predictions were validated against bacteria concentration data collected from six different points in the pond and showed good agreement.

Despite significant advances in computational resources, from the first studies to computationally model a stormwater pond (i.e. Shaw et al. 1997) until now, the modeling has not progressed significantly. Simulation of multiple grids to assess grid independence is now more feasible than ever before. Of the 11 studies, only 2 considered verification. CFD models of stormwater ponds in the literature typically solve the velocity field for the liquid phase and then use a transport equation for a tracer material to produce residence time distribution curves. This is partly because the benchmark data available for validation is most often in the form of a residence time distribution. Of the 11 studies, only 5 considered validation. Among these 5 studies, 2 were only validated against the residence time distribution. While useful, residence time distribution do not represent a comprehensive benchmark for validation of a CFD model, especially if the sediment does not follow the fluid. The residence time distribution method may be helpful in comparing the flow patterns for two different ponds, but it is not capable of predicting the transport in

complex ponds where the sediment is strongly affected by turbulence, complex geometry or other complicating features. It approximates the sediment transport by the convection-diffusion of a passive scalar, and does not consider particle settlement, and/or resuspension. Comparing to comprehensive flow measurements, e.g. velocity and turbulence properties in a pond, either scale model or prototype, would be a more effective method for validating single-phase models. Experimental capability in fluids measurements, e.g. Particle Image Velocimetry (PIV) and Acoustic Doppler Velocimeter (ADV) to some degree, now competes with CFD in terms of the comprehensiveness of the results. For example, tomographic PIV can provide time-resolved three-component measurements of the local velocity field. Notwithstanding the development of such methods, a lack of comprehensive experimental data sets appears to be a severe impediment to validation of single-phase CFD models in ponds.

Single-phase models cannot reproduce the particle trajectories and related sediment transport in a pond with complex features and large particles that do not follow the fluid trajectory. According to Balachandar and Eaton (2010), who reviewed the applicability of the single-phase approximation for modeling particle transport, this approach is only justified when the particle Stokes number is less than 0.2. For some pond conditions, the particle Stokes number of the largest particles, which are more likely to settle, exceeds 0.2. Given the rapid advancement in computing power and speed, moving towards a comprehensive multiphase model, even for prototype applications, no longer seems impossible.

2.3 Application of CFD in modeling sediment transport in stormwater retention ponds

If a multiphase model is required to more accurately model sediment transport in a pond, different approaches are available. The use of these models in the hydraulic engineering community has been limited (Pananicolaou et al. 2008). The first category of multiphase models is Lagrangian – Lagrangian, also called the mesh-free method, where both the liquid and solid phases are represented by a collection of discrete particles (Van der Hoef et al. 2008). Each particle possesses a set of properties such as mass and momentum, and the conservation equations are solved for each particle as they move through the domain (Shakibaeinia

and Jin 2011, Kolahdoozan et al. 2014). There are large computational and memory requirements for Lagrangian – Lagrangian modeling of sediment transport, and therefore the method has not yet been used for practical hydraulic modeling problems where the length scales are relatively large (Van der Hoef et al. 2008).

Alternatively, the governing equations of the liquid phase can be written in an Eulerian frame by adopting a continuum description governed by the Navier-Stokes equations, and the governing equations of the sediment phase formulated in a Lagrangian framework, resulting in a Eulerian-Lagrangian model that is often referred to as "particle tracking". In a third model formulation, both the liquid and sediment equations are written in an Eulerian framework, which is then called an Eulerian-Eulerian model. The most used Eulerian-Eulerian formulation is the so called "two-fluid model", where two sets of transport equations, one for each phase, are solved (Bakhtyar et al. 2009, Yan et al. 2014). The particle tracking and TFM approaches will be discussed in detail in the following sections.

2.3.1 The particle tracking model
2.3.1.1 Methodology

In particle tracking models, the Navier-Stokes equations are solved for the continuous liquid phase and the solid particle trajectories are integrated in time based on Newton's second law of motion. The hydrodynamic forces on the particles are due to the relative velocity field. The point-particle approach was the first among other particle tracking models (Balachandar and Eaton 2010). In a one-way coupled point-particle simulation, the particles follow the liquid passively, i.e. integrating the velocity field. In a two-way coupled point-particle simulation, the liquid phase momentum equation includes the drag of the particle on the fluid (Sommerfeld and Decker 2004, Garg et al. 2007).

When the particle concentration is high, the particles come together, displace the liquid between them, collide, and then rebound. In addition to sufficiently fine grids, simulating this phenomenon requires a high resolution time step. Resolved particle tracking models, also known as DNS models, resolve the flow

around the particles. These DNSs use an Eulerian grid at least an order of magnitude smaller than the size of the particles, so that the motion of each particle is computed from the hydrodynamic force exerted by the surrounding continuum (Van der Hoef et al. 2008). The resolved particle tracking methods are the most expensive to compute.

There are unresolved particle tracking models that use a collision model instead of resolving the collision phenomenon. The Discrete Element Methods (DEM) proposed by Cundall (1988) is a well-known category of collision models. The Eulerian grid is larger than the size of particles and the particle can be treated as a source of mass, momentum, and energy for the liquid phase (Van der Hoef 2008, Kloss et al. 2012, Norouzi et al. 2016). Yergey et al. (2010) simulated moving particles in an open channel flow using DEM. For modeling sediment transport in the bed region, more sophisticated collision models are required (Kempe and Fröhlich, 2012a). Kempe et al. (2014) investigated different collision models in a systematic way in open channel flow and found that the Adaptive Collision Model (ACM), developed by Kempe and Fröhlich (2012a), provided more physically realistic results.

The instantaneous flow field is required for tracking the particles. If RANS is used for the liquid phase, the fluctuating field has to be reconstructed artificially based on the length and time scales derived from the RANS turbulence field. One of the common techniques for reconstructing the instantaneous flow field is the random walk method, i.e. which is based on the use of stochastic methods employing a Gaussian distributed random velocity fluctuation. The simulation can approximate the flow turbulence effect on the particle if the calculations are repeated for a sufficient number of times (Adamsson et al. 2003, Yan 2013).

The bed boundary condition for sediment particles is known to be a key challenge in particle tracking models (Gu et al. 2017). The trap and reflect bed boundary conditions are the two most common (Adamsson et al. 2003, Yan et al. 2014). The trap boundary condition means that the trajectory of the particle terminates once it reaches the bed. The reflect boundary condition means that the particle is reflected back into the water domain when it reaches the bed (Yan et al. 2014). More physically realistic

bed boundary condition approaches have also been used in some particle tracking studies, e.g. a combination of trap and reflect features. For example, a critical bed shear stress is a combination of trap and reflect boundary conditions such that a particle hitting the bed is trapped if the local bed shear stress is below the critical bed shear stress, and is reflected if the local bed shear stress is larger than the critical bed shear stress. A critical issue is how to determine whether a particle settles or goes back into the water domain (Stovin and Saul 1998, Adamsson et al. 2003). Improved bed boundary conditions would need to admit a more complex description of the bed characteristics, e.g. the cohesion of sediment particles.

2.3.1.2 Survey of particle tracking studies

In this section, the studies that modeled sediment movement in the ponds using particle tracking methods are reviewed. Table 2.2 lists 4 studies that represent the use of particle tracking by the hydraulics engineering community for the study of retention ponds. These studies simulated either prototype or scale model ponds. The validation was performed against either the sediment removal efficiency or the sediment deposition zones.

Table 2.2 Summary of particle tracking studies investigated sediment in stormwater retention ponds

Author(s)	Prototype or scale model	Sediment particles	Type of model	Turbulence model	Code	Verification	Validation
Torres *et al.* (2008)	Prototype	-	3D RANS	$k - \omega$	ANSYS Fluent	Yes	Sediment deposition zones
Zhang (2009)	Scale model	47 μm 1500 kg/m^3	3D RANS	$k - \varepsilon$	ANSYS Fluent	No	Sediment removal efficiency
Dufresne *et al.* (2009)	Scale model	750 μm 1030 kg/m^3	3D RANS	$k - \varepsilon$ and RSM	ANSYS Fluent	No	Sediment deposition zones
Yan (2013)	Prototype	565 μm 1020 kg/m^3	3D unsteady RANS	$k - \varepsilon$	ANSYS Fluent	Yes	Sediment deposition zones

Torres et al. (2008) simulated the sediment deposition pattern in a full-size pond (32,200 m^3) in France using ANSYS Fluent. A $k - \omega$ turbulence model was applied with a standard wall function. The

flow domain was resolved using 900,000 cells based on a grid independence study. A total of 20,000 particles were injected at the inlet and then tracked. The dispersion of particles by the fluid turbulence was modeled using a random walk model. The free surface was resolved using the VOF method. In the search for a more realistic particle behaviour at the bed, a new particle bed boundary condition was also introduced: when a sediment particle reached the bed, it remained there if the turbulence kinetic energy was less than the particle kinetic energy defined by the particle settling velocity. The value of the settling velocity was calibrated to calculate the particle kinetic energy to give the closest fit to the experimental deposition patterns. The study is significant because it explores the particle tracking method in a prototype pond, however the calculation required empirical calibration of a number of model parameters.

Zhang (2009) implemented a 3D particle tracking model of a scale model stormwater retention pond ($2 \times 0.982 \times 0.45$ m) in ANSYS Fluent. A total of 328 particles were injected from the inlet into a computational domain resolved by 31,000 cells. The number of particles reaching the outlet was used to find the sediment removal efficiency of the pond. For the liquid phase, the RANS equations with a $k - \varepsilon$ turbulence model using standard wall functions were solved. The walls were modeled using no-slip boundary condition, while the free surface was modeled as a free-slip wall. Zhang (2009) compared two different bed boundary conditions: trap and critical bed shear stress. The bed shear stress boundary condition provided a closer prediction of the measured removal efficiency. However, the method is dependent on an empirically derived value for the critical shear stress at the bed, which will vary depending on the properties of the bed and the sediment characteristics.

When the number of particles is much less than in an actual pond, the model is unlikely to predict realistic behaviour for the particles. Dufresne et al. (2009) modeled the particle transport in a scale model experimental tank ($1.89 \times 0.76 \times 0.4$ m) using ANSYS Fluent. The liquid domain was solved with 100,000 cells, and 6400 spherical particles were tracked. A $k - \varepsilon$ turbulence model was used with standard wall functions to model the fluid phase. The authors included the effect of the fluid turbulence on the particle

motion and computed the particle trajectory using a random walk technique. The predictions for zones where sediment was deposited in the tank were compared against images taken from the scale model. The usefulness of their study was in representing the general deposition pattern of particles. However, the sediment deposition zones did not closely match to the experimental results. The turbulence kinetic energy boundary condition was used. This boundary condition improved the predictions for some cases, but resulted in poorer predictions for other cases. The authors also tested a Reynolds stress model (RSM) for the fluid turbulence; over the $k - \varepsilon$ model, however, it did not provide any improvements.

Yan (2013) implemented a model based on the URANS equations in ANSYS Fluent. A $k - \varepsilon$ turbulence model was used with a standard wall function. A random walk was also applied to model the effect of turbulence on the particle transport. The free surface was modeled as a free-slip wall. The bed roughness effect was considered using a modified law of the wall. The model was initially used to simulate the scale models of Dufresne et al. (2009) and Vosswinkel et al. (2012). The liquid phase velocity field was simulated as unsteady. Then, the unsteady particle tracking was performed using the liquid phase velocity field saved at the previous time step. Yan (2013) reported a significant improvement in prediction of the spatial and temporal deposition pattern of sediments on the bed compared to steady predictions. The authors claimed that the rational was that the physics of sediment particles can be better captured since a deposited particle at one time step may become entrained in the next time step due to the changes in the flow field. Some departure from the real deposition pattern in the pond was still present. Next, Yan (2013) modeled the full-size pond, previously modeled by Torres et al. (2008), considering unsteady effects on both the fluid and sediment transport. The number of cells selected was 850,000 based on a grid independence study.

Reviewing the literature on particle tracking methods used to model retention ponds, the method provides a detailed description of the particle transport. However, the large computational cost and convergence problems limit the application to low sediment concentrations. Particle tracking is not well suited to handling high concentration region near the bed where most of the particle dynamics occur. The

one-way models are not capable of capturing the particle collision effects at high concentrations. The fully-coupled particle tracking models involve intensive computational effort because they attempt to include particle collisions as well as the particles' effect on the liquid turbulence. The intensive computational effort of the fully-coupled particle tracking models is a limiting factor, since the largest number of particles simulated achieved in the literature at this moment is on the order of 10^{10} (Cheng et al. 2018). None of the current bed boundary conditions are capable of representing the physics of sediment behaviour in ponds, i.e. particle sliding, saltation and resuspension. The particle tracking models are not yet at a stage where there are confident deposition models. The number of particles to be tracked is a significant issue in modeling stormwater ponds using particle tracking methods. To provide a representative picture of the number of particles needed to simulate a stormwater retention pond, consider the measurements taken by Gillis (2017) in a pond located in Saskatoon, Saskatchewan. The approximate volume of the pond is 46,000 m^3. Gillis (2017) reported a particle density of 1300-2000 kg/m^3 and an average diameter of 0.014 mm. Assuming a solids volume fraction of 0.01% and spherical-shaped particles , then the total number of particles would be approximately 3.2×10^{15}. Given the intense computational cost of the particle tracking models, it is not yet feasible to track billions of particles and their interactions with each other. One way to avoid tracking large number of particles is to use of the two-fluid modeling (TFM) approach.

2.3.2 The two-fluid model
2.3.2.1 Background

A TFM, in which both phases are assumed to coexist in the form of interpenetrating continua, allows classic continuum mechanics to be employed to formulate multiphase flows based on fundamental conservation laws (Zhong et al. 2011). A TFM consists of separate sets of mass and momentum conservation equations written on fixed control volumes for each phase (Enwald et al. 1996). The model is able to include the influence of solid particles on the flow as well as particle-particle interactions (Greimann and Holly 2001). The TFM equations for each phase include the interactions between phases at their interface (Enwald et al. 1996). The equations are averaged either in space, in time or as an ensemble. Based

on the application, the modeller decides which interphase phenomena to include. The TFM introduces more variables than equations, so that additional expressions are required to close the set of averaged partial differential equations (Enwald et al. 1996). These closure expressions are mostly empirical, based on limited experimental data (Enwald et al. 1996). Depending on the averaging procedure and the closure expressions adopted, there are several ways to formulate a TFM (Enwald et al. 1996).

Early two-fluid-like models were mostly focused on deriving a revised single-phase equation for the liquid. Drew (1975) and McTigue (1981) were some of the first to use a TFM to describe sediment transport. Drew (1975) introduced a new averaging scheme for the sediment phase. However, he ignored the particle interactions and particle effects on the flow. McTigue (1981) was among the first studies to model sediment transport based on the assumption that both the fluid (water) and the dispersed particles (sediment) can be treated as continuous media. In subsequent studies, Cao et al. (1995) and Greimann et al. (1999) ignored the particle-particle interactions but retained the effect of particles on the flow. Note that this assumption is only valid if the concentration of the sediment phase is low, i.e. a volume fraction of less than 10^{-3} according to Elghobashi (1994).

For flows with high sediment concentration, the particle-particle interactions play a critical role and can no longer be ignored; a description for the sediment phase stress is required to close the sediment phase momentum equation. Introducing the kinetic theory of granular flow, Enwald et al. (1996) provided a model for particle-particle interactions. When collisional interactions play an important role in the motion of the particles, concepts from gas kinetic theory (Chapman and Cowling 1970) can be used to describe the effective stresses in the sediment phase resulting from kinetic and collisional contributions (Greimann and Holly 2001). Lun et al. (1984) considered the inelastic nature of particle collisions and derived expressions for the sediment phase stress based on kinetic theory. The concept of granular temperature was used to describe the particle velocity fluctuations. Jenkins and Hanes (1998) applied the kinetic theory of granular flow to derive relations for high concentration flows in which sediment particles are dominated by their

collisional interactions so that the effect of the fluid turbulence on the particles can be neglected. In high sediment concentrations, the frictional and buoyancy terms can also be included into the TFM equations. The sediment-induced density stratification will affect the hydrodynamics of the system including attenuation of the turbulence (Hsu et al. 2007, Cheng et al. 2017).

When RANS modeling is applied, the near bed region has to either be resolved to model the viscous and buffer sublayers, or avoided using bed treatment methods. As noted previously, a common method is to avoid the viscous and buffer sublayers by applying the logarithmic law of the wall above the bed boundary. For two-phase flow, either an empirical bed boundary condition is utilized, or as in the TFM, the model naturally predicts the sediment deposition. For the concentration at the first computational cell, in some cases an empirical bed boundary condition is used which relies on experimental data (Hsu et al., 2003, Jha and Bombardelli, 2009, Liang et al., 2017). An alternate and more consistent approach is the Johnson and Jackson (1987) boundary conditions, which specify the value of the particle shear stress and granular temperature at the wall. This wall boundary condition can include particles colliding with and sliding along the wall. The effect of particles on the fluid turbulence can be introduced into the TFM. This requires a so-called turbulence modulation term to be added to the turbulence model equations (Balachandar and Eaton 2010).

2.3.2.2 Survey of TFM studies

Two-fluid modeling has not yet been applied in pond simulations. Instead, Table 2.3 summarizes five studies that used the two-fluid to model to simulate sediment transport in open channel flow. Open channel flow with sediment transport captures some of the important features of a retention pond.

Table 2.3 Summary of studies used two-fluid modeling in open channel flows

Studies	Code	Turbulence model	Dilute/ dense	Verification	Validation	Highlight
Hsu *et al.* (2003)	In-house	$k-\varepsilon$	Dilute	No	Fluid velocity and sediment concentration	Effect of large particles on turbulence
Amoudry *et al.* (2008)	In-house code of Hsu *et al.* (2003)	$k-\varepsilon$	Dilute	No	sediment particle velocity and concentration	Modification of turbulence models to capture the effect of small particles
Jha and Bombardelli (2009)	In-house	$k-\varepsilon$	Dilute	Yes	Mixture velocity, sediment concentration, fluid velocity, sediment velocity, and turbulence statistics	Hierarchy of TFMs
Jha and Bombardelli (2010)	In-house	$k-\varepsilon$	Dense	Yes	Mixture velocity and sediment concentration	Dense flow modeling
Jha and Bombardelli (2011)	In-house	$k-\varepsilon$	Dense	Yes	Fluid velocity and sediment concentration	Non-uniform particle sizes
Cheng *et al.* (2018)	OpenFOAM	LES	Dense	Yes	Fluid velocity sediment, concentration, sediment velocity, and turbulence statistics	Application of LES
Ahadi *et al.* (2019)	ANSYS Fluent 19.2	Low Reynolds number $k-\varepsilon$	Dilute	Yes	Fluid velocity, sediment concentration, and turbulence statistics	Exploring the effect of particles on turbulence

Hsu et al. (2003) incorporated the damping effects of sediment on the turbulence of the flow using a $k-\varepsilon$ model. The authors validated their model against the experimental data of Sumer et al. (1996) and Asano (1995) in open channel flows. Their model was intended for transport of massive particles. The turbulence can either be enhanced or reduced depending on the particle characteristics and flow conditions (Tsuji and Morikawa 1982, Lyn 1991). Amoudry et al. (2008) modified the coefficients in the turbulence

model of Hsu et al. (2003) based on available experimental data to extend the turbulence closure to a wider range of particle sizes, i.e. smaller particles known as beach sand with a diameter of 0.2 mm.

Jha and Bombardelli (2009) proposed a hierarchy of different levels of two-fluid modeling for dilute transport of sediment in open channel flows. This study is significant since it validated the predictions against a variety of fluid and sediment measures for the first time in an open channel flow. Various efforts have been made to advance the TFM. Jha and Bombardelli (2010) improved their model for simulating the sediment transport for dense concentration, i.e. a maximum sediment concentration exceeding 2% (Torquato 1995). The predictions were validated against experimental data, from Einstein and Chien (1955), Taggart et al. (1972), and Wang and Qian (1992), for mean velocity of the mixture and the distribution of sediment across the flow depth. Their dense one-dimensional TFM was the first in an open channel flow. Turbulence in the fluid phase was modeled using the $k - \varepsilon$ model. Their work only focused on the suspended sediment, therefore they used a boundary condition at the bed based on experimental data to reflect the bedload. The authors also calculated the relative importance of interaction forces i.e. drag, lift and virtual mass. For dilute flows, the drag force was dominant, however for the dense flows, the virtual mass force also played a significant role. The lift force was found to be negligible for simulating both dilute and dense flows. Jha and Bombardelli (2011) also extended their one-dimensional model to simulate suspended sediment of different size. Each particle size class was modeled separately, and then all of them were combined to achieve the overall prediction, which resulted in better predictions compared to the measurements by Einstein and Chien (1955) and Taggart et al. (1972).

Cheng et al. (2018) adopted the LES approach to resolve the turbulence and turbulence-sediment interactions in sediment transport for a sheet flow condition. Sheet flow represents a sediment transport mode in which a layer of dense sediment moves above the bed. In sheet flows, the sediment concentration is so high that frictional stresses have to be included. According to Liu et al. (2016), near-bed turbulent motions are the main triggering mechanisms for large sediment entrainment. Using steady RANS, these

motions cannot be fully captured. The LES approach was used to explore the effect of these motions on the sediment dynamics. The authors validated their model against a comprehensive data set of Revil-Baudard et al. (2015).

Ahadi et al. (2019), applied the two-fluid formulation together with a low-Reynolds-number $k - \varepsilon$ turbulence model to explore the sediment transport in a fully developed open channel flow. The model was validated against fluid velocity, sediment concentration, turbulence kinetic energy, and Reynolds shear stress measurements form Lyn (1987). The presence of the sediment particles was observed to enhance the wall shear stress of the liquid phase.

It is not yet feasible to model sediment transport in stormwater retention ponds using particle tracking methods due to the high computational cost as the number of particles increases. Alternatively, the mass and momentum equations of the fluid and sediment phases can be solved with appropriate closures. The TFM has been applied to simulating sediment transport in open channel flow, which captures some of the significant features of a retention pond. The seven studies reviewed used different closure models for momentum transfer between phases, turbulence, and particle stresses. To simulate the sediment behavior in the near-bed region, including the frictional stress, as well as applying an appropriate boundary conditions for the particle-bed interactions are significant. Overall, the results from the reviewed studies were encouraging in so far as complete validation tests was performed against measurements, in some cases including turbulence. To the best knowledge of the authors, the TFM has not been yet applied to simulation of complex geometries such as stormwater retention ponds.

2.4 Discussion

A stormwater retention pond is to effectively remove sediment particles. In the literature, studies of stormwater retention ponds have mostly focused on the residence time distribution concept; the fluid velocity field is solved, and the behavior of a hypothetical neutral tracer is determined based on integration of that velocity field. However, the residence time distribution approach suffers from oversimplification

since it neglects the presence of sediment in the pond. Measurements in open channel flows show that sediment particles by no means act as a neutral tracer in a flow. They can affect both the mean and fluctuating characteristics of the velocity field of the carrier fluid (Kaftori et al. 1995, Muste et al. 2005, Balachandar and Eaton 2010). Significant information is lost when the presence of the sediment phase is neglected in modeling a stormwater retention pond, especially near the bed where the sediment concentration is high. This oversimplification can lead to inaccurate and incomplete predictions.

Any numerical study needs to consider verification and validation. It is necessary to demonstrate that the predictions are grid independent. Most of the studies reviewed in this paper have not appropriately addressed these two issues. One way to ensure that numerical errors are sufficiently small is to conduct a grid-independence study. Access to high performance computing resources has made this tests much more feasible than in the past. Regarding validation, the majority of studies documented above compared a number of pond configurations without validating the realism of their model. Two possible approaches are proposed for validation. One approach would be to use a simpler flow that captures the essential physics of a retention pond to benchmark the numerical predictions against experimental data. For example, a 2D open channel flow with sediment transport could be used to validate a model intended to solve a retention pond. Ideally, the benchmark flow should include deposition and resuspension. A second approach would be to configure a scale pond experiment for more rigorous validation. This would entail a comprehensive experimental study of a generic pond to provide data for benchmarking models. In either case, these two benchmarks would need to provide a more comprehensive set of measurements, i.e. mean and fluctuating velocity fields for both phases, particle concertation, and the Reynolds stresses in the fluid phase. The measurements would provide databases to incorporate new physics in the two-phase models, as well as validate existing two-phase models.

To improve the understanding of sediment removal efficiency in ponds, requires investigation of the sediment particle dynamics within the pond. Realistic predictions of sediment transport requires

authentic multiphase models to simulate the behaviour of the liquid and sediment phases, and their interactions. The sediment transport varies spatially within a pond with local and intermittent accelerated flow patterns. Particle tracking models have been widely used to model sediment transport in ponds. This model solves the fluid phase in an Eulerian frame and tracks each individual particle, however tracking each individual particle requires substantial computational effort which can limit the number of sediment particles considered. To simulate a full-size stormwater retention pond would likely require many millions or even billions of sediment particles. Notwithstanding the advancement in computing technology, it is still computationally impractical to simulate this number of particles and their interactions for an engineering study. Even for low sediment concentration flows, when the size of sediment particles is smaller than the grid size, it is both theoretically and computationally challenging to resolve information on the level of the sediment particles.

Stormwater retention ponds often function at high sediment concentrations, especially in the region near the bed where the important mechanisms of deposition and resuspension occur. At higher concentrations, particle collisions and friction become the dominant mechanisms of sediment transport. At high sediment concentrations, the sediment motion may include continuous contact of sediment particles with each other, as well as stratification effects. In this case, the influence of sediment particles on each other and their effect on the liquid needs to be included in the model formulation.

Two-fluid modeling is capable of bringing in the effect of sediment particles on the flow field and particle-particle interactions. Therefore, it is likely an efficient way to model the physics of sediment transport in ponds especially when the number of particles is large. In the hydraulic engineering literature, sediment particle transport is modeled either as bedload or suspended load. It should also be recognized that the open channel sediment transport specification as bedload and suspended load does not represent the same physics that we encounter in a pond. The near-bed region is responsible for most of the transport, and yet is the most unexplored region because it is the most challenging location to take measurements.

Most of the existing formulae for bedload transport are empirical. For example, the Bagnold (1956) formula calculates the total bedload as a function of the excess shear stress. Sediment motion is assumed to be initiated if the mean bed shear stress exceeds a critical value. This value is often quantified using the Shields (1936) parameter. However, the movement of sediment particles is actually related to the instantaneous wall shear stress, lift force and buoyant force. A TFM inherently predicts the near-bed region and therefore the traditional bedload and suspended load formulations are no longer required. A TFM avoids the various empirical correlations used by traditional sediment transport models and, if it is equipped with LES/DNS simulations and sufficient resolution, the movement of sediment particles can be predicted at an enhanced level of physical realism.

Two-fluid modeling of sediment transport in the complex environment of retention ponds represents a gap in the literature, even though it appears to be well suited to modeling particle dynamics in a pond. The development of two-fluid closure models has largely occurred in other engineering communities e.g. mechanical and chemical engineering. Therefore, different model formulations may be required to simulate hydraulic engineering problems. The two-fluid methodology in the hydraulic engineering community is still in the early development stage, and its capabilities have not been well-explored in the context of stormwater retention ponds. For example, it is not yet known how effective a TFM will be in reproducing the deposition and resuspension.

Even for low sediment concentrations, the combination of two of the most difficult subjects in fluid mechanics, i.e. turbulence and two-phase flows, presents a daunting challenge. The presence of particles and their random movement complicates the fluid phase turbulence. In the pond literature, turbulence is known to keep sediment in suspension and also to resuspend settled sediments. If the turbulence level is sufficiently high, it can be responsible for the negative sediment removal efficiencies observed in some ponds.

Both particle tracking and two-fluid modeling require a high fidelity simulation of the turbulent liquid velocity field. This remains a substantial challenge. For RANS, more advanced turbulence models are required to capture the complexity of the pond flow. The prevalent use of two-equation closures with eddy viscosity model formulations for the Reynolds stresses is not appropriate for complex flows; instead second-moment closures that solve transport equations for the Reynolds stresses promise much more realistic predictions. When the velocity field in the pond is solved using RANS methods, use of a particle-tracking method for the sediment will require reconstruction of an instantaneous velocity field for integration of the particle trajectories. This is currently an area that needs further study. An alternative to RANS is the use of LES, which resolves the large-scale turbulent motions in the pond. However, the large grid requirements and high computational costs make LES inappropriate for routine practical simulations, especially if multiple geometries are going to be explored. For both particle-tracking and TFM simulations, the present models for the turbulence modulation by sediment particle are not yet mature, especially for wall-bounded flows such as a pond.

Finally, there are many specific aspects of pond simulation by CFD that require further consideration. These include the treatment of the free surface, modelling vegetation at the bed, and the use of more realistic particles, e.g. particles of non-spherical shape and with a non-uniform size distribution.

2.5 Conclusion

The present study has reviewed recent developments in two-phase flow modeling of sediment transport in stormwater retention ponds using CFD. The hydraulic engineering community is presently at the point where single-phase models may not be the most effective method for modeling the sediment transport in complex pond configurations, especially as environmental regulations become more stringent. A viable complement to existing hydraulic engineering CFD methodologies, e.g. depth-averaged models, is the use of multiphase fully 3D CFD simulations. Both particle-tracking and TFM options are available to predict the sediment transport. Notwithstanding the advantages offered by a fully 3D simulation of the

water and particle velocity fields, these CFD models are not yet fully mature, and further research is required. A specific issue that needs to be clarified is the ability of the TFM to predict the deposition and re-suspension processes. The further development of the multi-phase CFD models will require new experimental studies that can provide comprehensive measurements of both the mean and fluctuating flow properties of both phases, in scale model and prototype ponds. Going forward, the application of two-phase CFD to model sediment transport in stormwater retention ponds promises to contribute to higher fidelity simulations, which in turn should support the goal of higher sediment removal efficiencies.

Chapter Three

3. INVESTIGATION OF A SCALE MODEL VORTEX-TYPE STORMWATER RETENTION POND: A COMPUTATIONAL AND EXPERIMENTAL STUDY

A similar version of this chapter is ready for submission:

- Ahadi, M., Bergstrom, D., Mazurek, K.A. (2021) Flow Pattern Investigation of a Scale Model Vortex-type Stormwater Retention Pond: Experimental and Computational, Journal of Hydraulic Engineering, ready for submission.

Preamble

Flow characterization of the pond provides a map of the flow pattern, which can be used to detect problematic regions such as stagnation regions. This map is essential for designing more effective ponds and minimizing damage to downstream water bodies. In this study, the flow in a 1:13.3 scale model of the vortex-type pond is characterized using computational and experimental study. The CFD model predictions were validated against measurements of the mean velocity, Reynolds shear stress, and turbulent kinetic energy. Three distinct flow regions of the pond were explored: the inlet jet and its subsequent decay; the rotational flow in the circular channel outside the berm; and the flow passing into the outlet within the berm.

Abstract

To design an effective stormwater retention pond capable of recovering the water quality before being discharged, the flow behaviour in the pond is insightful. In this study, we explore the mean and fluctuating velocity fields in a new vortex-type stormwater retention pond using computational and experimental studies to provide analysis and prediction.

To simulate the vortex-type pond, the 3D Reynolds averaged Navier-Stokes (RANS) equations together with a $k - \varepsilon$ turbulence model were solved using ANSYS Fluent 19.2. 3D velocity measurements were conducted in a scale laboratory model of the pond to obtain a detailed picture of the flow dynamics in the pond, and to guide the numerical modeling. The measurements provide a comprehensive database for CFD

validation of velocity and turbulence in the stormwater retention pond and the computational predictions provide enhanced knowledge of the flow pattern in this new pond design.

Three distinct flow patterns of the pond were explored: the inlet jet and its subsequent decay; the rotational flow in the circular channel outside the berm; and the flow passing into the outlet within the berm. The predictions revealed that despite using the berm and the tangential inlet pipe, a relatively large dead zone forms downstream of the jet clinging to outside the berm. The results also showed that the flow inside the berm does not operate as a single large vortex. Instead, there are two recirculation zones in opposite directions. A few parameters that affect the particle settlement, and as a result, the pond sediment retention performance, were investigated. The extent of the secondary flow pattern was also studied.

3.1 Introduction

Stormwater runoff in urban areas not only causes flooding, but also contaminates receiving water bodies. Stormwater retention ponds are used to manage stormwater flows, i.e. mitigating flooding, and to serve as water quality control structures, i.e. ensuring that the level of contaminants released to downstream water bodies is below the limit regulated by cities (Khan *et al.* 2009, Yan 2013, Gu *et al.* 2017). A useful concept for quantifying pond behaviour is the so-called residence time, which refers to the time that the water entering a pond resides within the pond. A favorable flow regime in a stormwater retention pond is one with a sufficiently long residence time, so that all the suspended sediment particles entering the pond can settle before being discharged. If a stormwater retention pond is subjected to detrimental flow patterns, such as dead zones and short-circuiting currents, the effective area of the pond is reduced, which negatively affects the pond performance (Shaw *et al.* 1997, Pettersson *et al.* 1998, Khan *et al.* 2012).

Knowledge of the flow pattern in the pond is necessary for assessing the pond performance, both qualitatively and quantitatively (Van Buren 1994, Persson 2000, Thaxton *et al.* 2004, Gu *et al.* 2017). Flow characterization of the pond provides a map of the flow pattern, which can be used to detect problematic regions such as low velocity zones and stagnation regions. This map is essential for designing more effective ponds and minimizing damage to downstream water bodies. The residence time distribution, i.e.

the distribution of travel times of tracer parcels injected into the pond, will reflect the detrimental effects of dead zones and short circuiting (Walker 1998). The residence time distribution of a pond is also directly related to the pond sediment retention (Persson and Wittgren 2003, Birch et al. 2007). It is common practice to evaluate the effects of pond shape, length-to-width ratio, vegetation, and retrofitting elements by comparing the corresponding residence time distribution curves (Persson 2000, Adamsson *et al.* 2005, Khan *et al.* 2009, He and Marsalek 2013, Tsavdaris *et al.* 2015, Farjood *et al.* 2014, Sonnenwald *et al.* 2017). A better approach would be to study the velocity field directly.

Advances in computer technology now enable CFD to be applied to different types of ponds, *e.g.* waste stabilization ponds (Shilton *et al.* 2008), sediment basins (Simpson *et al.* 2018), and stormwater retention ponds (Khan *et al.* 2012). CFD models are a promising tool for performing high quality "virtual experiments" on ponds to characterize the flow pattern. CFD models of stormwater retention ponds in the literature typically solve conservation equations for the liquid phase, along with a transport equation for a tracer material to produce residence time distribution curves, e.g. Shaw et al. (1997), Persson (2000), Adamsson et al. (2005), Khan et al. (2009), He and Marsalek (2013), Tsavdaris et al. (2015), and Sonnenwald et al. (2017). A tracer is released at the inlet and the tracer concentration is tracked at the outlet in time. Using the residence time distribution instead of the velocity field is partly because the benchmark data available for validation is often in the form of a residence time distribution curve. Although the residence time distribution method is useful for comparing the performance of different pond designs, a residence time distribution curve does not provide specific information regarding the flow field. In contrast, a CFD model of a pond can be used to study the specific features of the flow field.

A CFD simulation of a pond should be both verified and validated. Comparing against comprehensive velocity measurements in a pond is a more appropriate method for validating CFD models than using residence time distribution curves since a residence time distribution curve treats the pond as a blackbox. However, in many applications a set of experimental measurements of the velocity field in not

available. Furthermore, if a comprehensive set of measurements was available, there would be no need to perform a CFD study. Note that many current measurement methods, such as use of an ADV or a Particle Image Velocimetry (PIV) system, are able to provide three component measurements of the mean and fluctuating velocity field.

Given the context above, the present paper documents a CFD study of a new vortex-type stormwater retention pond designed to provide enhanced sediment removal. In a conceptual study, Albers and Amell (2010) demonstrated that the new circular pond geometry was more resistant to the formation of dead zones and short-circuiting currents. The focus of the CFD study is on the prediction of the mean velocity field and the associated flow patterns. The CFD simulation considers a scale-model of the pond, and a set of discrete velocity measurements are used to validate the predictions of the CFD model. The main purpose of the study is to use CFD to assess the flow pattern in a 3D stormwater retention pond and identify potential problems within the pond.

3.2 Experimental Model

A 1:13.3 scale model of the vortex-type pond was constructed to facilitate experimental measurements. The pond was constructed in the Hydraulic Laboratory at the University of Saskatchewan, designed using Froude scaling laws, assuming that gravitational effects are the most significant and that the viscosity and surface tension effects can be ignored. The Froude numbers are held constant between the model and its prototype. The pond was constructed of plywood coated with an oil-based primer and paint to make the model water-proof and durable; the inner surface was smooth. For more details regarding the physical model construction see Chowdhury (2016). As shown in Figure 3.1a), the pond structure consists of a circular pool with sloped walls (3H: 1V), a peripheral inlet pipe, a central elevated outlet, and an annular trapezoidal berm. The schematic cross section of the pond is also shown in Figure 3.1b). The pond model was 2.86 m in diameter at the bed. The scaled sizes of the inlets and outlets were D = 60 mm and 90 mm, respectively. The inlet pipe was at an angle of 30° with the tangent line to the pond circumference at the

point of entrance. A permanent pool was maintained in the model by using an elevated, top-closed outlet pipe perforated between 50% and 75% of the pipe's total height. The berm surrounds the central outlet and has sloped walls (2H: 1V). The optimum radial position of the berm causing the maximum amount of sediments to settle was determined to be at 60% of the bed diameter (Chowdhury 2016). An opening cuts through the top portion of the berm equal to 1/12th of the berm's circumference (opening width of 393 mm) at the location where the flow has almost completed one rotation. The opening directs the treated water from the main pool towards the outlet.

(a)

(b)

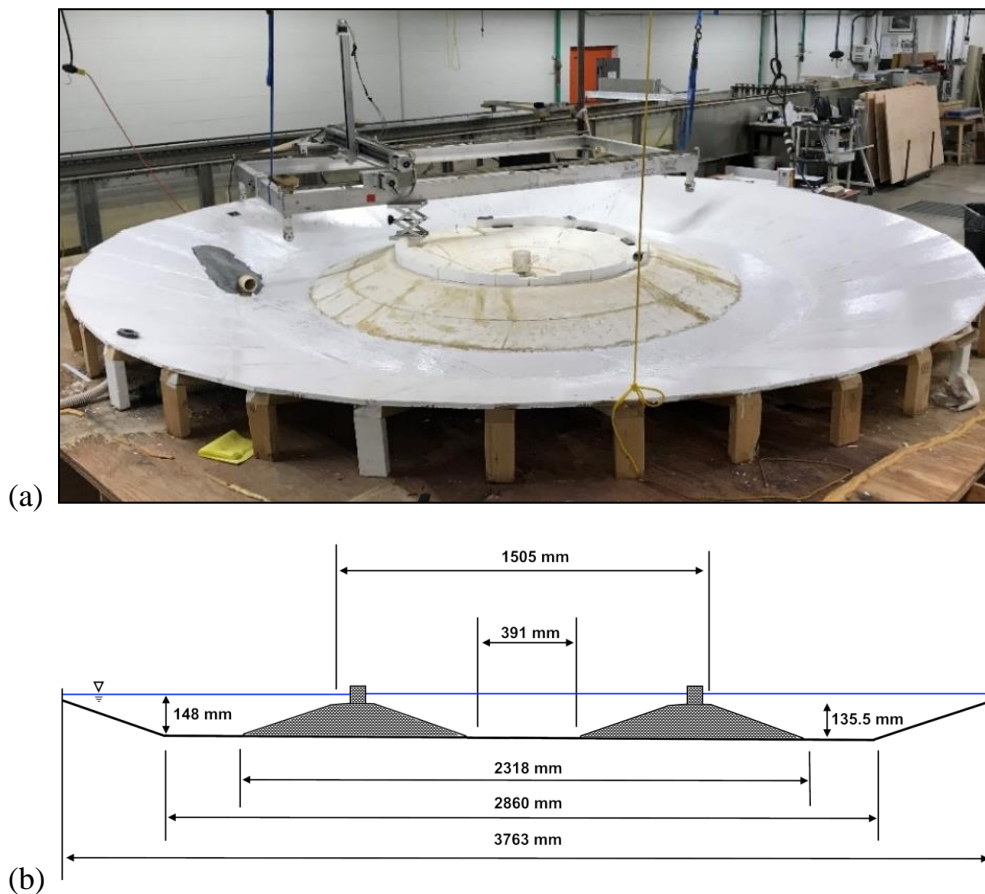Figure 3.1 a) Physical scale model (1:13.3) and b) schematic cross section of the vortex-type pond

The design peak flow rate of the prototype pond was appropriately scaled to Q = 1.55 L/s. This flow rate corresponds to a model inlet bulk velocity V = 0.56 m/s, and a Reynolds number ($VD\rho/\mu$) of Re = 33,600 at the inlet, where μ and ρ are the viscosity and density of water, respectively. The scaled flow

depth of the pool was h = 148 mm. 3D velocity measurements were taken at different radial locations and depths in the pond using two Sontek 16 MHz ADVs: an up-looking ADV for the top half of the flow depth and a down-looking ADV for the bottom half of the flow depth. The ADV probe was mounted on a traversing system as shown in Figure 1. The traversing system and the probe were oriented such that at each location it measured the azimuthal (v_θ), the radial (v_r), and the vertical (v_z), components. Going forward, for simplicity purposes they are called u, v, and w, respectively. Each ADV consists of a three-axis probe and an electrical processing unit. The ADVs have 50 mm focal lengths to allow for non-obtrusive velocity sampling.

Doppler noise is the main source of uncertainty in ADV measurements. At a sampling rate of 50 Hz and for a signal to noise ratio (SNR) above 20 db, the uncertainty due to Doppler noise can be estimated as 1% of the maximum velocity range (Chanson 2008). The quality of the velocity measurements can be assessed using a real-time output called the correlation statistic, which ranges from 0 -100%. Sontek recommends that the minimum correlation statistics be 70%. In the present study, the measured data has been filtered to ensure a minimum correlation statistics of 75% and a SNR of 30 db to ensure the quality of the ADV measurements. The measured data consisted of a time series of the three velocity spatial components, which was subsequently processed in the WinADV software. The software excluded the low-correlation and low signal-to-noise ratio samples. The measurements were typically taken over a period of 5 min for each sample. However, for some locations e.g. close to the inlet jet, an extended sampling time was required. Both the uplooking and downlooking ADVs were previously tested in a known open-channel flow against a rotameter. The depth-averaged velocity measurements from the ADVs agreed well with the rotameter and with each other in the overlapping regions i.e. the maximum deviation and normalized uncertainty were 8% and 5%, respectively.

As seen in Figure 3.2, nine radial sections were defined to cover significant regions of the pond. The sections are concentrated near the inlet jet and opening slot. At each section, measurement grids were

defined at intervals of 100 mm and 10 mm in the radial and vertical directions, respectively. At each section, instantaneous velocity measurements were taken at approximately 60 locations, giving a total of 540 measurement locations. The velocity measurements are presented in the results and discussion section for flow characterization as well as for comparison to the simulation results.
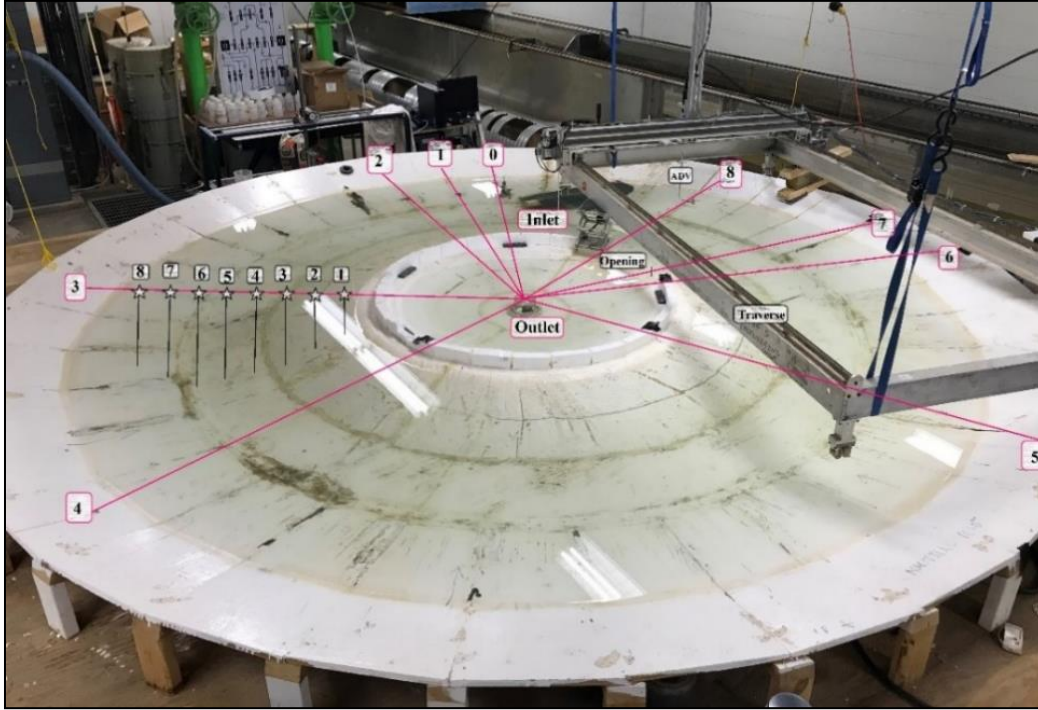
Radial line No.	0	1	2	3	4	5	6	7	8
Angle (degree)	0	15	30	60	90	180	270	285	315

Figure 3.2 Measurement locations at the scale model pond

3.3 Computational Model

The simulation considered a steady, 3D RANS formulation and assumed constant fluid properties. The mathematical model consisted of the transport equations for conservation of mass and momentum, given by Equation [3.1] and [3.2] below,

$$\frac{\partial U_i}{\partial x_i} = 0 \qquad\qquad [3.1]$$

$$U_j\left(\frac{\partial U_i}{\partial x_j}\right) = -\frac{1}{\rho}\frac{\partial P}{\partial x_i} + g_i + \nu\left(\frac{\partial^2 U_i}{\partial x_j \partial x_j}\right) - \frac{\partial}{\partial x_j}\langle u_i u_j \rangle \qquad\qquad [3.2]$$

where U_i, x_i, P, ρ, ν, and g_i are the mean velocity component in the x-direction, spatial coordinate in the x-direction, mean pressure, density, kinematic viscosity, and gravity vector, respectively.

The Reynolds stress tensor $\langle u_i u_j \rangle$, i.e., the correlation of the fluctuating velocity components representing the turbulent transport in the momentum balance, was obtained from an eddy viscosity model closure given by,

$$-\langle u_i u_j \rangle = \nu_t \left(\frac{\partial u_i}{\partial x_j} + \frac{\partial u_j}{\partial x_i} \right) - \frac{2}{3} \delta_{ij} k \qquad \text{[3.3]}$$

where k is the turbulence kinetic energy; ν_t is the eddy viscosity given by the relation $\nu_t = C_\mu \frac{k^2}{\varepsilon}$; and δ_{ij} is the Kronecker delta. The values of k and ε are solved from their own transport equations, i.e.

$$U_j(\frac{\partial k}{\partial x_j}) = \frac{\partial}{\partial x_j}\left((\nu + \frac{\nu_t}{\sigma_k})\frac{\partial k}{\partial x_j}\right) - \langle u_i u_j \rangle \frac{\partial U_i}{\partial x_j} - \varepsilon \qquad \text{[3.4]}$$

$$U_j(\frac{\partial \varepsilon}{\partial x_j}) = \frac{\partial}{\partial x_j}\left((\nu + \frac{\nu_t}{\sigma_\varepsilon})\frac{\partial \varepsilon}{\partial x_j}\right) - C_{1\varepsilon}\frac{\varepsilon}{k}\langle u_i u_j \rangle \frac{\partial U_i}{\partial x_j} - C_{2\varepsilon}\frac{\varepsilon^2}{k} \qquad \text{[3.5]}$$

where ε is the turbulence dissipation rate. The empirical constants in Equations [3.4] and [3.5] are given by: $C_\mu = 0.09$, $\sigma_k = 1$, $\sigma_\varepsilon = 1.3$, $C_{1\varepsilon} = 1.44$, and $C_{2\varepsilon} = 1.92$. In the near-wall region, the turbulence is suppressed and the high Reynolds number version of the $k - \varepsilon$ model is invalid. Instead, a standard wall function was used to patch the turbulent flow to the wall. The equations were numerically discretized and solved using the commercial software package ANSYS Fluent 19.2. The SIMPLE algorithm was used to solve the discrete equations for the mean velocity and pressure fields.

The geometry of the scale-model vortex-type pond was constructed in ANSYS Design Modeler 19.2. For the spatial discretization, an unstructured computational grid was generated in ANSYS Workbench 19.2. The numerical grid was refined near solid walls, e.g. the bed and sidewalls, to better capture the gradients in these regions. The grid dependence of the solution was assessed using three different grid resolutions. The coarsest grid used approximately 1 million control volumes; two finer grids were also considered, a medium grid with 2.2 million control volumes and a fine grid with 4.6 million

control volumes. Each of the grids was generated in an iterative manner until it satisfied the accepted range for the three grid metrics, i.e. aspect ratio, skewness, and smoothness. The profiles of the tangential velocity component at the channel centerline for radial sections 0 and 5 (presented in Figure 3.2) were used to assess the grid dependence. These two locations were selected because each of them is representative of a different region of the pond, i.e. the inlet jet region and the circular channel region.

For boundary conditions, a fully developed velocity profile for turbulent pipe flow corresponding to the desired flow rate, i.e. 1.55 L/s, was provided at the inlet. The turbulence intensity at the inlet was 0.1 and the dissipation rate was set to 0.045 m^2/s^3. A constant pressure boundary condition was specified at the outlet. The pond bed and walls were set as no-slip, smooth wall boundaries. The free surface was modelled as a rigid slip wall, i.e. zero normal velocity and zero normal gradient for the other variables. Based on previous studies of open-channel flow in tight bends by Zeng *et al.* (2008), this is a valid approximation. Zeng *et al.* (2008) found negligible difference between the present boundary condition and use of a deformable free surface.

Figure 3.3 represents a comparison of the tangential velocity profiles for the three different grids. In moving from the coarse grid to the medium grid, the velocity changed on average by approximately 4.5 %. In moving from the medium grid to the fine grid, the tangential velocity changed on average by less than 1 %. Based on this comparison, the medium grid using 2.2 million control volumes was selected for the simulations as a reasonable compromise based on numerical resolution and computational cost. The pond simulation on the medium grid required approximately 8 hours on a standard workstation.
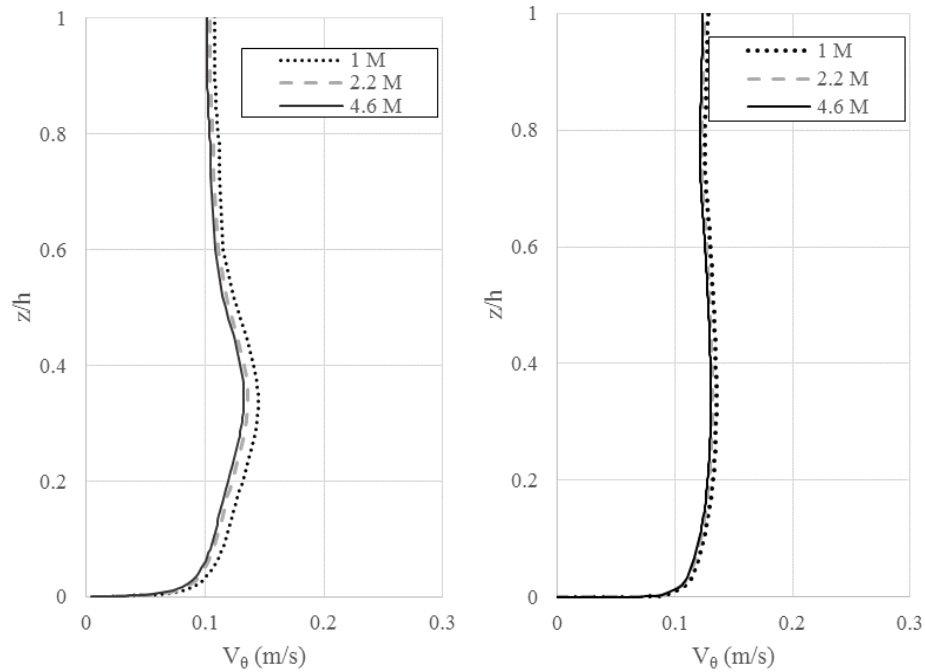
Figure 3.3 Centerline profiles of the tangential velocity component for radial sections (from left to right) 0 and 5 for three different grids

3.4 Results and Discussion

3.4.1 Overall Flow Pattern

The presentation of the simulation results begins with an investigation of the overall flow pattern in the pond. Figure 3.4 uses contours to present the velocity distribution on a plane parallel to the bed at the depth of the center of the inlet pipe, $z/h = 0.36$, as well as on several radial cross-sections perpendicular to the bed, where z is the distance from the pond bed and h is the flow depth at the pond. After a short distance, the jet attaches to the outer wall of the pond. The strength of the inlet jet becomes minimal by the time the inlet flow has traversed less than half-way around the pond, and thereafter the velocity distribution is almost uniform (~ 0.12 m/s) until the opening to the outlet. At the opening, the velocity increases as it enters the berm where the flow spirals down towards the outlet.
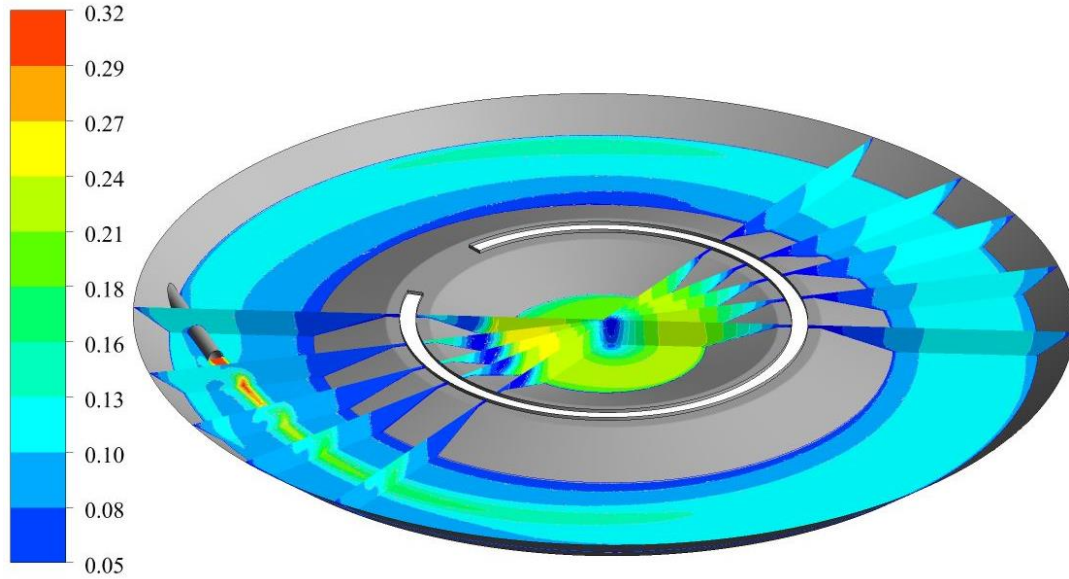
Figure 3.4 Resultant velocity contours (m/s) on a plane parallel to the bed at $z/h = 0.36$ and at specific radial sections

.

a)   b)
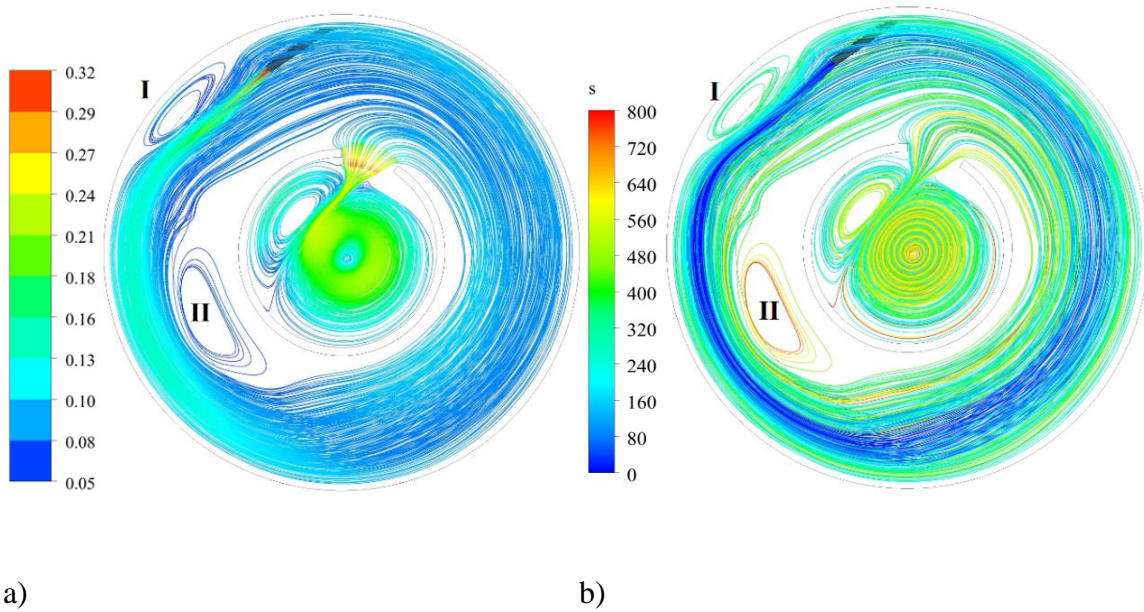
Figure 3.5 Plan view of 3D pathlines with color based on: a) total velocity (m/s), and b) residence time (s)

Figures 3.5a and 3.5b indicate how select water parcels travel within the pond once they are released at the inlet using pathlines. The pathlines are colored in Figure 3.5a and 3.5b based on the velocity magnitude and residence time, respectively. To produce Figures 3.5a and 3.5b, 300 neutral particles were

released at the inlet and tracked throughout the pond. The pathlines were obtained by integrating the velocity field. Three distinct flow regions are observed in the pond: 1) the inlet jet and its subsequent decay; 2) the rotational flow in the circular channel outside the berm, and 3) the flow passing into the outlet within the berm. The jet entrains the surrounding fluid as it spreads downstream, while also moving toward and attaching to the outer wall of the pond. The jet decays relatively quickly, and thereafter the flow becomes approximately uniform within the outer channel. In the circular channel, two strong recirculation zones are formed: (I) the region trapped between the jet and the outer wall, and (II) the region downstream of the jet that is trapped between the outer flow and the inner wall or berm. The characteristics of these two zones, e.g., shape and size, depend on the way the jet is introduced into the pond, i.e., the jet location, and orientation, as well as the berm geometry. From the pathlines in Figure 3.5a, the absolute velocity in these two zones is less than 0.01 m/s, indicating relatively slow recirculating flow. For the outlet region inside the berm, two distinct recirculation regions are observed, one smaller than the other. The color pathlines in Figure 3.5b indicate residence time, which is given by the total integration time for a given particle at that location. The color pathlines in Figure 3.5b indicate that most of the water parcels perform several orbits before exiting through the opening. The time required for a typical particle to travel from the inlet to the exit is approximately 450 s. Some of the particles can be trapped in the pond for a much longer time, e.g., 800 s for recirculation zone II.
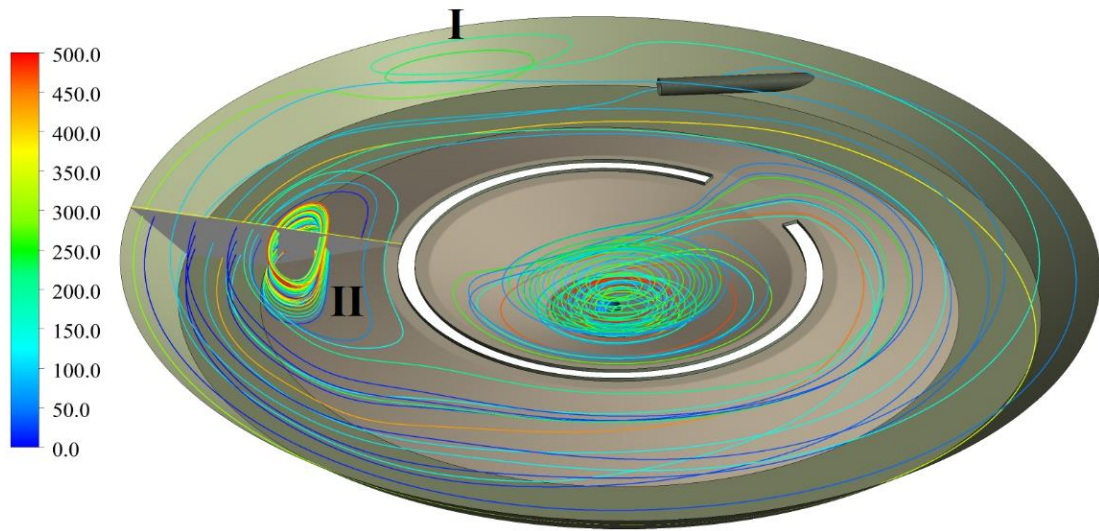
Figure 3.6 3D view of pathlines of water parcels released at a section through recirculation region II with the color based on residence time (s)

It is insightful to further explore the flow in the pond based on particles released at a section midway through the large recirculation zone II. In Figure 3.6, 100 fluid parcels released at a transverse section through recirculation zone II are tracked. The resultant pathlines are colored based on the residence time. Depending on the location of release, the particle paths differ significantly. The particles released near the outer wall are not affected by the recirculation zone and move downstream within the circular channel. Once these fluid parcels reach the vicinity of the inlet pipe, some cross over the pipe and enter recirculation zone I. The others either entrained the incoming jet or continue to proceed around the pond, but typically on a circular path of smaller radius. The fluid parcels released from the inner part of the section are effectively trapped and remain within recirculation zone II for an extended period of time. Careful examination of the trajectory and residence time of the particles in recirculation zone II, indicates that the vortex has an upward spiral motion such that the water parcels exit zone II close to the free surface. This is likely related to a residual effect of the jet on the flow close to the bed. The circulating particles that are not trapped by a recirculation zone eventually approach the inner wall and exit across the berm into the outlet section. Inside the berm, the flow spirals downward until it exits the pond at the outlet. Although there are

54

two recirculation zones within the berm, all of the 100 neutral particles that were released at zone II entered the larger recirculation zone in the outlet region.

Some photographs that document a dye-test performed in the physical model pond are shown in Figure 3.7. It should be noted that the orientation of the photographs is rotated clockwise by approximately 30 degrees compared to the pond image in Figure 3.5. The dye was injected at the inlet for 30 seconds. Although the physical test considered a finite amount of dye, and unlike the theoretical parcels, the dye is diffusive, some insightful comparisons can be drawn between the dye-test and parcel trajectories discussed above. During the first transit of the pond, the dye appears to enter recirculation zone I, and for the most part avoids entering recirculation zone II, as highlighted in the pictures taken at $t = 5$ and 25 s. At times $t = 55$ and 75 s, the pictures show some dye still lingering downstream of recirculation zone I along the outer wall of the pond. The CFD simulations predict that if a particle does not enter recirculation zone II, then it takes approximately 80 s to complete one rotation of the pond. This is consistent with the pictures of the dye slug at times t = 75 and 95 s. Finally, the picture at t = 95 s shows some dye exiting into the outlet after just one circulation of the pond. This is at variance with the CFD results in Figure 3.5b that clearly indicate that most of the particles do not enter the outlet after just one rotation. The reason for the difference in behavior can be attributed to the diffusion of the dye so that it does not indicate the pathlines of individual fluid parcels.
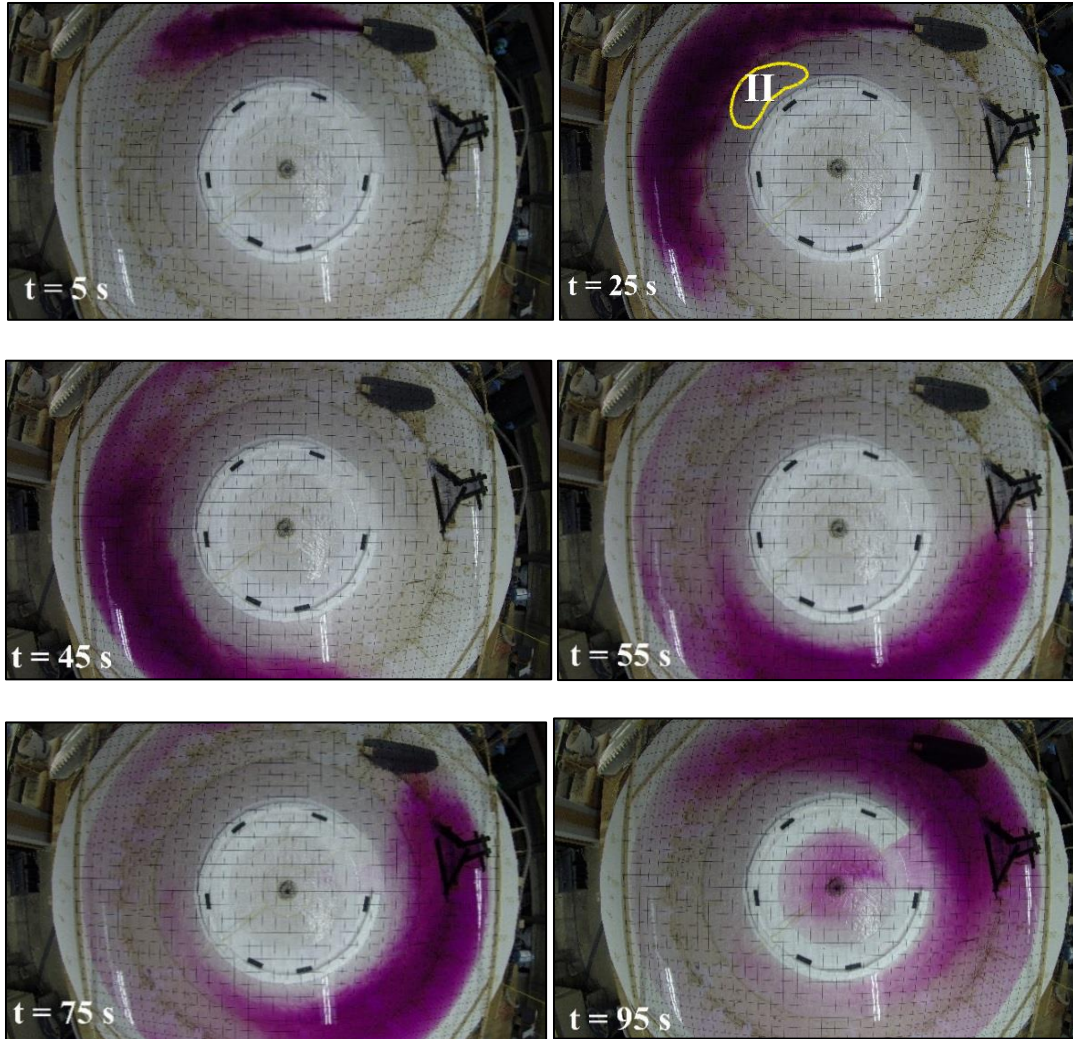
Figure 3.7 Experimental visualization using dye injection at different times

.

In a stormwater retention pond, it is desirable to dissipate the turbulence of the inlet jet as quickly as possible. A high level of turbulence is problematic since it can prevent the sediment from settling out, and also resuspend sediment that has already settled. The current pond model uses a circular turbulent offset inlet jet with its center located at $z/h = 0.36$. The turbulence level can be quantified by the turbulence intensity, which is the ratio of the streamwise velocity fluctuation over the magnitude of the local mean streamwise velocity, i.e.,

$$TI = \frac{u'}{U} \tag{3.6}$$

Figure 3.8 shows contours of the turbulence intensity at two different depths, $z/h = 0.36$ and 0.95, corresponding to the height of the jet and close to the top of the pond, respectively. The turbulence intensity (TI) is less than 10% throughout the pond except for two regions: 1) immediately downstream of the inlet jet, and 2) within the berm. In general, the turbulence intensity decreases as the flow circulates through the pond; initially it is 12% downstream of the inlet jet and after one rotation drops to approximately 1%. The highest turbulence intensity in the pond, i.e. $TI = 16\%$, occurs in a localized area near the outlet. In regions of relatively high mean shear, the turbulence level is also high due to the local production of turbulence kinetic energy. Both the region downstream of the jet and the outlet are characterised by stronger velocity gradients. Approximately 85% of the domain area at the inlet level ($z/h = 0.36$) has a turbulence intensity of 5% or less. Hence, over much of the pond the turbulence level is relatively low. This is consistent with the predictions (not shown) for the turbulent viscosity ratio (v_t/v), which ranges between 2 and 70 in the pond.
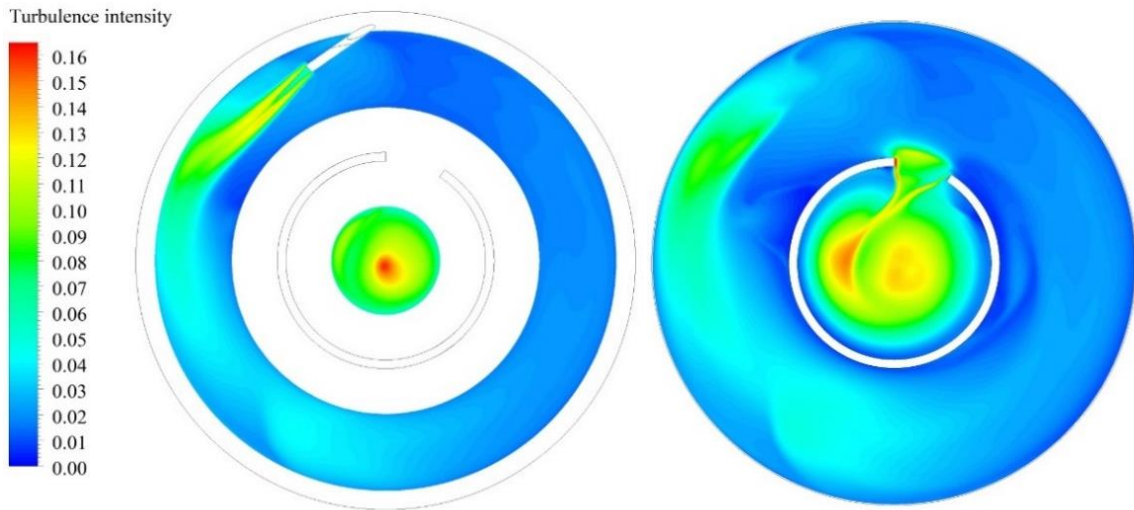
Figure 3.8 Turbulence intensity (TI) contours at z/h = 0.36 and 0.95

Figure 3.9 presents contours of the magnitude of the shear stress on the bottom wall of the pond. The bed shear stress on the bottom wall is relatively uniform and equal to approximately $\tau_b = 0.22$ Pa throughout the pond except for the regions downstream of the jet. Downstream of the jet, the bed shear stress reaches as high as $\tau_b = 0.45$ Pa. Using the Shields curve, the critical particle diameter (d_{cr}) for

initiating particle motion in the model pond was calculated as shown in Table 3.1. Here u_τ, Re_τ, and S are the friction velocity, Reynolds number based on friction velocity, and specific gravity, respectively. Based on this estimate, in most of the pond, particles with a diameter larger than 0.15 mm will not be resuspended by the flow. In the regions of high shear, the critical particle diameter increases to 0.41 mm.
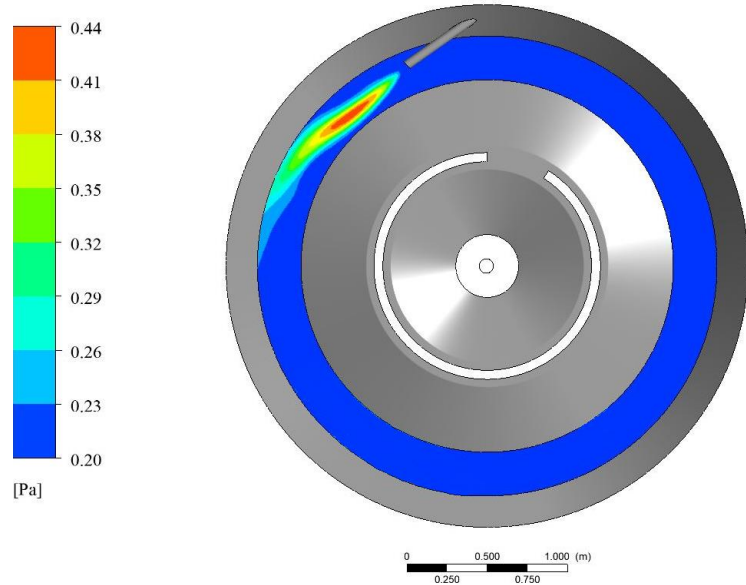
Figure 3.9 Contours of the magnitude of the shear stress on the bottom wall of the pond (Pa)

Table 3.1 Calculation of Shields parameter and the threshold particle size

Bed shear stress (Pa)	u_τ (m/s)	Re_τ	S	d_{cr} (mm)
0.45	0.021	8.69	2.65	0.41
0.22	0.015	2.32	2.65	0.15

Curved channels are typically characterized by cross-stream secondary currents, i.e. a recirculation pattern in which the fluid moves toward the inner wall along the bed and then changes direction to move toward the outer wall along the free surface. Periodically dredging the settled sediment is a necessary and expensive part of pond maintenance. It is more cost efficient if the pond design causes the sediment to settle closer to the outer walls where machinery access is easier. Due to the inward motion of the secondary flow near the bed, the sediment can be transported away from the outer walls of the pond. Therefore, it is of interest to investigate the presence and strength of the secondary flow in the pond's circular channel.

In Figure 3.10, the velocity field at nine different cross-sections is presented. In-plane velocity vectors based on measurements of the radial and vertical velocity components are plotted on the left side; the right side shows contours of the total velocity based on the CFD simulations. It should be noted that the viewpoint is looking downstream, therefore the right side represents the outer bank and the left side represents the inner bank or berm of the channel. The inlet jet flow is shown by the circular patterns observed in the streamwise velocity contours shown in the first three sections, i.e., 0, 1, and 2. For the same sections, the experimental velocity field shows a strong rotational pattern in the vicinity of the jet. The transverse circular pattern spreads as moving downstream and by the section no.3, the pattern is fully expanded in the outer half of the channel space. At the inner side of section no. 3, zero velocities confirm the presence of the dead zone in that region (both CFD and experiment). Further downstream, the flow in the curved channel is developing uniformly. In section no. 4, the experiment shows that the velocity vectors begin to accelerate inwards at the bottom. The typical secondary motion seen in a curved open channel is not observed here: the flow is not moving outward near the surface since the presence of the opening slot creates an inward motion near the free surface. At cross section no. 5, the relative secondary velocity (transverse velocity component over the streamwise velocity) is approximately 20%. At section no. 6, the CFD prediction shows no strong movement inward except for the opening area. In the experiment, the vectors in the inner region from the bottom to the free surface move towards the opening. At sections no. 7 and 8, this inward motion at free surface towards the opening is maximal and its influence extends throughout the depth. In general, as the main flow circulates in the channel around the vertical axis of the pond, a secondary motion, with maximum velocity of 0.6 m/s, moves inward near the bed towards the berm. At section no. 8, the experiment shows the impact of inlet beginning to emerge in the outer part of the section as as a circulating pattern.

No. 0

No. 1

No. 2

No. 3

No. 4

No. 5

No. 6

No. 7

No. 8

0   0.12   0.24   0.33
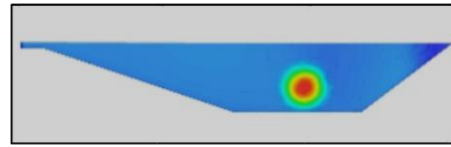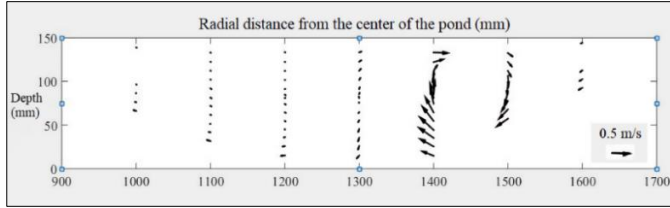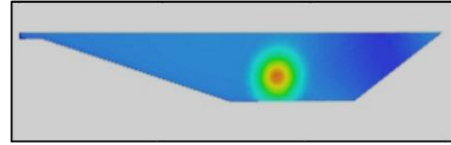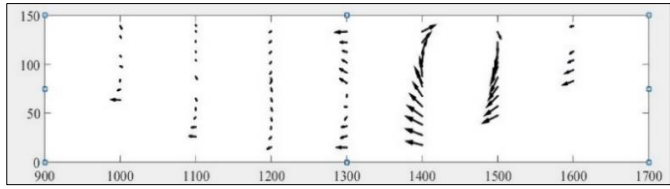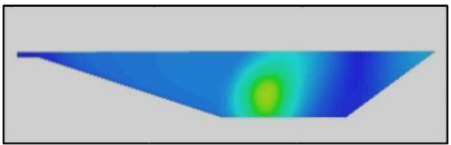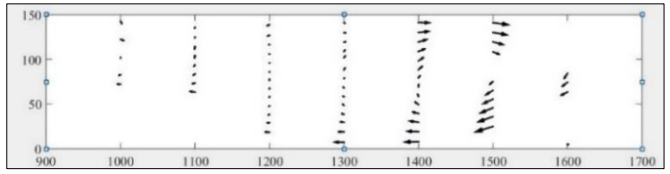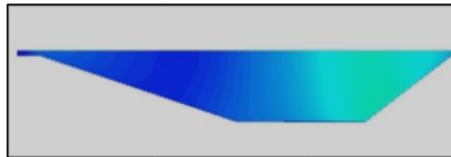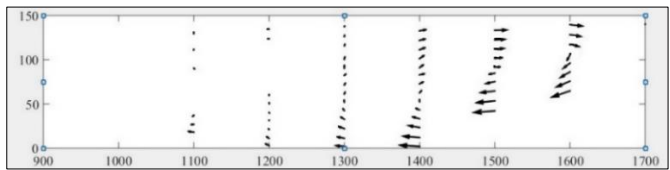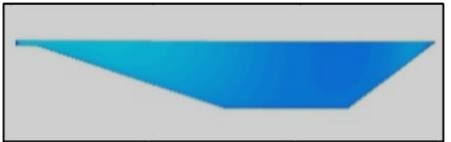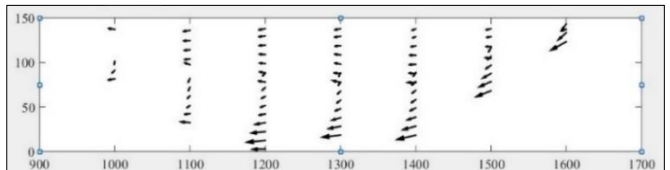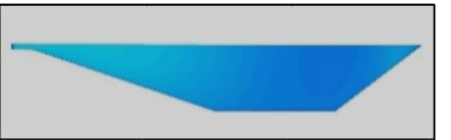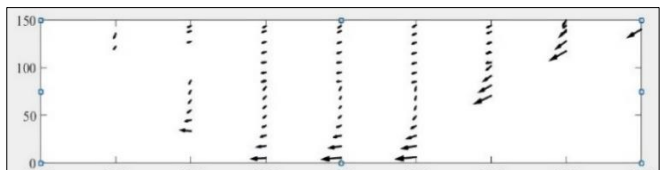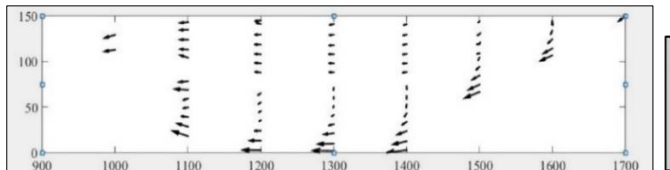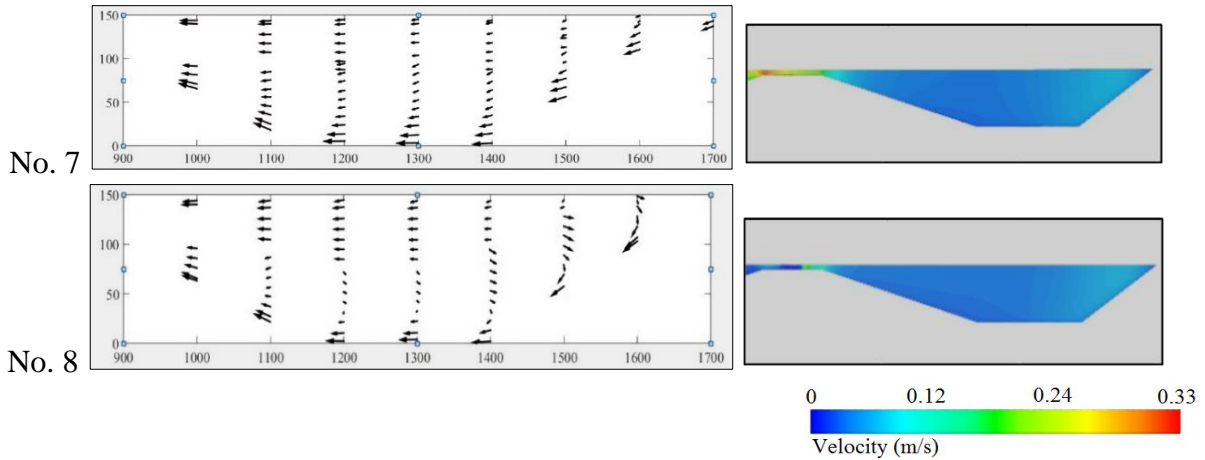
Velocity (m/s)

Figure 3.10 Velocity vectors (experimental) and total velocity contours (simulation) in radial cross-sections in the circular channel of the pond (sections: 0-8)

3.4.2 Selected Velocity Fields

Figure 3.11 shows the streamwise velocity (vertical and transverse profiles) at different radii and depths obtained from the CFD simulations at cross section no. 5 compared to the measured values. This section, i.e. no. 5, is sufficiently far away from the jet and not yet affected by the opening to the outlet. In general, the predictions are in close agreement with the measured values. A larger streamwise velocity can be observed at the outer radius than the inner. Transverse velocity profiles are uniform and smooth, but skewed towards the outer wall.

The jet behavior is a significant factor in stormwater retention ponds. The current jet is influenced by two sloped side walls and the pond bottom. Additionally, due to the pond geometry curvature, after the jet is introduced into the pond, it moves toward the outer wall after a short distance. There is not sufficient space for the jet to fully develop.

(a)

(b)
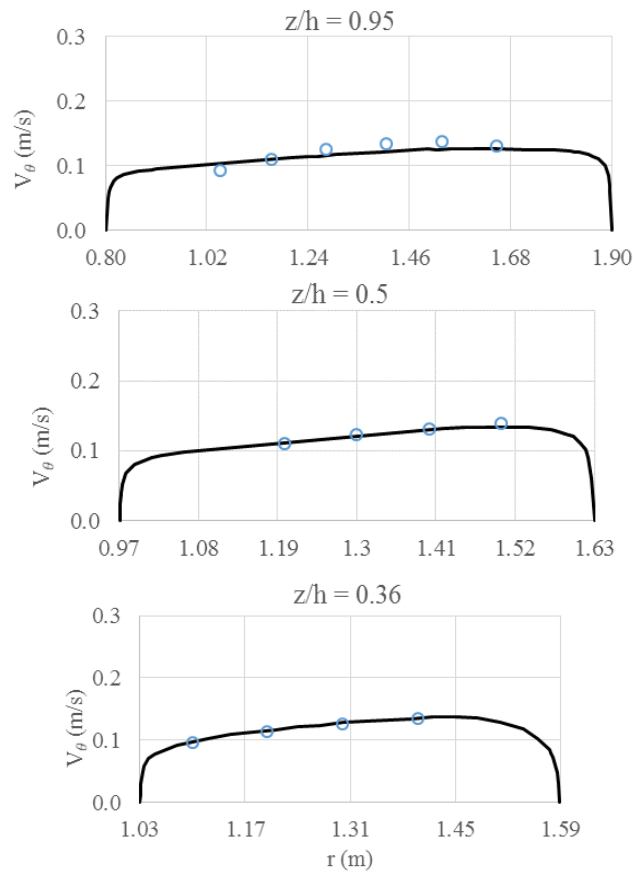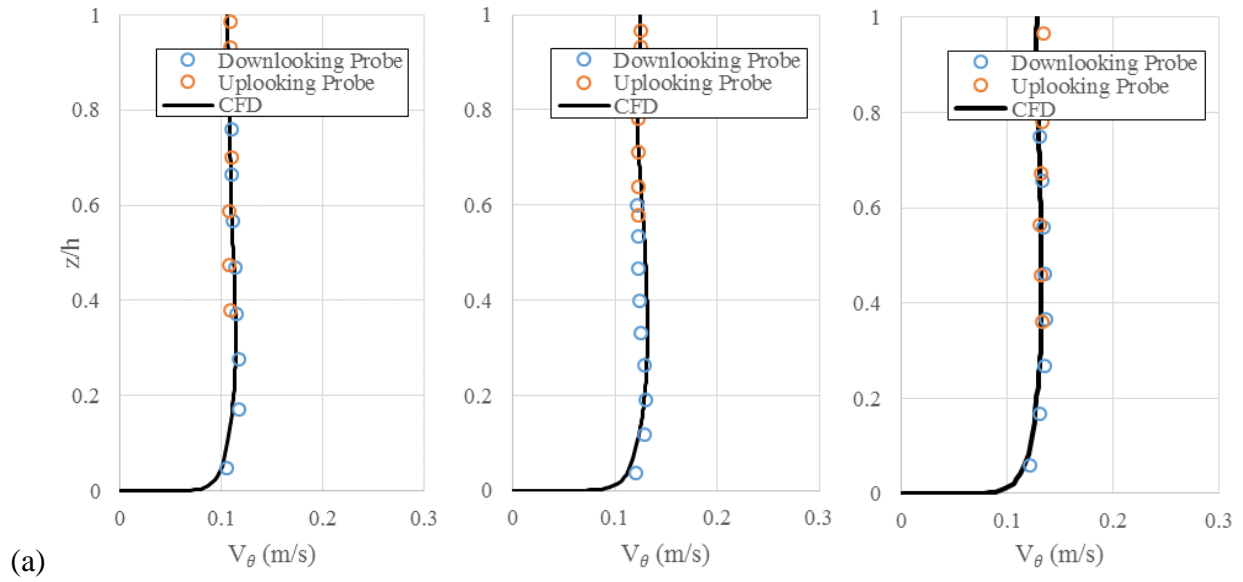
Figure 3.11 Predictions of streamwise (a) vertical and (b) transverse velocity profiles at cross section no. 5 against measurements
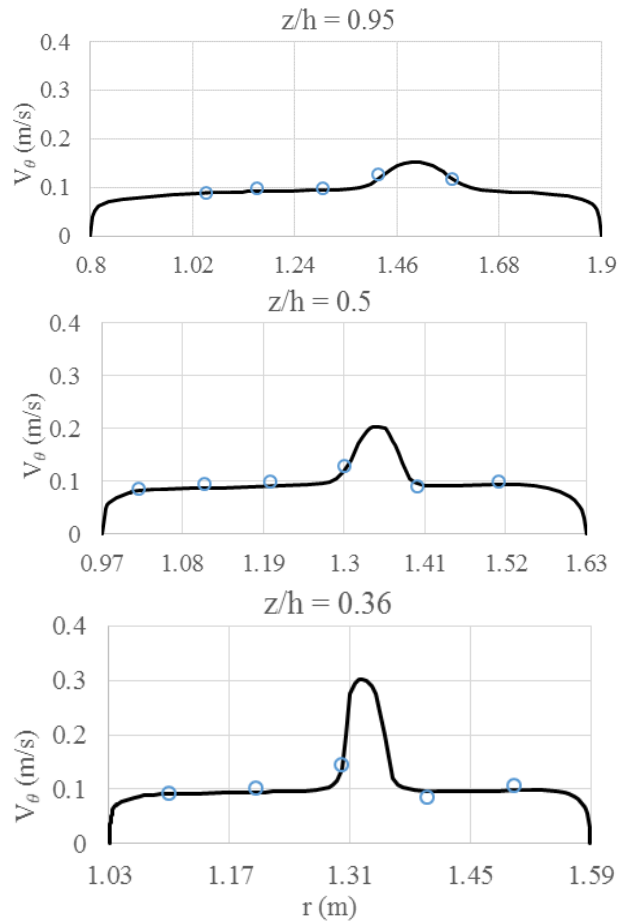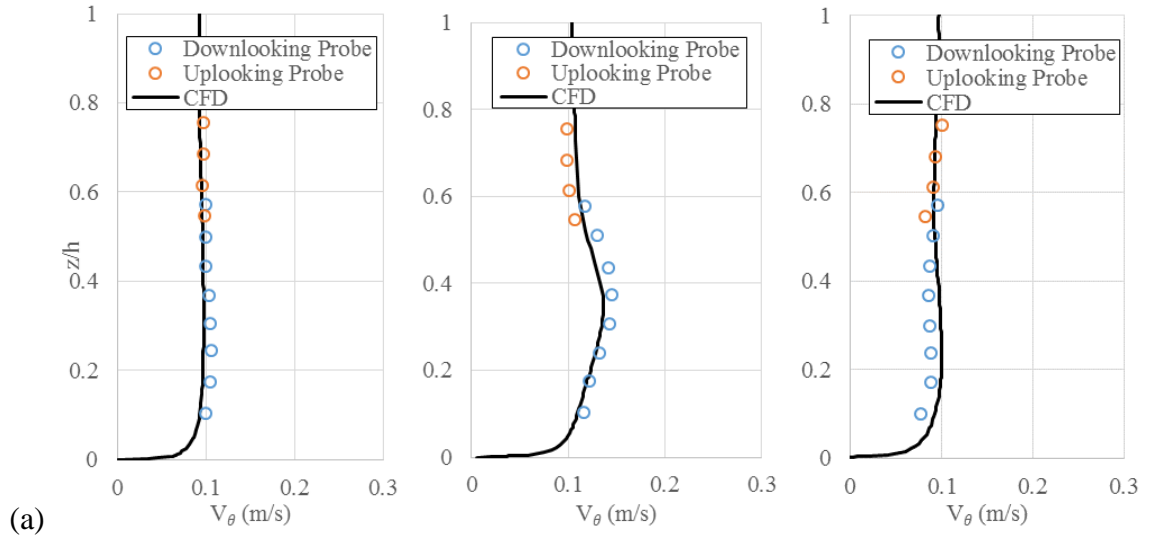
Figure 3.12 Jet characterization via (a) vertical and (b) transverse velocity profiles at cross section no. 0

Figure 3.12 presents the vertical and transverse velocity profiles for section no. 0, the closest section to the location where the jet is introduced into the pond, at different radii, i.e. 1.2, 1.3, and 1.4 m, and depths, i.e. z/h = 0.36, 0.5, and 0.95, compared to measured data. Note that these radial sections are not perpendicular to the jet since the jet is introduced to the pond at an angle of 30°. At this section, the jet spread is limited to the region between radii of r = 1.3 and 1.4 m. The elevated velocity of the jet is evident in the section at r = 1.3 m; it appears as blunt peak in the velocity profile near the pond bottom. The peak in the transverse velocity profile at z/h = 0.36 reduces from 0.3 m/s to 0.14 m/s at z/h = 0.95. The transverse velocity profiles at different depths indicate that as jet flow approaches the free surface of the pond, the velocity peak moves towards the outer wall. This feature is attributed to the pathline curvature.

Figure 3.13 compares the distribution of streamwise velocity at the center of the channel at section no. 5 to the canonical logarithmic law of the wall. The CFD predictions match the measured values, and deviate from the log-law plot in the wake region. This shows that the influence of the jet persists in this region.
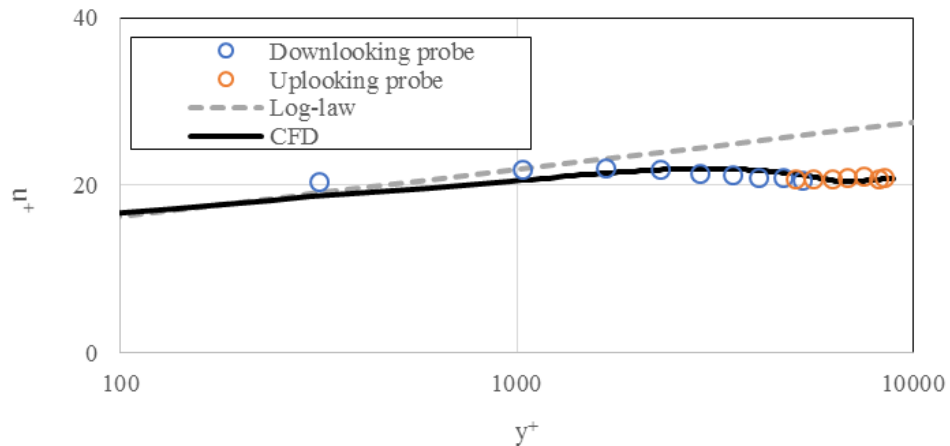
Figure 3.13 Comparison of the CFD predictions and measurements of the velocity profile at r = 1.3 m on section no. 5 to the logarithmic law of the wall formulation for a turbulent wall-bounded flow

Figure 3.14 represents the Reynolds shear stress, turbulent kinetic energy (TKE) normalized by the CFD shear velocity, and eddy viscosity at section no. 5. The normalized Reynolds shear stress increases

from a value of zero at the bed up to a maximum value of $\frac{u'v'}{u^2_\tau} = 0.5$ at z/h = 0.24 as predicted by the CFD

model. Thereafter, it decreases from the maximum value and reaches $\frac{u'v'}{u^2_\tau} = 0.18$ at the water surface. The

CFD predicted Reynolds shear stress compares most favorably with the measured data near the free surface.

The CFD turbulent kinetic energy is in good agreement with the data except for a small region near the wall

where the data shows higher turbulent kinetic energy compared to the model. The eddy viscosity follows

the same pattern as the Reynolds shear stress. The peak value normalized by the molecular value near the

wall is approximately 100.
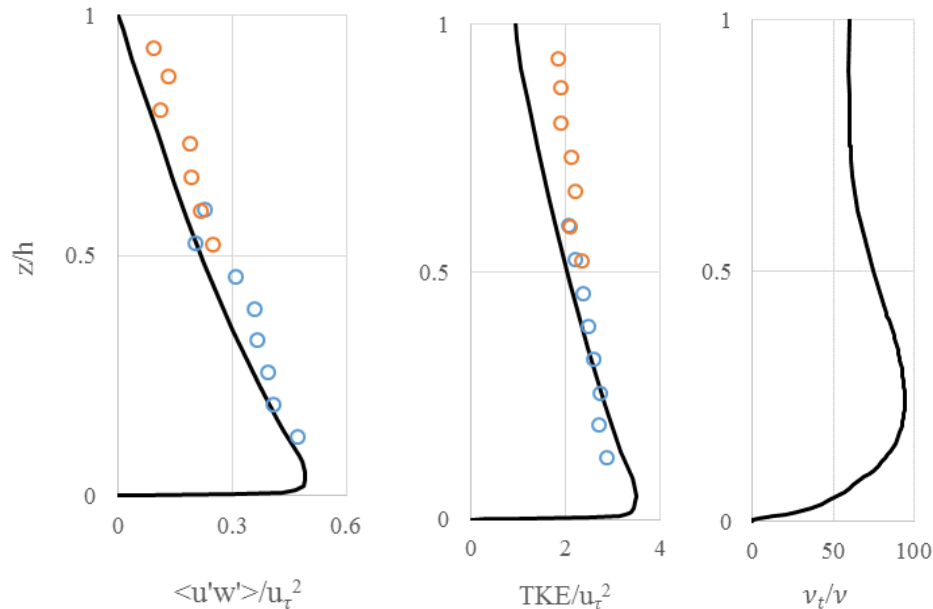
Figure 3.14 Distribution of Reynolds shear stress, turbulent kinetic energy, and eddy viscosity at the center of section no. 5

3.5 Conclusion

In this study, the flow pattern in a 1:13.3 scale-model of a vortex-type stormwater retention pond

was investigated using both experimental and numerical methods. The predictions of the CFD model were

compared to measurements of the mean velocity, Reynolds shear stress, and turbulent kinetic energy. Three

distinct flow regions of the pond were explored: the inlet jet and its subsequent decay; the rotational flow

in the circular channel outside the berm; and the flow passing into the outlet within the berm.

Fluid parcels were released from different locations within the pond and the pathlines were used to reveal the overall flow patterns. The CFD predictions revealed that a relatively large dead zone forms downstream of the jet clinging to the berm, with a second recirculation zone located further downstream along the inner wall of the channel. The extent of the secondary flow pattern was also studied and found to be disrupted by the flow into the outlet. In the fully developed flow region, the predominant transverse flow was inward along the bottom of the pond. The exit flow inside the berm was characterized by two recirculation zones in opposite directions. The turbulence intensity did not exceed TI = 12 % in the main channel. Using the Shields parameter based on the predicted wall shear stress on the bottom of the channel, it was determined that only particles larger than 0.15 mm in diameter would be susceptible to potential resuspension by the flow. Overall, comparison of the predicted velocity and turbulence kinetic energy profiles to the measurements indicated close agreement, demonstrating the ability of the CFD model to capture the flow patterns created by the novel pond design.

This study identified the potential of a CFD model as an engineering tool in the design of storm water retention ponds. The model showed to be a reliable tool to investigate the flow pattern before the pond is built and to detect problematic regions in the pond which is useful in suggesting design improvements.

Chapter Four

4. APPLICATION OF THE TWO-FLUID MODEL TO PREDICTION OF SEDIMENT TRANSPORT IN TURBULENT OPEN CHANNEL FLOW

A similar version of this chapter has been published as:

- Ahadi, M., Bergstrom, D., & Mazurek, K.A. (2019) Application of the Two-Fluid Model to Prediction of Sediment Transport in Turbulent Open Channel Flow, Physics and Chemistry of the Earth, Parts A/B/C, in press.

In addition, a part of this chapter was presented at the following conference:

- Ahadi, M., Bergstrom, D., & Mazurek, K.A. (2018) Application of the Two-Fluid Model to Prediction of Sediment Transport in Turbulent Open Channel Flow", 26th Annual Conference of the Computational Fluid Dynamics Society of Canada, 10–12 June 2018 | Winnipeg, Canada |

Preamble

Another fundamental step towards the higher fidelity simulation of the new vortex-type pond using the two-fluid methodology is to explore the TFM in a simpler problem. The TFM methology is a progressing method especially in the sediment transport community. There are elements to be further explored before applying the model to the complex case of stormwater retention pond e.g. effect of particles on the turbulence field, and particle-particle and particle-wall boundary conditions. In this chapter, a complete set of two-fluid equations with its closure models are explored in a fully developed open channel flow with available measurements of liquid velocity and particle concentration.

Abstract

The TFM formulation was used to predict the liquid and sediment transport in an open channel flow for dilute concentrations. A low-Reynolds-number $k-\varepsilon$ model was used to represent the turbulence in the liquid phase; it included the effect of the sediment particles on the turbulence field. The particle-wall interactions were implemented using the boundary condition of Johnson and Jackson (1987), which resulted in a finite value for the sediment velocity at the bottom wall. The values of the specularity coefficient and

coefficient of restitution for the particle-wall collisions were specified. Overall, the TFM prediction for the liquid velocity, sediment concentration, and turbulent statistics agreed well with two different experimental test cases by Lyn (1987). A key parameter for determining the sediment phase transport was the granular temperature, the level of which was set by the value of the specularity coefficient at the wall. In the context of the TFM, the presence of the sediment particles was found to enhance the wall shear stress of the liquid phase.

4.1 Introduction

In open channel flows, the transport of sediment has been traditionally described using empirical or semi-empirical formulations. For example, the commonly-used formula by Rouse (1937) was developed to predict the suspended sediment distribution based on a balance between the gravitational settling of particles and the diffusive flux of suspended sediment due to turbulence, but has and relies on empirical coefficients. Rouse's formula is only applicable for low sediment concentrations and, even then, limitations exist (e.g., near the bed where the concentration increases). An improvement to classical sediment transport models would be to develop a model able to appropriately capture the main features of sediment-laden flows with less empiricism. A model that suitably captures the physical mechanisms of sediment transport is thus required. Two-phase flow theory based on fundamental conservation principles supports this endeavor by bringing more of the physics of sediment transport into the modeling procedure.

Drew (1983) was the first to employ turbulence time-averaged mass and momentum equations for both the water and sediment phases to analyze sediment transport in open channels. The TFM was developed based on the fundamental assumption that both the water and sediment particles carried by water can be regarded as continuous media, governed by the partial differential equations of continuum mechanics (Drew 1983). The laws of conservation of mass and momentum are satisfied by each phase individually and provide a general modeling framework that potentially accounts for all the physical processes involved in sediment transport, such as liquid-particle and particle-particle interactions and

turbulence modulation. The phasic velocities and concentrations are obtained from solving the mass and momentum equations for each phase, as well as a turbulence closure for the liquid phase and the granular temperature equation and the required constitutive relations for the solid phase.

The coupling between phases can occur through the mass and momentum transfer terms in the equations. With no addition or removal of mass, momentum transfer due to drag is the only transfer mechanism between phases. For the sediment phase, when the collisional interactions play an important role in the motion of particles, the particle stresses can be computed by granular kinetic theory using the so-called granular temperature as a measure of the particle velocity fluctuations. Lun *et al.* (1983) derived the constitutive relations for the solid-phase stress based on kinetic theory allowing for the inelastic nature of particle collisions. For more dense sediment flows, particle-particle interactions in the higher concentration region close to the bed are different from the interactions in the low concentration region (1983). In the high concentration region, part of the particle stress is due to continuing contact among particles, rather than collisions.

Hsu *et al.* (2003) was the first to apply the kinetic theory based TFM to sediment transport problems in order to predict the suspended sediment concentration profile in a fully developed, free surface flow in a rectangular channel. The authors modeled the transport of dilute sediment transport in equilibrium (*i.e.,* erosion of the bed and deposition onto the bed were equal) and showed that the TFM predictions give a closer fit to the experimental data in comparison to Rouse's (1937) formula. No comparison of turbulence statistics with measurements was provided. In a similar study, Jha and Bombardelli (2009) also showed that the TFM is a compelling alternative for representing the physics of sediment transport in open channel flows. The authors focused on exploring the effect of different turbulence models and presented comparisons of turbulence kinetic energy and Reynolds shear stress for the model against measured data. Most of the subsequent studies of sediment transport in open channel flows shifted towards developing an

expression for relative velocity between the two phases (usually in terms of characteristics of the particles) to avoid solving the momentum equation for the solid phase (*e.g.*, Zhong et al. 2011 and Liang et al. 2017).

When the RANS equations are used in a wall bounded flow, a near bed treatment is required. A common empirical bed boundary condition was used in most previous studies; the sediment concentration at the first computational cell from the bed was found by interpolating the experimental concentration data [*e.g.,* 4,5,6,7]. Furthermore, in those studies, the viscous and buffer sublayers were avoided by applying the logarithmic law of the wall above the bed boundary. As an alternate approach to specifying the suspended sediment concentration at the bed, the Johnson and Jackson (1987) boundary condition can be used to specify the value of shear stress and granular temperature at the wall. This wall boundary condition assumes that particles can both collide with and slide on the wall.

Two key parameters used in the Johnson and Jackson (1987) wall boundary condition are the specularity and wall restitution coefficients. The specularity coefficient defines the amount of particle slip at the wall, depends on the wall roughness, and ranges from a value of zero for a smooth wall with perfectly specular collisions to a value of unity for a very rough wall with perfectly diffuse collisions (Li et al. 2010). The specularity coefficient depends on both the flow conditions and the wall properties. The wall restitution coefficient describes the amount of dissipation of granular energy at the wall due to inelastic collisions and ranges from zero to unity. The larger the value of the wall restitution coefficient, the smaller the dissipation of granular energy at the wall (Li et al. 2010).

In this paper, a kinetic-theory-based TFM was implemented with a low-Reynolds number formulation to predict the suspended sediment transport in an open channel flow in a rectangular channel from the free surface of the flow to the bed. As such, this is one of the first studies to implement a complete TFM set of equations with a low Reynolds number formulation for predicting of sediment transport in an open channel flow (see Table 4.1). Instead of the empirical specification of concentration for the boundary condition, the Johnson-Jackson boundary condition at the bed is tested. One of the outcomes of this

approach is to demonstrate the role of the specularity and wall restitution coefficients in determining the performance of the model in terms of velocity of both phases and sediment concentration.

Table 4.1 Numerical simulations of sediment transport using the TFM in open channel flow

Authors	Year	Complete TFM	Turbulence	Wall treatment	Validation against measurements
Drew	1983	No	Mixing length	-	Mixture velocity and concentration
Hsu *et al.*	2003	Yes	$k-\varepsilon$	Wall function (log-law displaced by roughness)	Liquid velocity and concentration
Jha and Bombardelli	2009	Yes	$k-\varepsilon$, $k-\omega$ RSM, and ASM	Wall function (standard log-law)	Liquid velocity, particle velocity, concentration, TKE, and Reynolds shear stress
Zhong *et al.*	2011	No	$k-\varepsilon$	Wall function (standard log-law)	Concentration
Liang *et al.*	2017	No	$k-\varepsilon$ for liquid phase and ASM for particle phase	Wall function (standard log-law)	Particle velocity, concentration, and TKE

For validation purposes, the experimental measurements of Lyn (1987), which include the liquid velocity, sediment concentration, turbulence kinetic energy, and Reynolds shear stress profiles, were used for two different test cases for which the channel bed was in equilibrium. Both test cases can be considered dilute since the maximum sediment concentrations were less than 2% (Torquato 1995). Therefore, the TFM formulation adopted does not include the effect of frictional contact between particles in the solids phase stress tensor.

4.2 Model equations

This section provides a summary of the transport equations used in the TFM for steady, constant density, two-dimensional flow. In the notation adopted, the subscript s is used to denote the sediment phase, while l is used to denote the liquid phase. The continuity equation for each phase is as follows:

$$\frac{\partial}{\partial x}(\alpha_l u_l) + \frac{\partial}{\partial y}(\alpha_l v_l) = 0 \qquad [4.1a]$$

$$\frac{\partial}{\partial x}(\alpha_s u_s) + \frac{\partial}{\partial y}(\alpha_s v_s) = 0 \qquad [4.1b]$$

where α_l, u_l and v_l are the volume fraction, the x-component velocity, and the y-component velocity for the liquid phase, respectively, and α_s, u_s and v_s are the corresponding variables for the sediment phase. The solution of Equation 1 for the sediment phase, along with the condition that the volume fractions sum to one, allows the volume fraction of each phase to be determined.

The momentum balances for the liquid and sediment phases are as follows:

$$\rho_l \frac{\partial}{\partial x}(\alpha_l u_l u_l) + \rho_l \frac{\partial}{\partial y}(\alpha_l u_l v_l) = -\alpha_l \frac{\partial P_l}{\partial x} + \alpha_l \left(\frac{\partial \tau_{xx,l}}{\partial x} + \frac{\partial \tau_{xy,l}}{\partial y}\right) + \alpha_l \rho_l g_x + R_{x,ls} \qquad [4.2a]$$

$$\rho_l \frac{\partial}{\partial y}(\alpha_l v_l v_l) + \rho_l \frac{\partial}{\partial x}(\alpha_l u_l v_l) = -\alpha_l \frac{\partial P_l}{\partial y} + \alpha_l \left(\frac{\partial \tau_{xy,l}}{\partial x} + \frac{\partial \tau_{yy,l}}{\partial y}\right) + \alpha_l \rho_l g_y + R_{y,ls}$$

$$[4.2b]$$

$$\rho_s \frac{\partial}{\partial x}(\alpha_s u_s u_s) + \rho_s \frac{\partial}{\partial y}(\alpha_s u_s v_s) = -\alpha_s \frac{\partial (P_s + P_l)}{\partial x} + \alpha_s \left(\frac{\partial \tau_{xx,s}}{\partial x} + \frac{\partial \tau_{xy,s}}{\partial y}\right) + \alpha_s \rho_s g_x - R_{x,ls}$$

$$[4.3a]$$

$$\rho_s \frac{\partial}{\partial y}(\alpha_s v_s v_s) + \rho_s \frac{\partial}{\partial x}(\alpha_s u_s v_s) = -\alpha_s \frac{\partial (P_s + P_l)}{\partial y} + \alpha_s \left(\frac{\partial \tau_{xy,s}}{\partial x} + \frac{\partial \tau_{yy,s}}{\partial y}\right) + \alpha_s \rho_s g_y - R_{y,ls}$$

$$[4.3b]$$

where P_l and P_s are the liquid and sediment pressure, and g_x and g_y are the gravity components in the x- and y- directions. $R_{x,ls}$ and $R_{y,ls}$ are components of the interaction forces between the liquid and sediment phases which are discussed later.

The stress tensor components for the liquid phase are modeled as follows:

$$\tau_{xx,l} = 2\mu_l \left(\frac{\partial u_l}{\partial x}\right) \tag{4.4a}$$

$$\tau_{yy,l} = 2\mu_l \left(\frac{\partial u_l}{\partial y}\right) \tag{4.4b}$$

$$\tau_{xy,l} = \mu_l \left(\frac{\partial u_l}{\partial y} + \frac{\partial v_l}{\partial x}\right) \tag{4.4c}$$

where μ_l is the liquid phase shear viscosity. The corresponding stresses for the sediment phase are given by:

$$\tau_{xx,s} = 2\mu_s \left(\frac{\partial u_s}{\partial x}\right) + \left(\lambda_s - \frac{2}{3}\mu_s\right)\left(\frac{\partial u_s}{\partial x} + \frac{\partial v_s}{\partial y}\right) \tag{4.5d}$$

$$\tau_{yy,s} = 2\mu_s \left(\frac{\partial v_s}{\partial y}\right) + \left(\lambda_s - \frac{2}{3}\mu_s\right)\left(\frac{\partial u_s}{\partial y} + \frac{\partial v_s}{\partial x}\right) \tag{4.5e}$$

$$\tau_{xy,s} = \mu_s \left(\frac{\partial u_s}{\partial y} + \frac{\partial v_s}{\partial x}\right) \tag{4.5f}$$

where μ_s and λ_s are the shear and bulk viscosity for the sediment phase. The solid shear and bulk viscosities for the sediment phase arise from the momentum exchange due to collisions. For example, the shear viscosity for the sediment phase is given by

$$\mu_s = \mu_{s,col} + \mu_{s,kin} \tag{4.6}$$

where $\mu_{s,col}$ and $\mu_{s,kin}$ are collisional and kinetic components of the sediment shear viscosity, respectively. For the models used for calculation of μ_s and λ_s in this study, the reader is referred to Table A.1 in the Appendix. Since the flow is considered to be dilute, no frictional component was considered in Equation [4.6].

Specification of the interaction forces is required to close Equations [4.2a], [4.2b], [4.3a], and [4.3b]. In general, this force depends on the friction, pressure, cohesion and other effects. The interaction force can be related to the slip velocity as follows,

$$R_{x,ls} = K_{x,ls}(u_l - u_s) \qquad \qquad [4.7a]$$

$$R_{y,ls} = K_{y,ls}(v_l - v_s) \qquad \qquad [4.7b]$$

where $K_{x,ls}$ and $K_{y,ls}$ are the interphase momentum exchange coefficients in x- and y-directions, which in this case, are modeled based on the particle relaxation time, particle diameter, and drag force. For granular flows (liquid-solid), the liquid-solid exchange coefficients are given by,

$$K_{x,ls} = \frac{3}{4} C_{Dx} \frac{\alpha_s \alpha_l \rho_l |u_s - u_l|}{d} \alpha_l^{-2.65} \qquad \qquad [4.8a]$$

$$K_{y,ls} = \frac{3}{4} C_{Dy} \frac{\alpha_s \alpha_l \rho_l |v_s - v_l|}{d} \alpha_l^{-2.65} \qquad \qquad [4.8b]$$

where d is the particle diameter. In the experiments to be modelled, the sediment particles had a distribution of sizes, although in the model the distribution was considered uniform. Here d is taken to be the D_{50} value of the particle distribution where D_{50} is the sediment grain size for which 50% of the particles are smaller than that size. The drag model of Wen and Yu (1966) (Equation 4.9) is appropriate for dilute systems and therefore used in the present study. For example, in the x-component, the drag coefficient is as follows:

$$C_{D_x} = \frac{24}{\alpha_l Re_s}[1 + 0.15(\alpha_l Re_s)^{0.687}]$$

[4.9]

$$Re_s = \frac{\rho_l d |u_s - u_l|}{\mu_l}$$

[4.10]

where Re_s is the sediment particle Reynolds number. The drag coefficient in the *y*-component is defined in a similar way.

For granular flows, the solid-phase stresses are obtained based on an analogy between the random particle motion arising from particle-particle collisions and the thermal motion of molecules in a gas. The resultant model formulation based on kinetic theory also considers the inelasticity of the granular phase. Like the case of a gas, the intensity of the particle velocity fluctuations determines the stresses, viscosity, and pressure of the solid phase. The granular temperature (Θ_s) is proportional to the kinetic energy of the fluctuating particle motion. A transport equation derived from kinetic theory is used to solve for the granular temperature given by,

$$\frac{2}{3}\left[\frac{\partial}{\partial x}(\alpha_s \rho_s u_s \Theta_s) + \frac{\partial}{\partial y}(\alpha_s \rho_s v_s \Theta_s)\right] = \mathcal{P}_s + \mathcal{D}_s - \gamma_{\Theta_s} + \emptyset_{ls}$$

[4.11]

where $\mathcal{P}_s$ is the generation of granular energy by the sediment stress tensor and $\mathcal{D}_s$ is the diffusion of granular energy. The collisional dissipation of energy, γ_{Θ_s}, is due to inelastic particle-particle interactions, and $\emptyset_{ls}$ is the so-called energy exchange (turbulence modulation) between the fluctuating liquid and solid phases. Each of these terms are presented in Table A.2 in the Appendix.

The fluctuating motion of the liquid and the sediment phase are coupled. The turbulence in the liquid is modeled by the low-Reynolds-number k–ε turbulence model of Launder and Sharma (1974). The k–ε turbulence model is modified to include additional source terms to account for effect of the sediment particles on the liquid turbulence (turbulence modulation). The set of equations for the turbulence model are given in Table A.3 in the Appendix. The current study adopts the model of Simonin and Viollet (1990)

to account for the turbulence modulation. Details of the equations used for the turbulence modulation are given in Table A.4 in the Appendix.

The TFM equations are solved together with the appropriate boundary conditions. Johnson and Jackson (1987) were the first to classify the particle interactions at the wall as either long or short contacts. The longer contacts are assumed to be frictional contacts (diffuse in nature) between particles and the wall, while the shorter contacts are collisional contacts (specular in nature). In general, the Johnson and Jackson (1987) relations approximate the total stress as the sum of both frictional and collisional stress contributions. In this case, no frictional effect is included. The Johnson and Jackson (1987) wall boundary condition for the shear stress at the wall ($\tau_{xy,s}$) and flux of granular temperature at the wall (q_s) are given, respectively, by

$$\tau_{xy,s} = -\frac{\pi}{6}\sqrt{3}\varphi \frac{\alpha_s}{\alpha_{s,max}} \rho_s g_{0,ss} \sqrt{\Theta_s}(u_s - u_l) \qquad [4.12]$$

$$q_s = \frac{\pi}{6}\sqrt{3}\varphi \frac{\alpha_s}{\alpha_{s,max}} \rho_s g_{0,ss} \sqrt{\Theta_s}(u_s - u_l)^2 - \frac{\pi}{4}\sqrt{3} \frac{\alpha_s}{\alpha_{s,max}} (1 - e_w^2)\rho_s g_{0,ss}^{3/2} \qquad [4.13]$$

where $\alpha_{s,max}$ is the maximum solid volume fraction (packing limit). The parameters φ and e_w are, respectively, the specularity coefficient and the wall restitution coefficient, which have to be specified for a given flow. The term $(u_s - u_l)$ is the particle slip velocity parallel to the wall.

4.3 Model Description

Lyn's (1987) experiment was conducted in a rectangular flume 13 m in length and 0.267 m in width. A schematic of this type of flow is presented in Figure 4.1. The flow conditions for the two test cases from Lyn (1987) are given in Table 4.2. Modeling two sediment concentrations allowed us to effectively test two flows, one with a larger bulk concentration, to see the effect of a greater number of particles on the flow. Lyn (1987) reported that the sand particles used in the test had a specific gravity of 2.65. The geometric standard deviation of the sand particles $\sigma_g = \sqrt{D_{84}/D_{16}}$ was reported as 1.18 and

1.12, where D_{84} and D_{16} are the sand particle sizes for which 84% and 16% of the material is finer. Since $\sigma_g < 1.35$, the sand particles can be considered to have a uniform gradation (Breusers and Raudkivi 1991). It is seen from the Reynolds numbers based on particle diameters (Table 4.2), the roughnesses are small so that we can approximate the surface as hydraulically smooth and apply a low-Reynolds number formulation to resolve the near wall region.
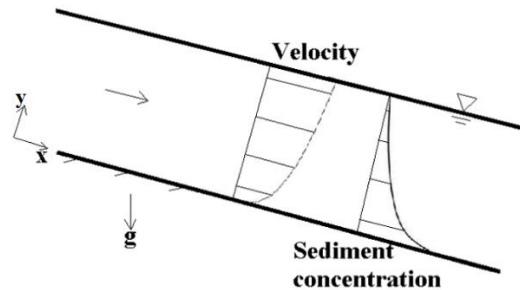
Figure 4.1 Free surface flow in a sloped open channel

In his experiment, Lyn initially placed 20-30 kg of the sand in the flume and then set the flow rate. By trial-and-error adjustment of the discharge and bed slope, the flow with a flat bed was achieved. Measurements of the water velocity and sediment concentration were taken at a section located 9 m from the flume entrance using Laser Doppler-Velocimetry (LDV) and a conventional suction sediment sampler, respectively.

Table 4.2 Flow conditions for experiment of Lyn (1987)

Test case #	Lyn's (1987) experiment #	Flow depth (m)	Bed slope, S	Bulk discharge (L/s)	Shear velocity, u_* [†] (m/s)	Average particle diameter (mm)	Particle settling velocity [††] (m/s)	$\dfrac{u_* d}{\nu}$
1	2565EQ	0.0654	0.00296	12.07	0.0357	0.24	0.031	8.55
2	1565EQ	0.0645	0.00244	10.8	0.0323	0.15	0.016	4.84

[†]   The shear velocity was calculated from $\sqrt{gSR_h}$, where R_h is the hydraulic radius of the channel
[††]   The water temperatures for test case #1 and 2, were $21.3°C$ and $20.7°C$, respectively

The phasic mass and momentum equations, together with a set of additional transport equations used to model the turbulence, were solved using the commercial software ANSYS Fluent 14.5. The TFM option referred to as "Eulerian model" in ANSYS Fluent was used. For test case #1, the 2D domain was 13 m $\times$ 0.0654 m in extent and used a total of 47,000 control volumes. The grid was non-uniform structured and denser close to the wall, and the control volume size increased gradually towards the free surface. In order to assess the grid dependence, three different grid sizes were tested: 32,000, 47,000, and 70,000 control volumes. The grid with a total 47,000 control volumes was selected for the study, since increasing the grid size to 70,000 control volumes resulted in less than 1% difference in the liquid velocity and sediment concentration (taken at $y/d = 100$ where y is the elevation from the bed normalized by the particle diameter d). In addition, the grid with a total of 47,000 control volumes was used for modeling the single-phase case, and the predictions agreed well with empirical results seen as the log-law plot. Using the same strategy, a 2D domain of 13 m$\times$ 0.0645 m was used with a total of 44,000 control volumes for test case #2.

At the inlet, uniform profiles for the water velocity, sediment velocity, and solids volume fraction were specified. The velocity of the water and sediment were set to 0.695 m/s and 0.627 m/s, respectively. The bulk solids volume fraction of the sediment was set to 0.01 and 0.025 for test case #1 and #2, respectively, at the inlet to match the experimental values reported by Lyn (1987) at 10% and 50% of the total depth, simultaneously. The free surface of the water was modeled as a free-slip wall (following previous studies, *e.g.* [4-7]) using a symmetry boundary condition for all flow properties. The bed boundary condition was a no-slip wall for the liquid phase and a partial-slip condition for the sediment phase using the boundary condition of Johnson and Jackson (1987).

For the Johnson and Jackson (1987) wall boundary condition, the specularity and wall restitution coefficients are two key parameters to be specified by the user. The values of the parameters tested in this

study were chosen based on suggested ranges in the literature, *e.g.* [9, 17]. The values of these parameters were determined using a two-step process. First, for a wall restitution coefficient of $e_w = 0.7$, three different values of the specularity coefficient were tested (φ = 0.001, 0.002, and 0.004). As discussed below, the value of $\varphi = 0.004$ was found to give predictions that best matched the experimental data. In the second step, for a specularity coefficient of φ = 0.004, three different values of the wall restitution coefficient were tested (e_w = 0.5, 0.7, and 0.9). The particle-particle restitution coefficient was set to be $e_{ss} = 0.9$.

4.4 Results and analysis

In this section, predictions of the liquid and particle velocity fields based on the TFM framework are presented and compared to the measurements by Lyn (1987), where available. Figure 4.2 shows the effect of different specularity coefficients (φ = 0.001, 0.002 and 0.004) on the water and sediment velocity profiles, which have been plotted versus dimensionless depth (y/d) for test case #1. As mentioned earlier, the wall restitution coefficient was kept constant at $e_w = 0.7$ for this set of tests.

Figure 4.2a shows the sediment velocity profile for different values of the specularity coefficient. Recall that the sediment velocity is modeled by a partial slip boundary condition at the wall. The larger the specularity coefficient, the smaller the sediment slip velocity at the wall which implies an effectively larger frictional effect. It was also observed that as the value of the specularity coefficient increases, the magnitude of the granular temperature also increases. For specularity coefficients of 0.001, 0.002, and 0.004 the sediment slip velocity at the wall was, respectively, 0.6, 0.49, and 0.435 m/s. This is accompanied by a higher magnitude of the sediment velocity in the upper region of the channel. Figure 4.2b shows the mean liquid velocity profile for different values of the specularity coefficient and includes the experimental measurements of Lyn (1987) for comparison. Like the sediment phase, increasing the value of the specularity coefficient reduces the value of the liquid velocity near the wall, with a corresponding increase in the level in the upper region of the channel. The dependence of the mean liquid velocity on the value of

the specularity coefficient is due to the coupling of the phasic momentum equations through the interaction

force. From Figure 4.2b, the value of φ =0.004 yields the best agreement with the experimental data.

(a)   (b)
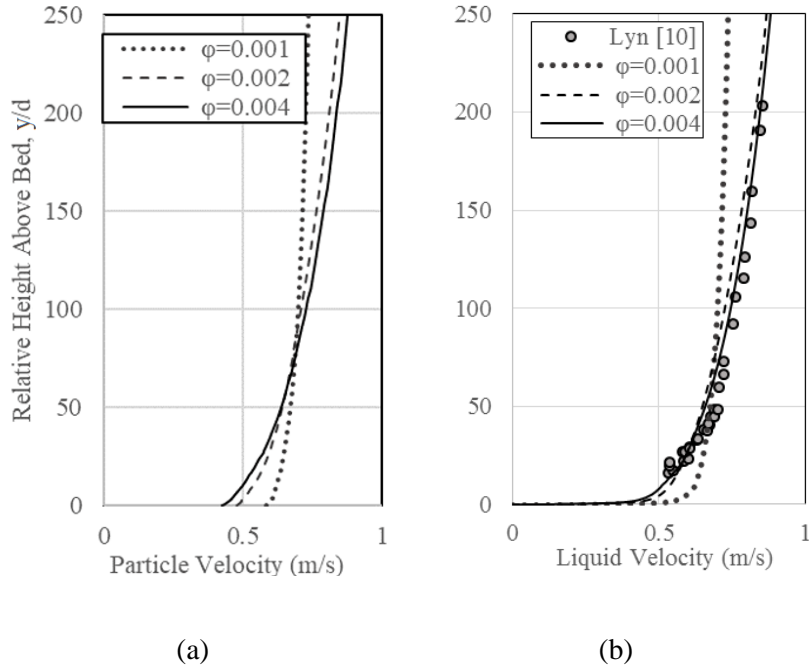
Figure 4.2 Effect of specularity coefficient on the TFM predictions of (a) particle velocity and (b)
liquid mean velocity compared to the experimental measurements of Lyn (1987) for test case #1

Next, different values of the wall restitution coefficient were assessed to illustrate their effect on

the model predictions. In this case, the specularity coefficient was fixed at $\varphi = 0.004$ and three different

values of the wall restitution coefficient were tested ($e_w = 0.5$, 0.7, and 0.9) for test case #1. All other

model parameters settings were kept constant so that the test was only representative of the effect of the

wall restitution coefficient.

Figure 4.3a gives the particle velocity for different values of the wall restitution coefficient. As the

value of the wall restitution coefficient increases and becomes closer to unity, the particle collisions with

the wall become more elastic, which implies more energetic particles near the wall. The partial slip velocity

of the sediment phase at the wall for restitution coefficients of 0.5, 0.7, and 0.9 was 0.57, 0.43, and 0.29

m/s, respectively. The reduction in the particle velocity at the wall is due to the enhanced sediment shear

stress associated with the more energetic particles. Figure 4.3b shows the liquid velocity for different values of the wall restitution coefficient for test case #1. The liquid velocity follows the same pattern as the particle velocity. Among the three values considered for the wall restitution coefficient, $e_w = 0.7$ gave the best agreement with the measured data for the liquid velocity. Hereafter, unless noted otherwise, all the simulations will use a specularity coefficient of $\varphi = 0.004$, and a wall restitution coefficient of $e_w = 0.7$.

(a)   (b)
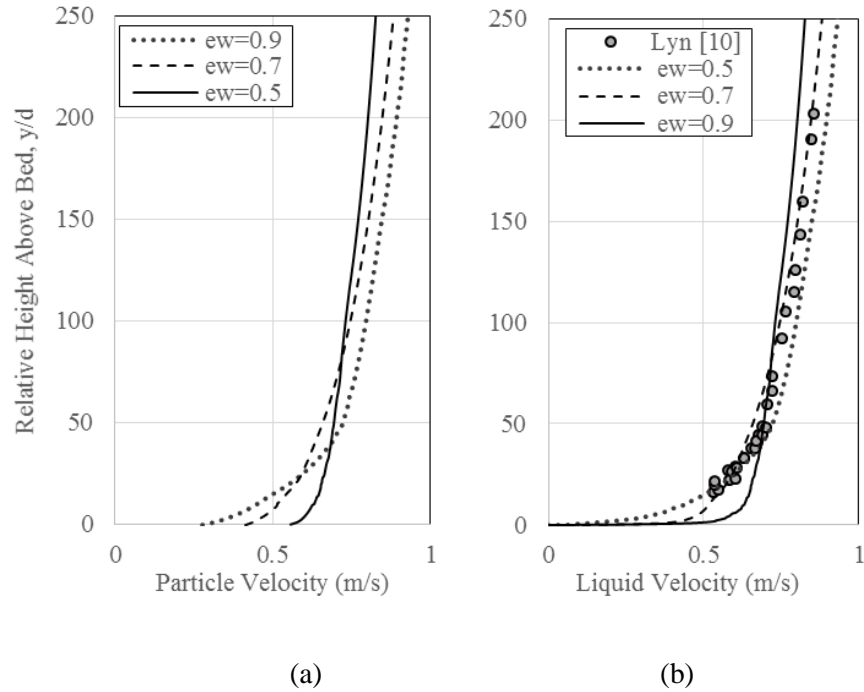
Figure 4.3 Effect of wall restitution coefficient on the TFM predictions of (a) particle velocity and (b) mean liquid velocity compared to the experimental measurements of Lyn (1987) for test case #1

Next, the TFM predictions are compared to test cases #1 and #2. As seen in Table 4.2, the flow carries a larger number of sediment particles of smaller size for test case #2 and the inlet velocity is somewhat (*i.e.* 10%) lower than for test case #1. Figure 4.4 shows the predictions for the liquid velocity for test cases # 1 and #2 compared to the corresponding measured values from Lyn (1987).
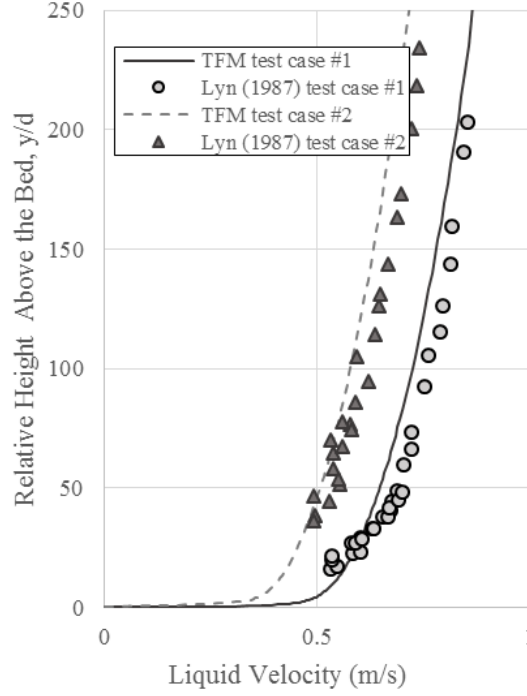
Figure 4.4 Mean liquid velocity for test cases #1 and #2

Figure 4.4 demonstrates that the TFM was able to capture successfully the measured mean liquid velocity for the both cases successfully. The larger number of particles in test case #2 caused the level of the liquid velocity to decrease overall.

Figure 4.5 presents the mean liquid velocity normalized by the friction velocity (u_*) for both the present two-phase flow and single-phase flow, which is a canonical formulation for a turbulent wall-bounded flow. Also shown in the figure are the log-law relation for single-phase turbulent flow in the overlap region, as well as the linear profile in the viscous sublayer, given respectively given by

$$u_l^+ = y^+ \tag{4.14a}$$

$$u_l^+ = \frac{1}{\kappa}\ln y^+ + B \tag{4.14b}$$

where $u_l^+ = u_l/u_*$ and $y^+ = y/u_*$. The von Karman constant was taken as $\kappa = 0.412$ and the constant B = 5.29 following Nezu and Rodi (1986). The value of the shear velocity ($u_* = \sqrt{\tau_w/\rho}$) for the single-phase flow and test cases #1 and #2 were, respectively, 0.039 and 0.044, and 0.041 m/s. The single-phase velocity profile behaves as expected for a low-Reynolds-number turbulence model closure, *i.e.* the velocity profile smoothly transitions from a log-law profile in the overlap region to the linear profile characterizing the viscous sublayer near the wall. The liquid velocity for the two-phase flow is in good agreement with the experimental data of Lyn (1987), although the measurements do not extend into the near-wall region. Due to the enhanced value of the shear velocity for the two-phase flow, the liquid velocity profile is displaced below the value of the log-law for a smooth surface, in a manner that is reminiscent of flow over a rough wall. For test case #2 this effect is less than for test case #1, even though the sediment concentration is greater for test case #2. However, within the buffer layer both two-phase flow velocity profile transition to match the linear relation in the viscous sublayer. Figure 4.5 clearly shows that the effect of the particles is to reduce the liquid velocity (using inner coordinates) below the value in single-phase flow. However, this effect is only evident in the overlap region and outer flow. Near the wall, the effect of the sediment disappears. As such, the TFM prediction indicated a minimal effect of the particle phase on the liquid velocity very near the wall, which warrants further investigation.
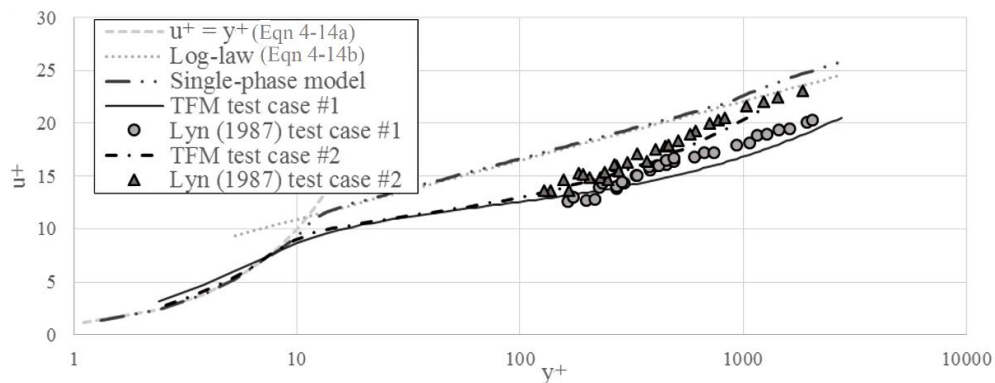
Figure 4.5 Comparison of the mean liquid velocity profiles predicted for single-phase and two-phase flow with the measurements of Lyn (1987) for test cases #1 and #2
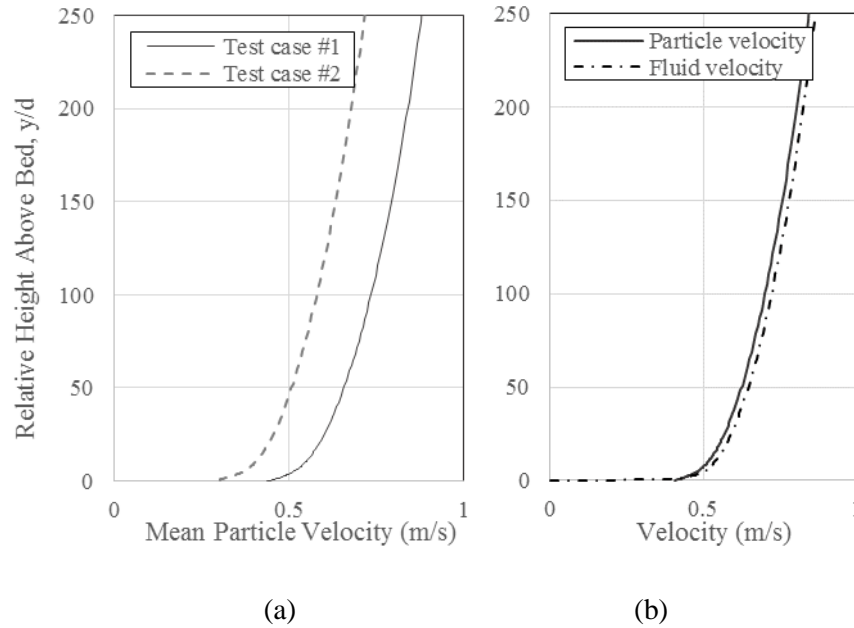
Figure 4.6 Comparison of a) mean particle velocity for test case #1 and #2, and b) mean particle and liquid velocity of test case #1 (slip velocity)

Figure 4.6a compares the mean particle velocity for test case #1 and test case #2 through the depth of the channel. Recall from Table 4.2 that test case #1 had a higher liquid flow rate than test case #2, which is also reflected in the level of the particle velocity in Figure 4.5a. At the bed, the particles have a slip velocity of respectively 0.43 and 0.31 m/s, respectively, for test case #1 and test case #2. In Figure 4.6b, the particle velocity predicted for test case #1 is shown alongside the liquid velocity. In general, the liquid velocity is only slightly greater than the sediment velocity, except near the wall where the liquid velocity goes to zero, while the sediment velocity remains finite (= 0.43 m/s) due to the partial-slip boundary condition. For example, at $y/d = 100$ the slip velocity equals 0.018 m/s which is only 2.5 % of the liquid velocity. At the wall, the liquid velocity goes to zero, while the sediment velocity retains a finite value (= 0.43 m/s) due to the partial-slip boundary condition.

Figure 4.7 compares the predicted particle concentration profiles to Lyn's (1987) measurements. Note that the plot only shows the lower region of the channel where there is the experimental data from Lyn (1987) available for comparison. In the numerical model, the sediment concentration was obtained

from the solids volume fraction which is calculated from the mass conservation equation. In Figure 4.7, the sediment concentration profiles steadily increase near the bottom wall of the flume, with a peak value at the wall that is less than 2.5%. Note that the bulk sediment volume concentrations of $\overline{\alpha_s}= 0.01$ and 0.025 corresponds to bulk mass concentrations of approximately 0.27 and 0.675 %, respectively. For both test cases, there is good agreement between the predicted and measured profiles. The concentration profile is predicted to reach a peak value at the bed.
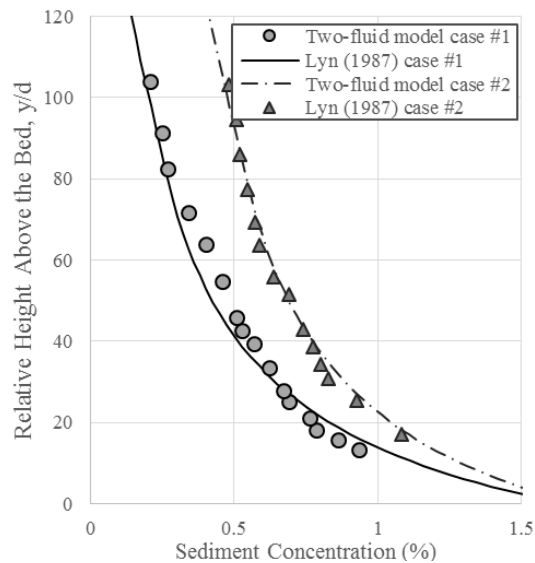
Figure 4.7 TFM prediction of the sediment concentration profile for cases #1 and #2 compared to the measurements of Lyn (1987)

Figure 4.8 examines the turbulence kinetic energy and Reynolds shear stress of the liquid phase predicted by the TFM for test cases #1 and #2 compared to the single-phase model as well as Lyn's (1987) measurements. Figure 4.8a shows the profile of the turbulence kinetic energy (normalized by the shear velocity squared). All three profiles show the characteristic near-wall peak for the turbulence kinetic energy in a near-wall flow. The profiles predicted for the two-phase flows both show general agreement with the experimental data: for test case #1 the profile and measurements coincide, while for test case #2 the trend is the same, but the measurements increase more quickly as they approach the wall. The numerical

predictions for both test cases indicate that the presence of particles decreases the level of the turbulence. The decrease is more pronounced for test case #1, which is characterized by a larger particle size.

(a)   (b)
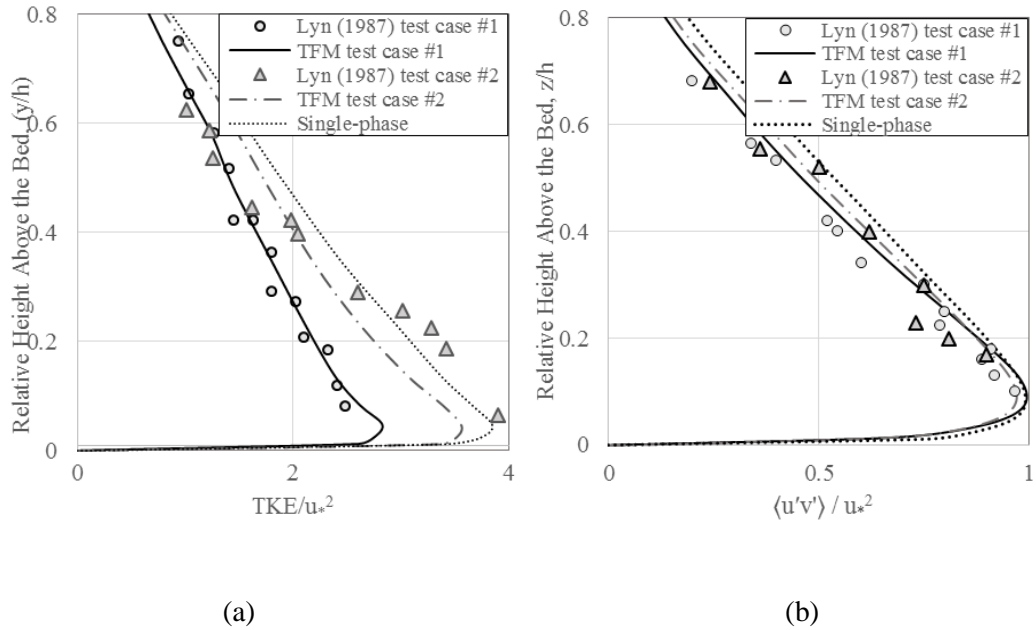
Figure 4.8 Predicted profiles for (a) the turbulence kinetic energy and (b) the Reynolds shear stress together with the measurements of Lyn (1987)

Figure 4.8b shows the Reynolds shear stress profile for the liquid phase for both single-phase and the two sediment-laden flows. All three profiles exhibit peak values near the bed and show that turbulent transport is dominant except in a narrow region very close to the bed. The predicted profiles for text cases #1 and #2 are close to each other, as are the experimental curves. As in the case of the turbulence kinetic energy, the effect of particles is to slightly reduce the level of the Reynolds shear stress, with a smaller reduction for test case #2.

Figure 4.9 shows the profile predicted for the eddy – or turbulent – viscosity in the liquid phase, normalized by the kinematic viscosity. The plot compares the value of the eddy viscosity for test case #1 and #2, as well as for single-phase flow. Recall that the eddy viscosity is the key parameter for determining the turbulent transport of momentum in the liquid using an eddy viscosity formulation.   From the figure,

the peak value of the eddy viscosity for all three cases in approximately two orders of magnitude greater than the molecular value. Furthermore, the figure indicates that the effect of the particles is to decrease slightly the value of the eddy viscosity. The decrease is most pronounced for test case #1, which is characterized by a larger particle diameter but a lower bulk concentration than test case #2. This result is consistent with the results for the turbulence kinetic energy, which is used to calculate the eddy viscosity.
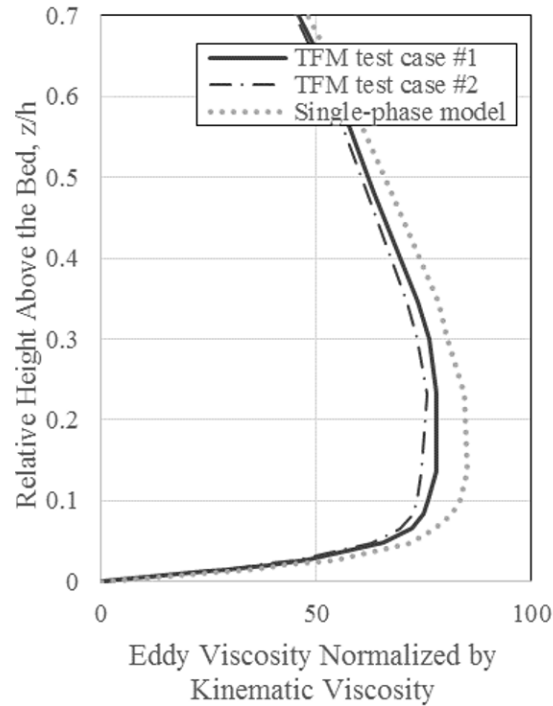
Figure 4.9 TFM predictions for the eddy viscosity in the liquid phase for the single phase and tests cases #1 and #2

Figure 4.10 shows profiles for the granular temperature, and the sediment particle shear stress across the depth of the channel. The granular temperature is a measure of the energy associated with the fluctuating particle velocity, and plays the same role as the turbulence kinetic energy for the fluctuating liquid velocity. From Figure 4.10a, for both test cases the granular temperature exhibits a peak value at the wall, which is due to the particle collisions with the bottom wall or bed. The value reduces with distance from the bottom wall, at first quite dramatically and then more gradually in the upper region of the channel. The level of the granular temperature is slightly higher for test case #2 compared to test case #1, which can be attributed to the higher

concentration of particles for test case #2. Figure 4.10b compares the particle/sediment shear stress for test cases #1 and #2. The figure indicates that the particle shear stress peaks near the wall, in a region where the mean particle velocity exhibits a relatively high gradient. The particle shear stress has a finite value at the wall, 0.00033 Pa for test case #1 and 0.0051 Pa for test case #2. From the constitutive relation, the sediment shear stress is strongly dependent on the granular temperature. As the level of the granular temperature increases, the magnitude of the sediment shear stress also increases. The higher particle shear stress at the wall for test case #2 is consistent with the prediction of a higher value for the granular temperature at the wall for test case #2.

(a)   (b)
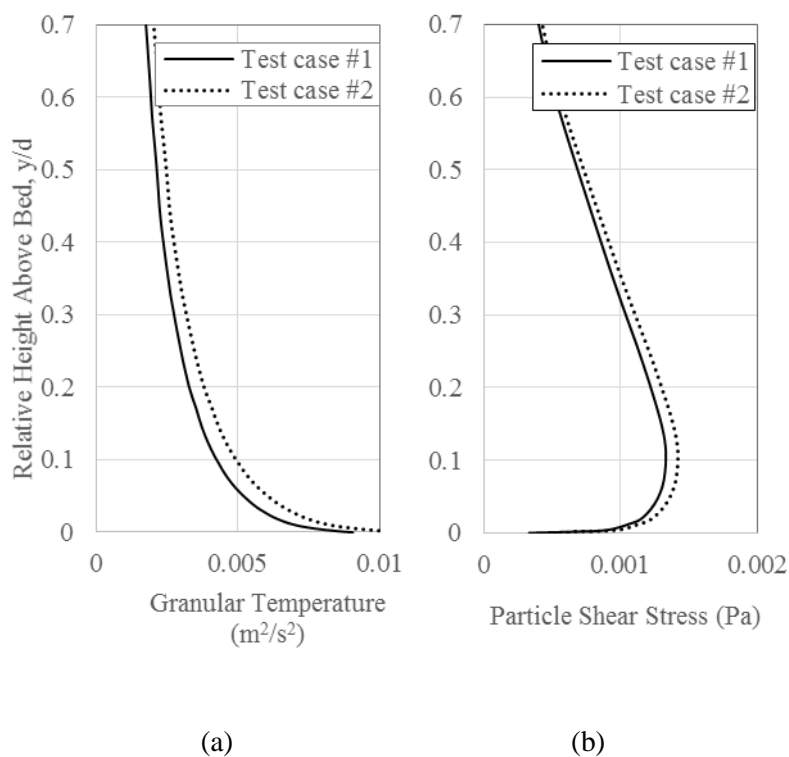
Figure 4.10 TFM predictions for the (a) granular temperature, and (b) sediment shear stress for test case #1 and #2

4.5 Conclusions

The TFM has significant potential for predicting sediment transport in open channel flows. The present study used the TFM formulation together with a low-Reynolds-number $k-\varepsilon$ turbulence model to investigate

the sediment transport in a fully developed open channel flow. In the TFM formulation, the concentration profile is calculated from the solids volume fraction, which is determined from mass conservation, while the particle velocity profile is determined from momentum conservation for the particle phase. The particle-wall interactions were characterized using the boundary condition of Johnson and Jackson (1987), which required that the values of the specularity coefficient and coefficient of restitution for the particle-wall collisions be specified for the flow under consideration. The model predictions of the liquid and sediment velocity profiles, sediment concentration, turbulence statistics and fluctuating particle velocity field were documented for two different test cases of the equilibrium open channel flow experiment of Lyn (1987).

The TFM prediction for the sediment concentration profile was in good agreement with the experimental data. It varied significantly over the depth of the channel, and exhibited a peak value at the wall. The sediment velocity profile was characterized by a partial-slip value at the bottom wall as determined by the Johnson and Jackson (1987) boundary conditions. The properties of the sediment phase strongly depend on the granular temperature, which is a measure of the fluctuating particle velocity and has a peak value at the bottom wall. The particle phase shear stress also exhibited a peak value located near the bottom wall and a finite value on the wall itself. The bottom wall or bed plays an important role in energizing the particle phase via the particle-wall collisions.

The flow was characterized by a small slip velocity between the two phases, with the liquid velocity being slightly larger than the particle velocity over most of the channel depth. When scaled using inner coordinates, the liquid velocity exhibited a downward shift in the overlap region due to the particle phase, in some ways similar to that produced by a rough surface, even though the roughness on the bed was minimal. Closer to the wall the effect of particles was negligible and the mean velocity profile for the liquid phase matched the canonical linear profile in the viscous sublayer. The particle phase produced a small reduction in both the level and peak value of the turbulence kinetic energy, Reynolds shear stress and eddy viscosity near

the wall, which indicated that the effect of particles was to suppress the turbulence in the liquid phase. This effect was more pronounced for the case of larger particles.

An important conclusion of the present study is that the TFM using constitutive equations based on granular kinetic theory, coupled with a low-Reynolds-number turbulence model, is able to predict the liquid and sediment transport in an equilibrium channel well without resorting to the empirical ad hoc relations often used to determine the concentration profile. A weakness of the Johnson and Jackson (1987) boundary condition relations is the need to specify the specularity coefficient and coefficient of restitution at the wall for the specific flow being considered. The next step in the application of the TFM to predicting sediment transport in open channel flow is to consider the case where sediment is being deposited on the bed and also being re-suspended into the flow.

Chapter Five

5. TWO-FLUID MODELING OF SEDIMENT TRANSPORT IN A VORTEX-TYPE STORMWATER RETENTION POND

A similar version of this chapter has been presented at the following conference:

- Ahadi, M. and Bergstrom, D. (2021) Two-fluid modeling of sediment transport in a vortex-type stormwater retention pond, 74th Canadian Water Resources Association (CWRA) 2021, Sharing knowledge and expertise: Managing water risks and opportunities, 31 May – 4 June 2021 | Quebec, Canada |

Preamble

The sediment transport varies spatially within a pond. Realistic prediction of sediment transport in the vortex-type stormwater retention pond requires an authentic 3D multiphase model. Two-fluid modeling is capable of bringing in the effect of sediment particles on the flow field and particle-particle interactions. The model showed promising results in predicting the movement of sediment particles in an enhanced level of physical realism in a fully developed open channel flow (Chapter 4). Two-fluid modeling of sediment transport in the environment of a retention pond was found to be a gap in the literature, even though it appears to be well suited to modeling particle dynamics in a pond. In this chapter, the TFM validated in Chapter 4 is applied to the vortex-type stormwater retention pond. This chapter is another step towards using the TFM in the stormwater retention ponds.

Abstract

A three-dimensional multiphase numerical model previously implemented and validated in a turbulent open channel flow in Chapter 4 is applied to the new design vortex-type stormwater retention pond. The flow in vortex-type stormwater retention pond was previously characterized experimentally and computationally in Chapter 3. The sediment and flow dynamics are now studied using the two-fluid method.

The TFM solves the transport equations for both phases of water and sediment. These models have the capacity of eventually bringing in the physics of sediment transport. TFMs are developing, and their

potential is not completely omitted in water resources engineering problems, yet. In this study, the TFM is tested for the first time in a new vortex-type stormwater retention pond. This study provided useful information for the design of stormwater retention ponds. Liquid and particle velocity profiles are provided. The sediment deposition spatial pattern in the pond is presented.

5.1 Introduction

Excessive sediment negatively impacts receiving waters. It reduces the lifetime and stability of downstream structures, degrades water quality, and disturbs aquatic habitats. Dredging is extremely costly and harmful to the environment. Stormwater retention ponds are facilities to prevent flooding through storage after storm events. If designed properly, they can also be effective at improving the quality of stormwater through sedimentation. Recently, more strenuous sediment removal requirements have been regulated to protect the downstream waters, e.g. North Carolina Department of Environment, Health, and Natural Resources 1995, Ontario Ministry of the Environment 2003, City of Edmonton 2008, City of Calgary 2011, and City of Brandon 2018. For example, according to the City of Calgary stormwater management and design manual (2011), the pond must provide a minimum 80 % removal of total suspended solids for particle sizes $\geq 75~\mu$m.

Stormwater retention ponds have been traditionally designed based on guidelines for pond volume, length-to-width ratio, and depth, e.g. according to the City of Saskatoon (2018), a stormwater retention pond should have a length-to-width ratio of 4:1 to 5:1 with a maximum depth of 1.8 m. Reviewing the literature, a wide variation of pond removal efficiencies was observed (Wu et al. 1996, Weiss 2007, Husna et al. 2011, The Center of Watershed protection 2007). This variation includes negative sediment removal efficiencies, i.e. the settled sediment at the pond bed is resuspended by the flow as it moves towards the pond outlet. For example, Gillis (2017) reported a removal efficiency of -67 % for a storm event in 2014 for a pond located in Saskatoon, Saskatchewan, Canada. The current ponds are nowhere near the new

92

sediment removal expectations, and the conventional methods of pond design need to be revisited (Wu et al. 1996, Khan et al. 2009, Gu et al. 2017).

Computational Fluid Dynamics (CFD) models have been playing a significant role in understanding sediment transport problems in hydraulic engineering. CFD is a numerical technique that solves the Reynolds Averaged Navier-Stokes (RANS) equations and the turbulent fluxes emerging from time-averaging the transport equations, i.e. the Reynolds stresses. A CFD model is also capable of solving the conservation equations for multiple phases and to simulate the interaction between phases.

Engineers typically need to investigate existing ponds, to test the effect of retrofitting elements on them, and to develop new designs capable of providing better performance. A validated CFD model is a promising tool to perform high quality virtual experiments on the pond that provide comprehensive information and reveal the transport mechanisms within the pond. Due to the predictive nature of a CFD model, it allows the simulation of new designs before they are built as well, as testing possible modifications to existing ponds.

Designing and optimizing stormwater ponds for the purpose of sediment removal requires a clear understanding of the flow field and sediment transport. In spite of the advances in multiphase CFD modeling approaches, in CFD studies of stormwater retention ponds, it is common practice to ignore the sediment phase, only solve the conservation equations for the liquid phase, and then to use an advection-diffusion equation for a tracer material. The tracer is released at the inlet and its concentration is then measured at the outlet at different times to estimate the so called residence time distribution e.g. Persson (2000), Adamsson (2005), Khan et al. (2009), He and Marsalek (2013), Sonnenwald et al. (2017), Nakhaei et al. (2018), Binns et al. (2019). This information is then used to characterize the sediment transport in the pond (Walker 1998).

Stormwater retention ponds deal with high sediment loads. Solving an advection-diffusion equation is incapable of bringing in important physics of the sediment transport. Exploring the sediment removal requires an authentic two-phase model to simulate the flow and sediment dynamics. In addition, the presence of sediment has been shown to affect the flow pattern (Ahadi et al. 2019). Two-phase models can be categorized as either a particle tracking model or a TFM. In both models the Navier-Stokes equations are solved for the continuous liquid phase in the Eulerian frame, but the sediment phase is treated differently in each model.

In particle tracking models, the particle trajectories are computed individually based on Newton's second law of motion. Particle tracking methods have been used to model sediment movement in the ponds (Zhang 2009, Dufresne et al. 2009, Torres et al. 2008, Yan 2013). However, for a full-size pond, the number of particles to be tracked using the particle tracking method is enormous. The computational cost to model large numbers of particles remains a challenge even with today's computing resources.

In the TFM, the particle phase is assumed to be a continuum like the liquid phase so that two separate sets of mass and momentum conservation equations (written in an Eulerian frame) are solved (Enwald et al. 1996, Zhong et al. 2011). For high concentrations, the particle-particle stresses should be included in the particle phase momentum equation. Lun et al. (1984) used the concept of kinetic theory of granular flow to provide a model for particle-particle interaction based on the inelastic nature of particle collisions. The two-fluid methodology has shown promising predictions in open channel flow problems. The TFMs have been increasingly applied to investigations of sediment-laden open channel flows in the literature (e.g., Drew 1975, McTigue 1981, Cao et al. 1995, Greimann et al. 1999, Greimann and Holly 2001, Hsu et al. 2003, Jha and Bombardelli 2009, and Zhong et al. 2011, Amoudry et al. 2014, Ahadi et al. 2019). However, the method has not been explored in the context of stormwater ponds.

In this study, the Eulerian-Eulerian TFM is applied to model sediment transport in a new vortex-type stormwater retention pond. This vortex-type pond design was initially developed in a simplified

conceptual study by Albers and Amell (2010); it demonstrated more resistance to the formation of dead zones and short-circuiting currents. The flow pattern in this vortex-type pond was further studied, i.e. Chapter 3, using physical modeling of a scale model (1:13.3) of the pond design and computational modeling using a 3D single-phase numerical model. The experimental and numerical results indicated that an inlet jet, the rotating flow in the circular channel outside the berm, and the flow moving towards the outlet inside the berm are the three important patterns of behavior are observed in the pond as shown in Figure 5.1. The jet entrains the surrounding water and spreads toward the outer wall of the pond. After less than half a round of circulation, the jet has decayed such that the flow becomes approximately uniform in the circular channel. Two strong recirculation zones were formed: (I) the region trapped between the incoming jet and the outer wall, and (II) the region downstream of the jet trapped between the jet and the inner wall, i.e. the berm.
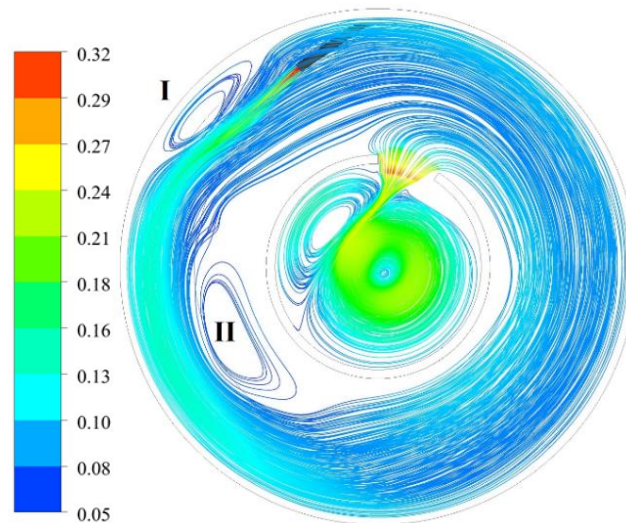
Figure 5.1 Plan view of 3D pathlines with color based on the total velocity (m/s)

In Chapter 4, a TFM prediction of flow and sediment transport in an open channel flow was explored. The results were compared to velocity, turbulence, and sediment concentration data from the literature. In the current chapter, the TFM was applied to study the sediment transport in the vortex-type

pond. Although no experimental data on the sediment transport are available for direct comparison, the TFM model has been extensively tested in the open channel flow noted above. The simulations presented below represent a first-step in exploring the sediment transport in the vortex-type pond previously studied using a single-phase CFD model. It demonstrates the potential of a TFM to predict features of sediment transport that cannot be captured by a single-phase model.

5.2 Methodology

This section provides a summary of the conservation equations used in the TFM for a two-phase three-dimensional steady flow. The continuity equation for each phase q (liquid or solid) is as follows:

$$\nabla \cdot \left(\alpha_q \rho_q \vec{v}_q \right) = 0 \tag{5.1}$$

where α_q, ρ_q, and $\vec{v}_q$ are the volume fraction, density, and velocity of phase q (either water or particles), respectively. The solution of Equation [5.1] for the sediment phase, along with the condition that the volume fractions sum to one, allows the volume fraction of each phase to be determined. The momentum balance for each phase q is as follows:

$$\nabla \cdot \left(\alpha_q \rho_q \vec{v}_q \vec{v}_q \right) = -\alpha_q \nabla P + \nabla \cdot \overline{\tau_q} + \alpha_q \rho_q \vec{g} + \vec{R}_{pq} \tag{5.2}$$

where P is the fluid pressure, $\vec{g}$ is gravity, $\overline{\tau_q}$ is the phasic stress tensor, and $\vec{R}_{pq}$ is the phase interaction force. In Table A.1 in the Appendix, the reader can find the 2D form of the conservation equations for the liquid and solid phases.

The phasic stress tensor is modeled using Equation [5.3]:

$$\overline{\tau_q} = \alpha_q \mu_q \left(\nabla \vec{v}_q + \nabla \vec{v}_q{}^T \right) + \alpha_q \left(\lambda_q - \frac{2}{3}\mu_q \right) \nabla \cdot \vec{v}_q \bar{I} \tag{5.3}$$

where μ_q and λ_q are the shear and bulk viscosity, respectively. The particle shear and bulk viscosities arise from the momentum exchange due to collisions,

$$\mu_s = \mu_{s,col} + \mu_{s,kin} \qquad [5.4]$$

where $\mu_{s,col}$ and $\mu_{s,kin}$ are the collisional and kinetic components of sediment shear viscosity, respectively. For the models used for calculation of $\mu_{s,col}$ and $\mu_{s,kin}$ in this study, the reader is referred to Table A.2 in the Appendix. Since the flow being considered is dilute, no frictional component was considered.

An expression for the interaction force $(\vec{R}_{pq})$ between phases q and p is required to close Equation 2. This force depends on frictional, pressure, cohesion and other effects. In general, it is written as:

$$\vec{R}_{pq} = \vec{K}_{pq}(\vec{v}_p - \vec{v}_q) \qquad [5.5]$$

where $\vec{K}_{pq}$ $(= \vec{K}_{qp})$ is the interphase momentum exchange coefficient, which in this case, is modeled based on the drag force. For granular flows (liquid-solid), the liquid-solid exchange coefficient $\vec{K}_{ls}$ is given by,

$$\vec{K}_{ls} = \frac{3}{4} C_D \frac{\alpha_s \alpha_l \rho_l |\vec{v}_s - \vec{v}_l|}{d_s} \alpha_l^{-2.65} \qquad [5.6]$$

where the subscript l is for the liquid, and the subscript s for the solid phase, and d_s is the particle diameter. The value of D_{50} of the particle distribution is used as d_s , where D_{50} represents the sediment grain size for which 50 % of the mass of the particles are smaller than this value. The drag model of Wen and Yu (1966) (Equation 5.7) is appropriate for dilute systems.

$$C_D = \frac{24}{\alpha_l Re_p}[1 + 0.15(\alpha_l Re_p)^{0.687}] \qquad [5.7]$$

$$Re_p = \frac{\rho_l d_s |\vec{v}_s - \vec{v}_l|}{\mu_l} \qquad [5.8]$$

where Re_p is the Reynolds number of the particle.

For granular flows, the solid-phase stresses are obtained based on an analogy between the random particle motion arising from particle-particle collisions and the thermal motion of molecules in a gas. The resultant model formulation based on kinetic theory also takes into account the inelasticity of the granular phase. Similar to the case of a gas, the intensity of the particle velocity fluctuations determines the stresses, viscosity, and pressure of the solid phase. The kinetic energy associated with the particle velocity fluctuations is represented by the granular temperature (Θ_s), which is proportional to the kinetic energy of the fluctuating particle motion ($3\Theta_s$ = solids fluctuating velocity).

A transport equation derived from kinetic theory is used to solve for the granular temperature,

$$\frac{2}{3}[\nabla \cdot (\alpha_s \rho_s \overrightarrow{v_s} \Theta_s)] = \left(-p_s \bar{\bar{I}} + \bar{\bar{\tau}}_s\right) : \nabla \overrightarrow{v_s} + \nabla \cdot \left(K_{\Theta_s} \nabla \Theta_s\right) - \gamma_{\Theta_s} + \emptyset_{ls} \tag{5.9}$$

where $\left(-p_s \bar{\bar{I}} + \bar{\bar{\tau}}_s\right) : \nabla \overrightarrow{v_s}$ is the generation of granular energy by the solids stress tensor and $K_{\Theta_s} \nabla \Theta_s$ is the diffusive flux of granular energy based on the particle thermal conductivity K_{Θ_s}. The collisional dissipation of energy, γ_{Θ_s}, is due to inelastic particle-particle interactions, and $\emptyset_{ls}$ is the so-called energy exchange between the fluctuating liquid and solid phases. Each of these terms is given in Table A.2 in the Appendix.

The fluctuating motion of the fluid and the sediment phase are coupled. The turbulence in the fluid is modeled by the low-Reynolds number k–ε turbulence model of Launder and Sharma (1974). The set of equations for turbulence modeling can be found in Table A.3 in the Appendix. The k–ε turbulence model is modified to include additional source terms to account for effects of the sediment particles on the fluid turbulence, i.e. turbulence modulation. The current study adopts the model of Simonin and Viollet (1990) to account for the turbulence modulation. Further details of the equations used for turbulence modulation modeling are given in Table A.4 in the Appendix.

The TFM equations are solved together with the appropriate boundary conditions. Johnson and Jackson (1987) were the first to classify the particle interactions at the wall as involving either long or short contacts. The longer contacts are assumed to be frictional contacts (diffuse in nature) between particles and the wall, while the shorter contacts are collisional contacts (specular in nature). Using the Johnson and Jackson (1987) boundary condition relations, the total stress is approximated as the sum of both frictional and collisional stress mechanism contributions. The Johnson and Jackson (1987) wall boundary conditions expresses the shear force at the wall ($\vec{\tau_s}$) and granular temperature at the wall (q_s) as follows:

$$\vec{\tau_s} = -\frac{\pi}{6}\sqrt{3}\varphi\frac{\alpha_s}{\alpha_{s,max}}\rho_s g_{0,ss}\sqrt{\Theta_s}\vec{U}_{s,II} \qquad [5.10]$$

$$q_s = \frac{\pi}{6}\sqrt{3}\varphi\frac{\alpha_s}{\alpha_{s,max}}\rho_s g_{0,ss}\sqrt{\Theta_s}\vec{U}_{s,II}.\vec{U}_{s,II} - \frac{\pi}{4}\sqrt{3}\frac{\alpha_s}{\alpha_{s,max}}(1-e_w{}^2)\rho_s g_{0,ss}{}^{3}/_{2} \qquad [5.11]$$

where $\vec{U}_{s,II}$ is the particle slip velocity parallel to the wall and $\alpha_{s,max}$ is the maximum solids volume fraction (packing limit). The parameter $g_{0,ss}$, called the radial distribution function, is presented in Appendix A.1 in the Appendix. The parameters φ and e_w are the specularity coefficient and the wall restitution coefficient, respectively, and they have to be specified for a given flow.

The Johnson and Jackson (1987) wall boundary condition assumes that particles can both collide with and slide on the wall. Two key parameters used in the Johnson and Jackson (1987) wall boundary condition are the specularity and wall restitution coefficients. The specularity coefficient defines the amount of particle slip at the wall, and the wall restitution coefficient describes the granular energy dissipation at the wall due to inelastic collisions (Li et al., 2010). The values of the parameters used in this study taken from Ahadi et al. (2019): the particle-particle restitution coefficient (e_{ss}), specularity coefficient (φ), and wall restitution coefficient (e_w) are set to 0.9, 0.004, and 0.7, respectively.

5.3 Description of simulation

A 1:13.3 scale model of the vortex-type pond based on Froude scaling laws was constructed in the Hydraulic Laboratory at the University of Saskatchewan to facilitate experimental measurements. For more details regarding the physical model construction see Chowdhury (2016). The pond structure consists of a circular pool with sloped walls (3H: 1V), a peripheral inlet pipe, a central elevated outlet, and an annular trapezoidal berm. The pond model was 2.86 m in diameter at the bed. The scaled sizes of the inlets and outlets were D = 60 mm and 90 mm, respectively. The inlet pipe is at an angle of 30° with the tangent line to the pond circumference at the point of entrance. A permanent pool is maintained in the model by using an elevated, top-closed outlet pipe perforated between 50% and 75% of the pipe's total height. The berm surrounds the central outlet and has sloped walls (2H: 1V). The optimum radial position of the berm causing the maximum amount of sediments to settle was determined to be at 60% of the bed diameter (Chowdhury 2016). An opening cuts through the top portion of 1/12th of the berm's circumference at the location where the flow completes one round of rotation. The opening directs the treated water from the main pool towards the outlet. The peak flow rate observed in the prototype pond was scaled down based on the Froude scaling law to Q = 1.55 L/s.

The 3D phasic mass and momentum equations along with a set of additional transport equations used to model the turbulence, were solved using the commercial software ANSYS Fluent 19.2. The TFM option referred to as "Eulerian model" in ANSYS Fluent 19.2 was used. FLUENT uses a control-volume-based technique to convert the governing partial differential equations to algebraic equations that can be solved numerically. The discretization used a second order upwind, except for the volume fraction equation where the QUICK scheme was used. A phase-coupled SIMPLE method was implemented for the pressure-velocity coupling.

The boundary conditions for the water phase are the same as those used in Chapter 3, the study wherein the flow pattern in this vortex type stormwater pond was previously simulated and partially

validated against experimental data. The boundary conditions for the solid phase follow those used in Ahadi et al. (2019), the study in which the sediment transport in an open channel flow was simulated and validated against flow and sediment concentration data. At the inlet, uniform profiles for the water velocity, sediment velocity, and solids volume fraction were specified. The velocity of the water and sediment were set to V = 0.55 m/s, the velocity corresponding to a flow rate of Q = 1.55 L/s. Two sets of simulations were carried out with two different bulk solid volume fractions of the sediment: $\alpha_s = 0.01$ and 0.025 (as used in Ahadi et al. 2019). The free surface of the water was modeled using a symmetry boundary condition for all flow properties, following previous studies, e.g. Hsu et al. (2003), Bombardelli and Jha (2009), and Liang et al. (2017). The bed boundary condition was a no-slip wall for the liquid phase and a partial-slip condition for the sediment phase using the boundary condition of Johnson and Jackson (1987). The Johnson and Jackson boundary condition was investigated previously in a TFM of open channel flow (Ahadi et al. 2019).

For the spatial discretization, an unstructured computational grid was generated in ANSYS Workbench 19.2. The numerical grid was refined near solid walls, e.g. the bed and sidewalls, to better capture the gradients in these regions. The grid dependence of the solution was assessed using three different grid resolutions. The coarsest grid used approximately 1.5 million control volumes; two finer grids were also considered, a medium grid with 2.5 million control volumes and a fine grid with 5 million control volumes. Each of the grids was generated in an iterative manner until it satisfied the accepted range for the three grid metrics, i.e. aspect ratio, skewness, and smoothness. These grid configurations were tested in Chapter 3 for the same geometry in the case of single-phase flow to assess grid dependence. In this study, the particle velocity profile at the channel centerline for radial section 0 (presented in Figure 5.2) for an inlet volume fraction of 0.025 was used to assess the grid dependence as an additional test in the two-phase case. This location was selected because it is representative of the most challenging region of the pond, i.e. the inlet jet region. The case with higher volume fraction was selected because it is more challenging to capture the particle velocity as the sediment concentration increases. In moving from the coarse grid to the medium grid, the velocity changed on average by approximately 5.3 %. In moving from the medium grid

to the fine grid, the tangential velocity changed on average by less than 1.2 %. Based on this comparison, the medium grid using 2.5 million control volumes was selected for the simulations as a reasonable compromise based on numerical resolution and computational cost. The time step selected for the simulations was 0.003 s. The simulation of a total real time of 30 s required from 180 to 240 hours (depending on the solids loading) to run on a Core™ i7-6800K CPU @ 3.4 GHz with a 128 GB RAM.
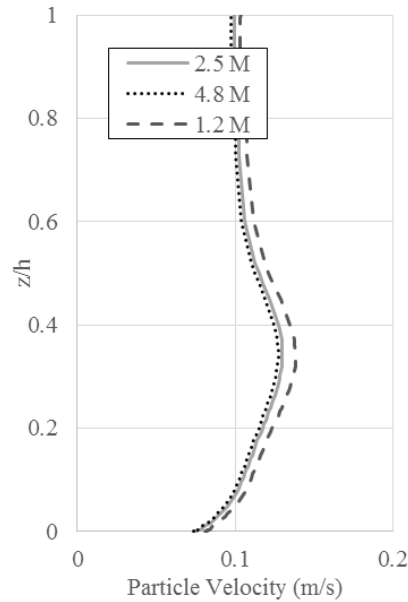
Figure 5.2 Centerline profiles of particle velocity on radial section 0 for inlet volume fraction of 0.025

5.4 Results and discussion

In this section, predictions of the liquid and particle velocity fields for two different inflow sediment concentrations based on the TFM framework are presented. The flow pattern was previously investigated in a parallel study using a 3D single-phase CFD simulation, and assessed against the mean and fluctuating velocity measurements. The results revealed that despite using a berm and tangential inlet pipe, two recirculation zones forms downstream of the jet. The first on the outside of the berm immediately downstream of the jet and the second further yet downstream on the inside of the berm (See Figure 5.1). The predictions also showed that inside the berm, there are two recirculation zones with opposite direction of rotation.

Figure 5.3 a), b) and c) show the liquid and particle velocity profiles at different radii, i.e. $r = 1.2$, 1.3, and 1.4 m, for an inflow volume fraction of 0.01 at section 0, the closest section to the location where the inflow enters the pond. At this location, the particle velocity follows the same pattern as for the liquid. The particle velocity remains slightly smaller than the liquid velocity throughout the depth and width of section 0, except for the near-bed region (up to z = 3 mm). The sediment transport is largely driven by the drag force of the liquid on the particle, hence the slip velocity observed. Recall that the sediment velocity is modeled by a partial slip boundary condition at the wall. Figure 5.3 d) compares the effect of volume fraction on the profiles at $r = 1.3$. With increase in the volume fraction, the mean liquid velocity drops because of the enhanced drag of the particles. While the liquid velocity approaches zero at the wall, the particle velocity at the wall is, respectively, 0.077 and 0.083 m/s for particle inflow volume fractions of 0.01 and 0.025.

In Figure 5.4, the transverse mean liquid velocity profile for $\alpha_s = 0.01$ is presented at section 0 (jet section). The jet diffuses as move above the discharge plane, and also shifts to the outer wall of the channel. For $\alpha_s = 0.025$, the same trend was seen. Overall, the velocity magnitude was reduced slightly due to the higher mass of particles being convected.

(a)   (b)

(c)   (d)
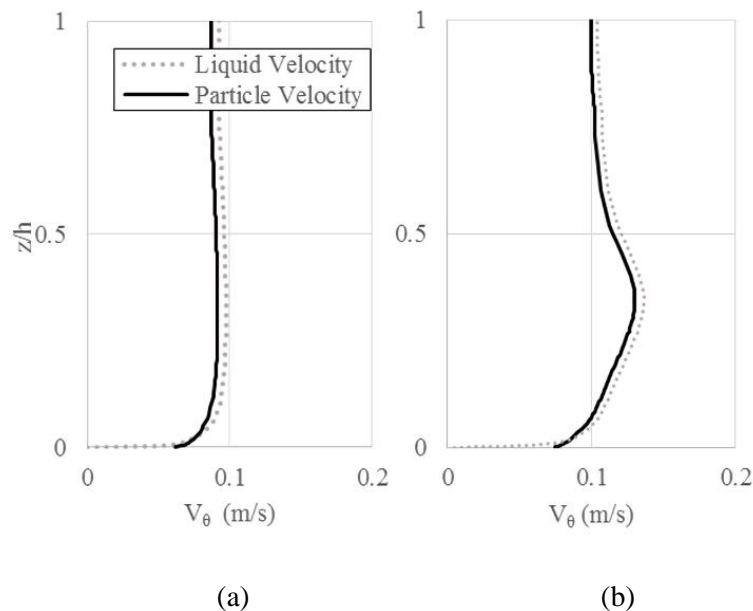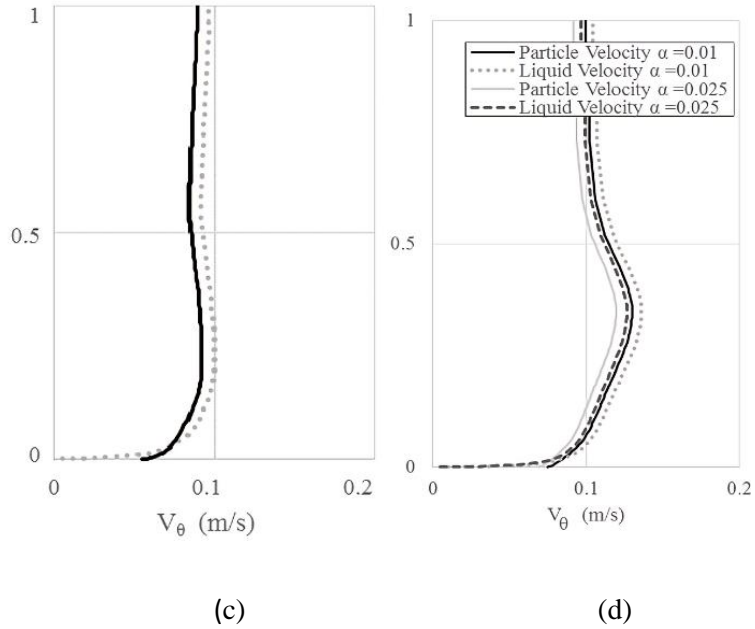
Figure 5.3 Mean liquid and particle velocity at section 0 at: (a) r = 1.2, (b) 1.3, and (c) 1.4 m for a volume fraction of 0.01, and (d) at r = 1.3 m for volume fractions of 0.01 and 0.025
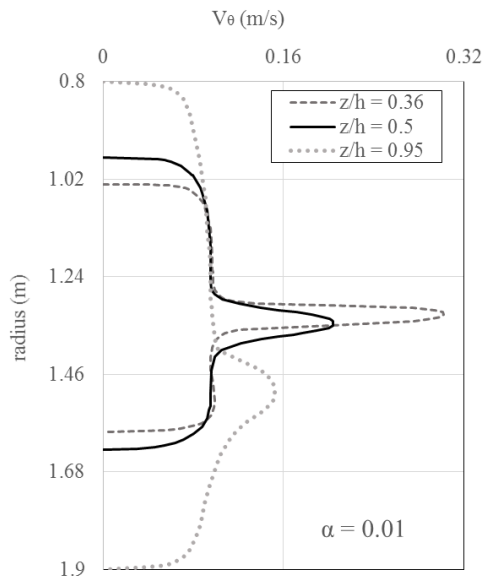
Figure 5.4 Mean liquid transverse velocity profiles at different depths for α = 0.01 at section 0

Figure 5.5 presents the mean liquid velocity at section 5 normalized by the friction velocity (u_*) for both sediment volume fractions, which is a canonical formulation of the velocity for a turbulent wall-

bounded flow. Also shown in the figure are the log-law relation for single-phase turbulent flow in the overlap region, as well as the linear profile in the viscous sublayer, given, respectively, by Equations [5.12a] and b.

$$u_l^+ = y^+ \qquad\qquad\qquad [5.12a]$$

$$u_l^+ = \frac{1}{\kappa}\ln y^+ + B \qquad\qquad\qquad [5.12b]$$

where $u_l^+ = u_l/u_*$ and $y^+ = y/u_*$. The von Karman constant was taken as $\kappa = 0.412$ and the constant B = 5.29 following Nezu and Rodi (1986). The values of the friction velocity ($u_* = \sqrt{\tau_w/\rho}$) for the flow at sediment volume fraction of $\alpha_s = 0.01$ and 0.025 were, respectively, 0.041 and 0.044 m/s. Both velocity profiles follow the general slope of the log-law curve over most of the channel depth and exhibit a reduction in magnitude near the water surface. The dimensionless liquid velocity profile for the larger volume fraction is displaced further downward from the log-law curve for single-phase flow due to a higher shear velocity at the wall.
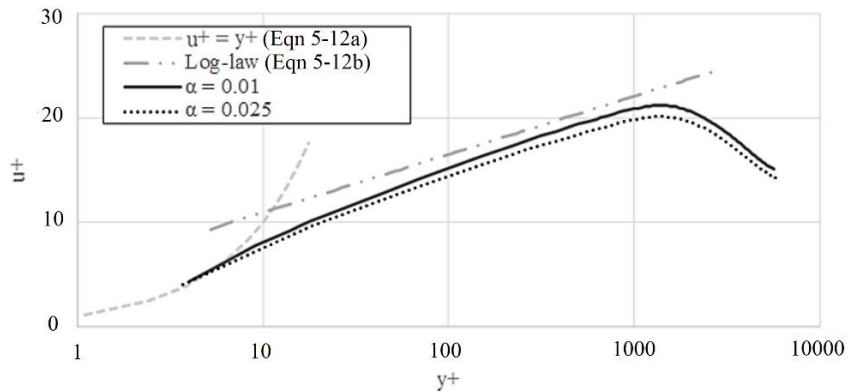
Figure 5.5 Mean liquid velocity profiles predicted for two bulk volume fractions

In Figure 5.6, the spatial variation of the sediment volume fraction is shown at different depths (z/h = 0.36, 0.5, and 0.95). The sediment volume fraction at the inlet is $\alpha_s = 0.01$. A significant fraction of sediments accumulates in the vicinity of the dead zone downstream of the jet (zone II characterized in

Figure 5.1). At z/h = 0.36, the small deadzone beside the inlet jet (zone I in Figure 5.1) also seems to trap some of the sediment. Moving towards the free surface, the sediment volume fraction reduces. In addition, the sediment is located more towards the outer wall, while the recirculation zone is actually located along the inner wall.

(a)   (b)   (c)
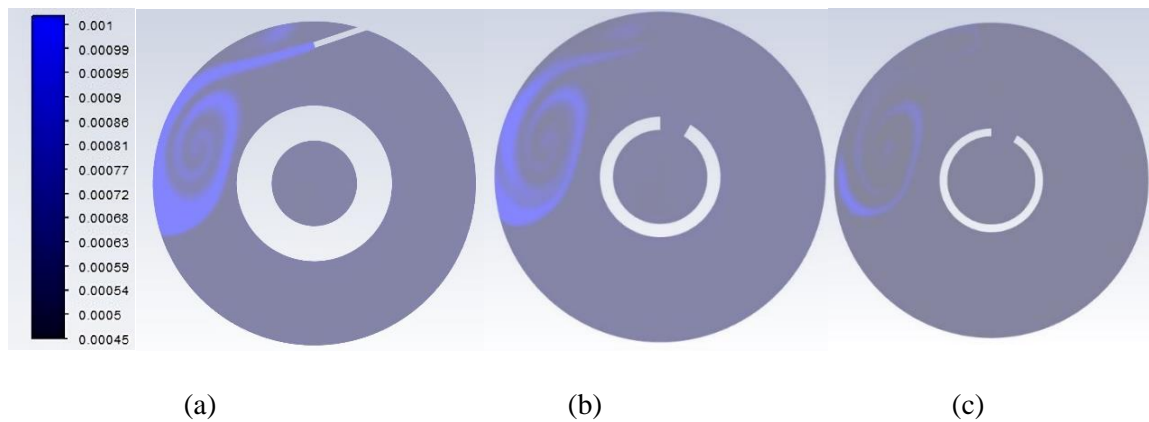
Figure 5.6 TFM predictions for sediment volume fraction distribution for α = 0.01 on different horizontal planes z/h = (a) 0.36, (b) 0.5, and (c) 0.95

Figure 5.7 presents profiles of the sediment volume fraction and granular temperature across the depth of the channel at the centerline of section 5. The sediment volume fraction and granular temperature both exhibit a peak value at the wall. Although the concetration peaks at the wall, the velocity at the wall is still finite due to the no-slip condition. The magnitudes of both properties reduce with distance from the bottom wall, quite dramatically at first and then more gradually in the upper region of the channel. For the two different sediment volume fractions, the profiles have the maximum difference at the bed. The granular temperature is greatest at the wall, where the particles are collide with the wall.

106
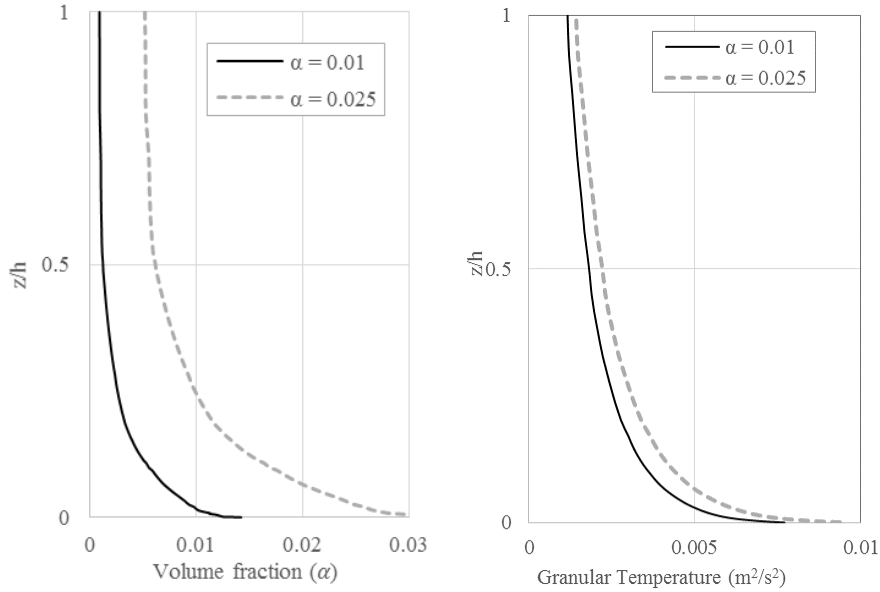
Figure 5.7 Profiles of sediment volume fraction and granular temperature at section 5 for $\alpha = 0.01$ and 0.025

5.5 Conclusion

Modern stormwater retention ponds sediment removal requirements lead to the need for understanding the sediment transport phenomenon in ponds. A TFM formulation together with a low-Reynolds-number $k-\varepsilon$ turbulence model was used to investigate the sediment transport in a new vortex-type stormwater retention pond. Different from traditional sediment transport models, the TFM uses two-phase theory, and thus, has no need to invoke any empirical sediment transport formulas. After validating the TFM in simulating sediment transport in an open channel flow in Chapter 4, and studying the flow pattern in the new vortex-type stormwater retention pond experimentally and computationally in Chapter 3, in this chapter, the TFM was applied to explore the sediment transport in the new vortex-type pond. The model predictions of the liquid and sediment velocity profiles and sediment volume fraction were documented for two different inflow sediment volume fractions.

The TFM prediction for the sediment concentration varied significantly over the pond area: most of the sediment was accumulated in the areas characterized as dead zones I and II in Chapter 3. The sediment velocity profile was characterized by a partial-slip value at the bottom wall as determined by the Johnson

and Jackson (1987) boundary conditions. The flow was characterized by a small slip velocity between the two phases, with the liquid velocity being slightly larger than the particle velocity over most of the channel depth. This steady flow dilute sediment concentration case is a starting point in applying the TFM in the context of storage ponds. The next step would be to incorporate even more physics by testing non-dilute sediment concentration and include deposition/resuspension phonemenon.

Chapter Six

6. CONCLUDING REMARKS AND FUTURE WORK

6.1 Thesis Summary

CFD modeling has been shown to provide useful information for improving new pond designs and testing the capability of retrofitting elements to improve pond performance. To begin with, the literature of stormwater retention ponds was reviewed to identify the role of different computational modeling approaches. Computational modeling of the ponds is performed using either single-phase or two-phase modeling. Both single-phase and two-phase modeling approaches were implemented and demonstrated in a new vortex-type pond. The key charateristics of this pond are its circular shape, peripheral inlet, and central outlet.

To demonstrate the use of single-phase numerical models, a 3D CFD model of a new vortex-type pond was validated against the flow measurements taken by the author in a scale physical model. Single-phase models ignore the presence of sediment and focus on the fluid flow pattern. Understanding the flow pattern within the pond provided useful information to understand the sediment removal potential because flow and sediment behaviour are interconnected. For example, flow patterns containing dead-zones or short-circuiting reduce the ability of the pond to remove sediment.

For developing a two-phase CFD model of sediment transport, an Eulerian-Eulerian TFM was chosen. TFMs are able to include significant features of sediment transport in a pond, including the sediment-fluid, sediment-sediment, and sediment-wall interactions. The computational time required for two-phase modeling can be more than double that of single-phase models due to solving extra sets of coupled nonlinear partial differential equations. To apply the TFM to the vortex-type pond with multiple levels of complexity, a step-by-step modeling approach was required. Before applying the model to the vortex-type pond, the predictions of the TFM were assessed using a known problem with available data.

An open channel flow, for which the sediment data was available, was modeled to explore the TFM performance and to evaluate the predictions for the velocity and sediment concentration in the channel.

Lastly, in a preliminary study of the dilute sediment distribution in the pond, the TFM was to used to assess the vortex-type pond performance (without sediment deposition). Insight on sediment phase velocity and concentration in the pond was obtained.

6.2 Conclusions and contributions

This thesis provided specific insight on the flow features of a vortex-type pond and demonstrated the use of multiphase CFD modeling to predict the fluid flow and sediment distribution in the pond for the case of steady and dilute flow.

A comprehensive data base of measured mean and fluctuating velocity field in the vortex-type pond was provided. The flow pattern in the pond was modeled using a 3D single-phase CFD simulation, and then assessed against the measurements. In general, the agreement between predictions and measurements was good. The computational predictions provided enhanced knowledge of the flow pattern in this new pond design. The results revealed that despite using a berm and tangential inlet pipe, two relatively large recirculation zones form downstream of the jet clinging to the outer and inner walls of the berm. The results also showed that discharge flow from the berm does not form a single large vortex pattern as expected. Instead, there are two recirculation zones inside the outlet pipe, swirling in opposite directions. Overall, the flow predictions obtained with CFD were informative in terms of assessing the performance of the vortex-type pond.

An Eulerian-Eulerian TFM was tested in a fully developed open channel flow against flow and sediment measurements (Chapter 4). The TFM formulation together with a low-Reynolds-number $k-\varepsilon$ turbulence model was applied; it included the effect of the sediment particles on the turbulence field. The particle-wall boundary condition was also investigated. The model predictions of the liquid and

sediment velocity profiles, sediment concentration, turbulence statistics and fluctuating particle velocity field were documented for two different test cases of the equilibrium open channel flow. An important conclusion was that the TFM using constitutive equations based on granular kinetic theory, coupled with a low-Reynolds-number turbulence model, was able to predict the liquid and sediment transport well in an equilibrium channel without resorting to the empirical ad hoc relations often used to determine the concentration profile.

Lastly, the flow and sediment dynamics in the vortex-type stormwater retention pond were computationally studied using the two-fluid methodology. To our knowledge, this was the first study of applying the TFM to investigate flow and sediment transport in a stormwater retention pond. The model predictions of the liquid and sediment velocity profiles, and sediment concentration were documented for two different inflow sediment volume fractions. A significant conclusion is that the recirculation zones documented single-phase CFD study are characterized by relatively high concentrations of sediment.

6.3 Future work

Going forward, in the pursuit of higher sediment removal efficiency, the application of CFD to model flow and sediment transport in stormwater retention ponds is promising. However, the methodology of the TFM is still under development and the capability is still being explored. Based on the contributions and conclusions of this research work, some recommendations for future work are as follows:

(1) Further development of the two-fluid CFD model will require new experimental studies that can provide comprehensive measurements of both the mean and fluctuating flow properties of both phases, in scale-model and prototype ponds. In particular, taking velocity and concentration measurements of sediment particles will provide data that can be used for validation of the TFM in the pond.

(2) The next step in the application of the TFM to predicting sediment transport in open channel flow, and in turn in stormwater ponds, is to consider the case where sediment is being deposited on the

bed and also being re-suspended into the flow. The current model is complete and theoretically capable of predicting the deposition and re-suspension of particles. An important factor to explore would be effect of turbulence on deposition and re-suspension of the sediment partciels.

(3) Related to the above challenge is the need to model transport with non-dilute (or dense) sediment concentrations using the TFM methodology. In this case, the frictional stress components must be included since there is sustained contact between particles.

(4) Another effort that would advance modeling of storage ponds is to extend sediment transport models in the TFM to consider more realistic sizes and shapes of particles, e.g. polydisperse flow which is most often the case in natural ponds. One possible approach is to regard different sediment sizes as separate phases. Particle-particle momentum interaction terms need to be developed between sediment phases of different sizes.

(5) Exploring the effect of other turbulence model formulations can further advance the application of TFMs to retention ponds. Advanced turbulence models, i.e. LES and DNS, with sufficient resolution, are able to provide an enhanced level of physical realism by resolving the flow around the sediment particles. Investigation of the effect of a second moment closure is another possible direction for future development. A second moment treatment can give superior predictive accuracy by removing the isotropy assumption. This can be specifically functional in modeling turbulence-driven secondary motions in curved channels such as the vortex-type stormwater pond.

(6) Finally, there are specific aspects of pond simulation by CFD that require further consideration. These include the following:

- the treatment of boundaries such as the free surface including the effects of wind, and modelling bed roughness due to the sediment particles and/or vegetation.

- Modeling a more realistic unsteady discharge event; this will require an unsteady simulation, which is much more costly.

- Modeling an actual pond versus a model pond; the scale will change, and the simulation will be more costly.

Appendix

This appendix contains the tables referenced in Chapters 4 and 5.

Table A.1 Set of TFM closure equations

Sediment bulk viscosity λ_s by Lun *et al.* (1984) e_{ss} =particle-particle restitution coefficient	$$\lambda_s = \frac{4}{3}\alpha_s\rho_s d g_{0,ss}(1 + e_{ss})\left(\frac{\Theta_s}{\pi}\right)^{0.5}$$
Collisional part of sediment shear viscosity $\mu_{s,col}$ by Syamlal *et al.* (1993)	$$\mu_{s,col} = \frac{4}{5}\alpha_s\rho_s d g_{0,ss}(1 + e_{ss})\left(\frac{\Theta_s}{\pi}\right)^{0.5}$$
Kinetic part of sediment shear viscosity $\mu_{s,kin}$ by Syamlal *et al.* (1993)	$$\mu_{s,kin} = \frac{\alpha_s\rho_s d\sqrt{\pi\Theta_s}}{6(3 - e_{ss})}[1 + \frac{2}{5}(1 + e_{ss})$$ $$(3e_{ss} - 1)\alpha_s g_{0,ss}$$
Solid pressure	$$P_s = \alpha_s\rho_s\Theta_s + 2\rho_s(1 + e_{ss})\alpha_s^2 g_{0,ss}\Theta_s$$
Radial distribution function, $g_{0,ss}$	$$g_{0,ss} = \left[1 - \left(\frac{\alpha_s}{\alpha_{s,max}}\right)^{\frac{1}{3}}\right]^{-1}$$

Table 6.2 Set of sediment phase granular temperature equations

The sediment granular temperature (Θ_s)	$3\Theta_s = \langle u_s'u_s'\rangle + \langle v_s'v_s'\rangle + \langle w_s'w_s'\rangle$
Granular temperature production term ($\mathcal{P}_s$)	$\mathcal{P}_s = (\tau_{xx,s})\frac{2\partial u}{\partial x} + (\tau_{xx,s})\left(\frac{\partial u}{\partial y} + \frac{\partial v}{\partial x}\right) + (\tau_{y,s})\frac{2\partial v}{\partial y}$
Granular temperature diffusion term ($\mathcal{D}_s$)	$$\mathcal{D}_s = \frac{\partial}{\partial x}\left(K_{\Theta_s}\frac{\partial\Theta_s}{\partial x}\right) + \frac{\partial}{\partial y}\left(K_{\Theta_s}\frac{\partial\Theta_s}{\partial y}\right)$$
Diffusion coefficient for granular energy (K_{Θ_s}) $\eta = 0.5(1 + e_{ss})$	$$K_{\Theta_s} = \frac{15\alpha_s\rho_s d_s\sqrt{\pi\Theta_s}}{4(41-33\eta)}[1 + \frac{12}{5}\eta^2(4\eta - 3)\alpha_s g_{0,ss} +$$ $$\frac{16}{15\pi}(41 - 33\eta)\eta\alpha_s g_{0,ss}$$
Rate of energy dissipation within the sediment phase due to collisions from Lun *et al.* (1984)	$$\gamma_{\Theta_s} = \frac{12(1-e_{ss}^2)g_{0,ss}}{d_s\sqrt{\pi}}\alpha_s^2\rho_s\Theta_s^{3/2}$$

Energy exchange between liquid and sediment phases from Gidaspow *et al.* (1992)	$\emptyset_{ls} = -3K_{ls}\Theta_s$

Table A.3 Set of liquid phase turbulence modeling equations

Reynolds stress tensor for liquid phase (Boussinesq hypothesis)	$\tau_{turb,l} = \rho_l \mu_{turb,l}\left(\nabla\vec{U}_l + \nabla\vec{U}_l^{\ T}\right) - \dfrac{2}{3}\rho_l\left(k_l + \mu_{turb,l}\nabla.\vec{U}_l\right)\bar{\bar{I}}$
Turbulent viscosity in terms of turbulence kinetic energy $(C_\mu = 0.09)$	$\mu_{turb,l} = \rho_l C_\mu \dfrac{k_l^{\ 2}}{\epsilon_l}$
k equation for liquid phase $(\sigma_k = 1)$	$\nabla.(\alpha_l\rho_l\vec{u}_l k_l) = \nabla.\left(\alpha_l\dfrac{\mu_{turb,l}}{\sigma_k}\nabla k_l\right) + \alpha_l G_l - \alpha_l\rho_l\epsilon_l + \alpha_l\rho_l\Pi_{k_l}$
ϵ equation for liquid phase $(C_{1\epsilon} = 1.44, C_{2\epsilon} = 1.92, \sigma_\epsilon = 0.75)$	$\nabla.(\alpha_l\rho_l\vec{u}_l\epsilon_l) = \nabla.\left(\alpha_l\dfrac{\mu_{turb,l}}{\sigma_\epsilon}\nabla\epsilon_l\right) + \alpha_l\dfrac{\epsilon_l}{k_l}(C_{1\epsilon}G_l - C_{2\epsilon}\rho_l\epsilon_l) + \alpha_l\rho_l\Pi_{\epsilon_l}$
Production of turbulence kinetic energy due to mean velocity gradients (G_l)	$G_l = \mu_{turb,l}\,S^2$
Modulus of the mean rate-of-strain tensor (S)	$S = \sqrt{2S_{ij}S_{ji}}$

Table A.4 Turbulence modulation equations

Influence of the dispersed phase on the continuous phase Π_{k_l} by Simonin and Viollet (1990)	$\Pi_{k_l} = \dfrac{K_{ls}}{\alpha_l\rho_l}[k_{ls} - 2k_l + (\vec{v}_l - \vec{v}_s).\vec{v}_{dr}]$

Influence of the dispersed phase on the continuous phase Π_{ϵ_l} by Simonin and Viollet (1990)	$$\Pi_{\epsilon_l} = C_{3\epsilon} \frac{\epsilon_l}{k_l} \Pi_{k_l}$$
Drift velocity ($\vec{v}_{dr}$)	$$u_{dr} = -D_{ls}.\left(\frac{1}{\alpha_s}\frac{\partial \alpha_s}{\partial x} - \frac{1}{\alpha_l}\frac{\partial \alpha_l}{\partial x}\right)$$ $$v_{dr} = -D_{ls}.\left(\frac{1}{\alpha_s}\frac{\partial \alpha_s}{\partial y} - \frac{1}{\alpha_l}\frac{\partial \alpha_l}{\partial y}\right)$$
Liquid-particle dispersion tensor by Tchen theory ($D_{ls} = D_{t,ls}$)	$$D_{t,ls} = \frac{1}{3}k_{ls}\tau^t{}_{ls}$$
Turbulence quantities for sediment phase based on Simonin and Viollet (1990)	$$k_s = k_l\left(\frac{\eta_{ls}}{1+\eta_{ls}}\right)$$ $$k_{ls} = 2k_l\left(\frac{\eta_{ls}}{1+\eta_{ls}}\right)$$ $$D_s = D_{t,ls} + \left(\frac{2}{3}k_s\right)\tau^F{}_{ls}$$
Ratio between these two characteristic times (η_{ls})	$$\eta_{ls} = \frac{\tau^t{}_{ls}}{\tau^F{}_{ls}}$$
Characteristic particle relaxation time connected with inertial effects acting on sediment phase ($\tau^F{}_{ls}$)	$$\tau^F{}_{ls} = \frac{\rho_l d_l^2}{18\mu_c f}\left(1 + 0.5\frac{\rho_l}{\rho_s}\right)$$ $$f = \frac{C_D . Re}{24}$$
Eddy particle interaction time or the Lagrangian integral time scale calculated along particle trajectories ($\tau^t{}_{ls}$) by Csanady (1963)	$$\tau^t{}_{ls} = \frac{\tau^t{}_l}{\sqrt{(1 + C_\beta \xi_\tau{}^2)}}$$ $$\xi_\tau = \frac{|\vec{U_s} - \vec{U_l}|}{\sqrt{\frac{2}{3}k_l}}$$
θ is the angle between the mean particle velocity and the mean relative velocity	$$C_\beta = 1.8 - 1.35\cos^2\theta$$
Time scale of the energetic turbulence eddies	$$\tau^t{}_l = \frac{3}{2}C_\mu\frac{k_l}{\epsilon_l}$$

References

Adamsson, Å. (1999). Computational fluid dynamics for detention tanks: simulation of flow pattern and sedimentation.

Adamsson, Å., Stovin, V., and Bergdahl, L. (2003). Bed shear stress boundary condition for storage tank sedimentation. Journal of Environmental Engineering, 129(7), 651-658.

Adamsson, Å., Bergdahl, L., and Lyngfelt, S. (2005). Measurement and three-dimensional simulation of flow in a rectangular detention tank. Urban Water Journal, 2(4), 277-287.

Aghaee, Y., and Hakimzadeh, H. (2010). Three dimensional numerical modeling of flow around bridge piers using LES and RANS. River Flow, Dittrich, Koll, Aberle & Geisenhainer. 211–218.

Ahadi, M., Bergstrom, D. J., and Mazurek, K. A. (2019). Application of the two-fluid model to prediction of sediment transport in turbulent open channel flow. Physics and Chemistry of the Earth, Parts A/B/C, 113, 73-82.

Ahadi, M., Bergstrom, D. J., and Mazurek, K. A. (2020). Computational Fluid-Dynamics Modeling of the Flow and Sediment Transport in Stormwater Retention Ponds: A Review. Journal of Environmental Engineering, 146(9), 03120008, 14 pages.

Al-Rubaei, A. M., Merriman, L. S., Hunt, W. F., Viklander, M., Marsalek, J., and Blecken, G. T. (2017). Survey of the operational status of 25 Swedish municipal stormwater management ponds. Journal of Environmental Engineering, 143(6), 05017001.

Allafchi, F., Valeo, C., He, J., and Neumann, N. F. (2019). An Integrated Hydrological-CFD Model for Estimating Bacterial Levels in Stormwater Ponds. Water, 11(5), 1016.

Albers, C., and Amell, B. (2010). Changing the Stormwater Pond Design Game. NOVATECH 2010.

Amoudry, L., Hsu, T. J., and Liu, P. F. (2008). Two-phase model for sand transport in sheet flow regime. Journal of Geophysical Research: Oceans, 113(C03011). Doi: 10.1029/2007/JC004179.

Arnold, J.A., D.E. Line, S. W. Coffey, and J. Spooner. (1993). Stormwater Management Guidance Manual. North Carolina Cooperative Extension Service and North Carolina Division of Environmental Management. Raleigh, N.C.

Aryal, R., Vigneswaran, S., Kandasamy, J., and Naidu, R. (2010). Urban stormwater quality and treatment. Korean Journal of Chemical Engineering, 27(5), 1343-1359.

Asano, T. (1995). Sediment transport under sheet-flow conditions. J. Wtrwy Port Coastal Ocean Engng 121(5), 1-8.

Bagnold, R. A. (1956). The flow of cohesionless grains in fluids. Philosophical Transactions of the Royal Society of London. Series A, Mathematical and Physical Sciences, 249(964), 235-297.

Baines, W. D., and Knapp, D. J. (1965). Wind driven water currents. Journal of the Hydraulics Division, ASCE, 91(2), 205-221.

Bakhtyar, R., Barry, D. A., Li, L., Jeng, D. S., and Yeganeh-Bakhtiary, A. (2009). Modeling sediment transport in the swash zone: A review. Ocean Engineering, 36(9), 767-783.

Balachandar, S., and Eaton, J. K. (2010). Turbulent dispersed multiphase flow. Annual Review of Fluid Mechanics, 42, 111-133.

Barbosa, A. E., Fernandes, J. N., and David, L. M. (2012). Key issues for sustainable urban stormwater management. Water research, 46(20), 6787-6798.

Birch, S., Donahue, R., Biggar, K. W., and Sego, D. C. (2007). Prediction of flow rates for potable water supply from directionally drilled horizontal wells in river sediments. Journal of Environmental Engineering and Science, 6(2), 231-245.

Binns, A. D., Fata, A., Ferreira da Silva, A. M., Bonakdari, H., and Gharabaghi, B. (2019). Modeling Performance of Sediment Control Wet Ponds at Two Construction Sites in Ontario, Canada. Journal of Hydraulic Engineering, 145(4), 05019001.

Birch, S., Donahue, R., Biggar, K. W., and Sego, D. C. (2007). Prediction of flow rates for potable water supply from directionally drilled horizontal wells in river sediments. Journal of Environmental Engineering and Science, 6(2), 231-245.

Bombardelli, F. A., & Jha, S. K. (2009). Hierarchical modeling of the dilute transport of suspended sediment in open channels. Environmental fluid mechanics, 9(2), 207.

H. N. C. Breusers, and A. J. Raudkivi. Scouring. International association for Hydraulic Research (IAHR), Hydraulic Structures Design Manual 2. A.A. Balkema, Rotterdam, The Netherlands, 1991.

Cao, Z., Wei. L., and Xie, J. (1995). Sediment-laden flow in open channels from two-phase flow viewpoint. Journal of Hydraulic Engineering. 121(10), 725-735.

Center for Watershed Protection (2007). National Pollutant Removal Performance Database: Version 3. Center for Watershed Protection, Elliot City, MD, United States.

Chanson, H. (2008). Acoustic Doppler velocimetry (ADV) in the field and in laboratory: practical experiences. International Meeting on Measurements and Hydraulics of Sewers, Hydraulic Model Report No. CH70/08, Division of Civil Engineering, The University of Queensland, Brisbane, Australia.

Chowdhury, R. (2016). Assessment of flow conditions in a new vortex-type stormwater retention pond using a physical model. M.Sc. Thesis. Department of Civil and Geological Engineering, University of Saskatchewan, Saskatoon, Canada.

Chen, H. C., and Patel, V. C. (1988). Near-wall turbulence models for complex flows including separation. AIAA journal, 26(6), 641-648.

Cheng, Z., Hsu, T. J., & Calantoni, J. (2017). SedFoam: A multi-dimensional Eulerian two-phase model for sediment transport and its application to momentary bed failure. Coastal Engineering, 119, 32-50.

Cheng, Z., Hsu, T. J., and Chauchat, J. (2018). An Eulerian two-phase model for steady sheet flow using large-eddy simulation methodology. Advances in Water Resources, 111, 205-223.

Chapman, S., and Cowling, T. G. (1970). The Mathematical Theory of Non-Uniform Gases, Cambridge Univ. Press, Cambridge, England.

Chen, X. (2005). A comparison of hydrostatic and nonhydrostatic pressure components in seiche oscillations. Mathematical and computer modelling, 41(8-9), 887-902.

City of Calgary. (2011). Stormwater management and design manual. Calgary, Alberta, Canada.

City of Edmonton (2008). Stormwater quality control strategy ad action plan, Edmonton, Alberta, Canada.

City of Saskatoon (2018). Design and development standard manual. Section six. Stormwater drainage system, Saskatoon, Saskatchewan, Canada

Comings, K. J., Booth, D. B. and Horner, R. R. (2000). Storm water pollutant removal by two wet ponds in Bellevue, Washington. Journal of Environmental Engineering. 126, 321–30.

G.T. Csanady. Turbulent diffusion of heavy particles in the atmosphere. J. Atmospheric Sci., 20(3), 201-208, 1963.

Cundall, Peter A. (1988). Formulation of a three-dimensional distinct element model—Part I. A scheme to detect and represent contacts in a system composed of many polyhedral blocks. International Journal of Rock Mechanics and Mining Sciences and Geomechanics Abstracts, 25 (3).

Danish Hydraulic Institute (DHI) (1996). MIKE 21 user guide and reference manual. Horsholm, Denmark.

Drew, D. A. (1975). Turbulent sediment transport over a flat bottom using momentum balance. Transactions of the ASME, 38-44.

D.A. Drew. Mathematical Modeling of Two-phase Flow. Annu. Rev. Fluid Mech., 15:261–291, 1983.

Dufresne, M., Vazquez, J., Terfous, A., Ghenaim, A., and Poulet, J. B. (2009). Experimental investigation and CFD modelling of flow, sedimentation, and solids separation in a combined sewer detention tank. Computers and Fluids, 38(5), 1042-1049.

Durbin, P. A., Medic, G., Seo, J. M., Eaton, J. K., and Song, S. (2001). Rough wall modification of two-layer $k-\varepsilon$. Journal of Fluids Engineering, 123(1), 16-21.

Einstein H.A., and Chien N. (1955). Effects of heavy sediment concentration near the bed on velocity and sediment distribution. MRD sediment series report. University of California, Berkley.

Elghobashi, S. (1994). On predicting particle-laden turbulent flows. Applied scientific research, 52(4), 309-329.

Enwald, H., Peirano, E., and Almstedt, A. E. (1996). Eulerian two-phase flow theory applied to fluidization. International Journal of Multiphase Flow, 22 (S), 21-66.

Farjood, A. (2016). A Study in the Performance of Sediment Retention Ponds, Ph.D. thesis, Civil Engineering, University of Auckland, Auckland, New Zealand.

Farjood, A., Melville, B. W., and Shamseldin, A. Y. (2014). A study in hydraulic performance indices for Sediment Retention Ponds. 7th International Conference on Fluvial Hydraulics (River Flow2014), 3-5 September, Lausanne, Switzerland.

Fraga, B., Peña, E., and Cea, L. (2012). Modeling of shallow curved flows with 3D unsteady RANS. Numerical Methods for Hyperbolic Equations: Theory and Applications, 113-120, CRC Press, Taylor & Francis Group, New York, US.

Garg, R., Narayanan, C., Lakehal, D., and Subramaniam S. (2007). Accurate numerical estimation of interphase momentum transfer in Lagrangian-Eulerian simulations of dispersed two-phase flows. International Journal of Multiphase Flow 33 (12), 1337–1364.

German, J., and Svensson, G. (2005). Stormwater pond sediments and water characterization and assessment. Urban Water Journal, 2(1), 39-50.

D. Gidaspow, R. Bezburuah, and J. Ding. Hydrodynamics of circulating fluidized beds, kinetic theory approach. In Fluidization VII, Proceedings of the 7th Engineering Foundation Conference on Fluidization, Brisbane, Australia, 75-82, 1992.

Gillis, C., Mazurek, K., Putz, G., and Albers, C. Gillis, C., Mazurek, K., Putz, G., and Albers, C. (2015). Field measurements of the flow pattern in a stormwater retention pond. E-proceedings of the 36th IAHR World Congress, 28 June, Hague, Netherlands.

Gillis, C. J. (2017). The Flow Pattern, Solids Settling, and Characteristics of a Saskatoon, Saskatchewan Stormwater Management Pond. Master thesis. Civil, Environmental, and Geological Engineering, University of Saskatchewan.

T. Li, J. Grace, and X. Bi. Study of wall boundary condition in numerical simulations of bubbling fluidized beds. Powder Technol., 203(3), 447-457, 2010.

Greimann, B. P., Muste, M., and Holly Jr, F. M. (1999). Two-phase formulation of suspended sediment transport. Journal of Hydraulic Research. 37, 479-500.

Greimann, B. P., and Holly Jr, F. M. (2001). Two-phase flow analysis of concentration profiles. Journal of Hydraulic Engineering. 127(9), 753-762.

Gu, L., Dai, B., Zhu, D. Z., Hua, Z., Liu, X., van Duin, B., and Mahmood, K. (2017). Sediment modelling and design optimization for stormwater ponds. Canadian Water Resources Journal/Revue canadienne des ressources hydriques, 42(1), 70-87.

Hanjalić, K., and Launder, B. (2011). Modelling turbulence in engineering and the environment: second-moment routes to closure. Cambridge university press.

He, C., and Marsalek, J. (2013). Enhancing sedimentation and trapping sediment with a bottom grid structure. Journal of Environmental Engineering, 140(1), 21-29.

Hirt C. W., and Nichols B.D. (1981). Volume of fluid methods for the dynamics of free boundaries. Journal of computational physiscs, 39.

Hodges, B. R. (2000). Numerical Techniques in CWR-ELCOM (code release v.1), CWR, Manuscript WP, 1422 BH. Centre Water Resources, Nedlands, Western Australia, Australia.

Hsu, T.J., Jenkins, J.T. and Liu, P.L.F (2003). On two-phase sediment transport: Dilute flow. Journal of Geophysics Research: Oceans, 108(C3), 3057.

Hsu, T. J., Traykovski, P. A., & Kineke, G. C. (2007). On modeling boundary layer and gravity-driven fluid mud transport. Journal of Geophysical Research: Oceans, 112(C04011).

Jarman, D. S., Faram, M. G., Butler, D., Tabor, G., Stovin, V. R., Burt, D., and Throp, E. (2008). Computational fluid dynamics as a tool for urban drainage system analysis: A review of applications and best practice. 11th International Conference on Urban Drainage, 31 August- 5 September, Edinburgh, Scotland, United Kingdom.

Jaw, S. Y., and Chen, C. J. (1998). Present status of second order closure turbulence models. II. Applications. Journal of Engineering Mechanics, 124(5), 502-512.

Jha, S.K., and Bombardelli, F.A. (2009). Hierarchical modeling of the dilute transport of suspended sediment in open channels. Environmental Fluid Mechanics, 9 (2), 207.

Jha, S. K., and Bombardelli, F. A. (2010). Toward two-phase flow modeling of non-dilute sediment transport in open channels. Journal of Geophysical Research: Earth Surface, 115(F03015).

Jha, S. K., and Bombardelli, F. A. (2011). Theoretical/numerical model for the transport of non-uniform suspended sediment in open channels. Advances in water resources, 34(5), 577-591.

Jenkins, J. T., and Hanes, D. M. (1998). Collisional sheet flows of sediment driven by a turbulent fluid. Journal of Fluid Mechanics, 370, 29-52.

Johnson, P.C., Jackson, R., (1987). Frictional–collisional constitutive relations for granular materials, with application to plane shearing. J. Fluid Mech. 176, 67–93.

Kaftori, D., Hetsroni, G., and Banerjee, S. (1995). Particle behavior in the turbulent boundary layer. I. Motion, deposition, and entrainment. Physics of Fluids, 7(5), 1095-1106.

Kantrowitz, I. H., & Woodham, W. M. (1995). Efficiency of a stormwater detention pond in reducing loads of chemical and physical constituents in urban streamflow, Pinellas County, Florida (Vol. 94, No. 4217). US Department of the Interior, US Geological Survey.

Kempe, T., & Fröhlich, J. (2012). Collision modelling for the interface-resolved simulation of spherical particles in viscous fluids. Journal of Fluid Mechanics, 709, 445-489.

Kempe, T., Vowinckel, B., & Fröhlich, J. (2014). On the relevance of collision modeling for interface-resolving simulations of sediment transport in open channel flow. International Journal of Multiphase Flow, 58, 214-235.

Kjelland, M. E., Woodley, C. M., Swannack, T. M., and Smith, D. L. (2015). A review of the potential effects of suspended sediment on fishes: potential dredging-related physiological, behavioral, and transgenerational implications. Environment Systems and Decisions, 35(3), 334-350.

Khan, S., Melville, B. W., Shamseldin, A. Y., and Fischer, C. (2012). Investigation of flow patterns in storm water retention ponds using CFD. Journal of Environmental Engineering, 139(1), 61-69.

Khan, S., Melville, B. W., and Shamseldin, A. Y. (2009). Modeling the layouts of stormwater retention ponds using residence time. In 4th IASME/WSEAS International Conference on Water Resources, Hydraulics and Hydrology, 77-83, University of Auckland, Auckland, New Zealand.

Khosronejad, A., and Sotiropoulos, F. (2014). Numerical simulation of sand waves in a turbulent open channel flow. Journal of Fluid Mechanics, 753 (2), 150–216.

Kloss, C., Goniva, C., Hager, A., Amberger, S., and Pirker, S. (2012). Models, algorithms and validation for open source DEM and CFD-DEM, 12(23), 140–152.

Kolahdoozan, M., Ahadi, M. S., and Shirazpoor, S. (2014). Effect of turbulence closer models on the accuracy of MPS method for the viscous free surface flow. Scientia Iranica, 21(4), 1217-1230.

Launder, B. E. (1989). Second-moment closure: present… and future?. International Journal of Heat and fluid flow, 10(4), 282-300.

B.E. Launder, B.I. Sharma. Application of the energy-dissipation model of turbulence to the calculation of flow near a spinning disc. Lett. Heat Mass Transfer, 1:131-138, 1974.

Laurent, J., Finaud-Guyot, P., Wanko, A., Bois, P., and Mosé, R. (2013). Hydrodynamic of artificial wetlands at the outlet of urban catchment: complementarity of the systemic approach and computational fluid dynamics tools. Récents Progrès en Génie des Procédés, 104.

Leupi, C., & Altinakar, M. S. (2005, May). 3D Finite Element Modeling of Free-Surface Flows with Efficient k–ε Turbulence Model and Non-hydrostatic Pressure. In International Conference on Computational Science (pp. 33-40). Springer, Berlin, Heidelberg.

Levenspiel, O. (2012). The tanks-in-series model. In Tracer Technology (pp. 81-97). Springer, New York, NY.

Li, Y., Deletic, A., and Fletcher, T. D. (2007). Modelling wet weather sediment removal by stormwater constructed wetlands: Insights from a laboratory study. Journal of Hydrology, 338(3-4), 285-296.

Lin, B., and Falconer, R. A. (1997). Three-dimensional layer-integrated modelling of estuarine flows with flooding and drying. Estuarine, coastal and shelf science, 44(6), 737-751.

Liang, L., Yu, X., and Bombardelli, F. (2017). A general mixture model for sediment laden flows. Advances in Water Resources, 107, 108-125.

Liu, D., Liu, X., Fu, X., Wang, G., (2016). Quantification of the bed load effects on turbulent open-channel flows. Journal of Geophysics Research on Earth Surface. 121 (4), 767–789, ISSN 2169–9011.

Lun, C.K.K., Savage, S.B., Jeffrey, D.J. and Chepurniy, N. (1984). Kinetic theories for granular flow: Inelastic Particles in Couette flow and slightly inelastic particles in a general flow field. Journal of Fluid Mechanics, 140, 223-256.

Lyn D.A. (1987). Turbulence and turbulent transport in sediment-laden open-channel flows. Ph.D. Thesis, Engineering and Applied Science Division, California Institute of Technology, Pasadena, California, United States.

Lyn, D. A. (1991). Resistance in flat-bed sediment-laden flows. Journal of Hydraulic Engineering, 117(1), 94-114.

McTigue, D. F. (1981). Mixture theory for suspended sediment transport. Journal of Hydraulics. Division, ASCE 107 (6), 659-673.

Menter, F. R. (1994). Two-equation eddy-viscosity turbulence models for engineering applications. AIAA journal, 32(8), 1598-1605.

Moin, P., and Mahesh, K. (1998). Direct numerical simulation: a tool in turbulence research. Annual Review of Fluid Mechanics, 30(1), 539-578.

Muste, M., Yu, K., Fujita, I., and Ettema, R. (2005). Two-phase versus mixed-flow perspective on suspended sediment transport in turbulent channel flows. Water Resources Research, 41(10), W10402.

Nakhaei, N., Boegman, L., Mehdizadeh, M., and Loewen, M. (2018). Hydrodynamic modeling of Edmonton storm-water ponds. Environmental Fluid Mechanics, 19 (2), 305-327.

I. Nezu, and W. Rodi. Open-channel flow measurements with a laser Doppler anemometer. J Hydraul Eng, 112(5), 335-355, 1986.

Norouzi, H. R., Zarghami, R., Sotudeh-Gharebagh, R., and Mostoufi, N. (2016). Coupled CFD-DEM modeling: Formulation, implementation and application to multiphase flows. John Wiley & Sons.

North Carolina Department of Environment, Health, and Natural Resources (1995). Stormwater best management practices. NC- DEHNR, Division of Water Quality, Water Quality Section, Raleigh, US.

Ontario Ministry of the Environment (2003). Stormwater management planning and design manual. Toronto, Canada.

Papanicolaou, A. T. N., Elhakeem, M., Krallis, G., Prakash, S., and Edinger, J. (2008). Sediment transport modeling review—current and future developments. Journal of Hydraulic Engineering, 134(1), 1-14.

Pedlosky, Geophysical Fluid Dynamics, Springer-Verlag, New York, (1979).

Persson, J. (1999). Hydraulic efficiency in pond design, Doctoral dissertation, Department of Hydraulics, Chalmers University of Technology).

Persson, J. (2000). The hydraulic performance of ponds of various layouts. Urban Water, 2(3), 243-250.

Persson, J., & Wittgren, H. B. (2003). How hydrological and hydraulic conditions affect performance of ponds. Ecological Engineering, 21(4-5), 259-269.

Pettersson, T. J. R., German, J., and Svensson, G. (1998). Modeling of flow pattern and particle removal in an open stormwater detention pond. In Proceedings of Hydra Storm 98, Walker, D.J. and Daniell, T.M. (eds), 27-30 September, Adelaide, Australia.

Pettersson, T.J.R., German, J. and Svensson, G. (1998). Modelling of flow pattern and particle removal in an open stormwater detention pond. In Proceedings of the HydraStorm '98, Walker, D.J. and Daniell, T.M. (eds), Adelaide, Australia, pp. 63– 68, September 27 – 30.

Revil-Baudard, T., Chauchat, J., Hurther, D., Barraud, P.A. (2015). Investigation of sheet flow processes based on novel acoustic high-resolution velocity and concentration measurements. Journal of Fluid Mechanics. 767, 1-30,.

Rodi, W. (2017). Turbulence modeling and simulation in hydraulics: a historical review. Journal of Hydraulic Engineering, 143(5), 03117001.

Ross, L., Dupuis, L., Unterschultz, K., & Raizenne, J. (2018). City of Brandon Naturalized Stormwater Pond Guidelines, Manitoba, Canada.

Rouse H. Modern conceptions of the mechanics of fluid turbulence. Transactions of the ASCE, 102:436-451, 1937.

Shakibaeinia, A., and Jin, Y. C. (2011). A mesh-free particle model for simulation of mobile-bed dam break. Advances in Water Resources, 34(6), 794-807.

Shaw, J. K. E., Watt, W. E., Marsalek, J., Anderson, B. C., and Crowder, A. A. (1997). Flow pattern characterization in an urban stormwater detention pond and implications for water quality. Water Quality Research Journal of Canada, 32(1), 53-71.

Shields, A. (1936). Application of similarity principles and turbulence research to bed-load movement, California Institute of Technology, Pasadena, CA, United States.

Shilton, A. (2000). Potential application of computational fluid dynamics to pond design. Water science and technology. 42(10-11), 327-334.

Shilton, 2005, A. Pond Treatment Technology, 1843390205, IWA Publishing, London, UK.Sommerfeld, M., and Decker, S. (2004). State of the Art and Future Trends in CFD Simulation of Stirred Vessel Hydrodynamics. Chemical Engineering & Technology 27(3), 215-24.

Shilton, A., Kreegher, S., and Grigg, N. (2008). Comparison of computation fluid dynamics simulation against tracer data from a scale model and full-sized waste stabilization pond. Journal of Environmental Engineering, 134(10), 845-850.

Simonin C., and Viollet P. L. (1990) Predictions of an oxygen droplet pulverization in a compressible subsonic co-flowing hydrogen flow. J. Comput. Multiphase Flows, 91: 65-82.

Simpson, T., Wang, J., and Vasconcelos, J. G. (2018). Cellular Confinement Systems to Prevent Resuspension in Sediment Basins. Journal of Environmental Engineering, 144(5).

Song, K., Xenopoulos, M. A., Buttle, J. M., Marsalek, J., Wagner, N. D., Pick, F. R., and Frost, P. C. (2013). Thermal stratification patterns in urban ponds and their relationships with vertical nutrient gradients. Journal of environmental management, 127, 317-323.

Sonnenwald, F. C., Guymer, I., and Stovin, V. (2017). Computational fluid dynamics modelling of residence times in vegetated stormwater ponds. In Proceedings of the Institution of Civil Engineers. Water Management. Thomas Telford, 171 (2), 76-86

Spencer, K. L., Droppo, I. G., He, C., Grapentine, L., and Exall, K. (2011). A novel tracer technique for the assessment of fine sediment dynamics in urban water management systems. Water research. 45(8), 2595-2606.

Stovin, V.R., and Saul A. J. (1998). A computational fluid dynamics (CFD) particle tracking approach to efficiency prediction. Water Science and Technology. 37(1)285-293.

Sumer, B. M., Kozakiewicz, A., Fredsoe, J. and Deigaard, R. 1996 Velocity and concentration profiles in sheet-flow layer of movable bed. Journal of Hydraulic Engineering. 122, 549-558.

M. Syamlal, W. Rogers, and T. J. O'Brien. MFIX documentation: Theory guide. National Energy Technology Laboratory, U.S. Department of Energy, Morgantown, West Virginia, USA, 1993.

Taggart W.C., Yermoli C.A., Montes S., and Ippen A. (1972). Effects of sediment size and gradation on concentration profiles for turbulent flow. Massachusetts Institute of Technology.

Husna, T., Ahmad, M. H., Nur, H., & Kamaruzaman, J. (2011). Assessment on pollutant removal of interconnected wet detention pond. American-Eurasian Journal of Agricultural & Environmental Sciences, 10(3), 324-329.

Thaxton, C. S., Calantoni, J., and McLaughlin, R. A. (2004). Hydrodynamic assessment of various types of baffles in a sediment retention pond. Transactions of the ASAE. 47(3), 741.

Torquato, S. (1995). Nearest-neighbor statistics for packings of hard spheres and disks. Physical Review E, 51(4), 3170.

Torres, A., Lipeme Kouyi, G., Bertrand-Krajewski, J. L., Guilloux, J., Barraud, S., and Paquier, A. (2008). Modelling of hydrodynamics and solid transport in a large stormwater detention and settling basin.

University of Lyon, Lyon, France, In 11th International Conference on Urban Drainage. 31 August - 5 September, Edinburgh, Scotland.

Troitsky, B., Zhu, D. Z., Loewen, M., van Duin, B., and Mahmood, K. (2019). Nutrient processes and modeling in urban stormwater ponds and constructed wetlands. Canadian Water Resources Journal/Revue canadienne des ressources hydriques, 1-18.

Tsavdaris, A., Mitchell, S., and Williams, J. B. (2015). Computational fluid dynamics modelling of different detention pond configurations in the interest of sustainable flow regimes and gravity sedimentation potential. Water and Environment Journal, 29(1), 129-139.

Tsuji, Y., and Morikawa, Y. (1982). LDV measurements of an air-solid two-phase flow in a horizontal pipe. Journal of Fluid Mechanics, 120, 385-409.

Uchida, T., and Fukuoka, S. (2009). A depth integrated model for 3D turbulence flows using shallow water equations and horizontal vorticity equations. Chuo University, Tokyo, Japan. In 33rd IAHR Congress: Water Engineering for a Sustainable Environment, Vancouver, British Columbia, Canada, 1428-1435.

USEPA (United States Environmental Protection Agency) (1998). EPA's Contaminated Sediment Management Strategy, Office of Water, 823- R-98-001.

Van Buren, M.A. (1994). Constituent Mass Balance for an Urban Stormwater Detention Pond in Kingston Township. M.Sc. Thesis, Department of Civil Engineering, Queen's University, Kingston, Ontario, Canada.

Van der Hoef, M. A., Van Sint Annaland, M., Deen, N. G., and Kuipers, J. A. M. (2008). Numerical simulation of dense gas-solid fluidized beds: a multiscale modeling strategy. Annual Review of Fluid Mechanics, 40, 47-70.

Vosswinkel N., Lipeme Kouyi G., Ebbert S., Schnieders A., Maus C., Laily A.-G., Mohn R. and Uhl M. (2012). Influence of unsteady behaviour on the settling of solids in storm water tanks. University of Lyon, Lyon, France, Proceedings of the 9th Urban Drainage Modelling International Conference, 3rd - 7th September, Belgrade, Serbia.

Walker, D. J. (1998). "Modelling residence time in stormwater ponds." Ecol. Eng., 10(3), 247–262.

Wang, X., and N. Qian (1992), Velocity profiles of sediment laden flow. International Journal of Sediment Research, 7(1), 27–58.

Wang, L. K., and Yang, C. T.. (2014). Modern water resources engineering. Humana Press.

Wu, J. S., Holman, R. E., and Dorney, J. R. (1996). Systematic evaluation of pollutant removal by urban wet detention ponds. Journal of Environmental Engineering, 122(11), 983-988.

Weiss, P. T., Gulliver, J. S., and Erickson, A. J. (2007). Cost and pollutant removal of storm-water treatment practices. Journal of Water Resources Planning and Management, 133(3), 218-229.

Yan, H., Kouyi, G. L., Gonzalez-Merchan, C., Becouze-Lareure, C., Sebastian, C., Barraud, S., and Bertrand-Krajewski, J. L. (2014). Computational fluid dynamics modelling of flow and particulate contaminants sedimentation in an urban stormwater detention and settling basin. Environmental Science and Pollution Research, 21(8), 5347-5356.

Yan, H. (2013). Experiments and 3D modelling of hydrodynamics, sediment transport, settling and resuspension under unsteady conditions in an urban stormwater detention basin, Ph.D. thesis, Institut National des Sciences Appliquées (INSA) de Lyon, France

Yergey, B.A., Beninati, M.L., Marshall, J.S., 2010. Sensitivity of incipient particle motion to fluid flow penetration depth within a packed bed. Sedimentology 57, 418–428.

Yousef, Y. A., Lin, L. Y., Lindeman, W., and Hvitved-Jacobsen, T. (1994). Transport of heavy metals through accumulated sediments in wet ponds. Science of the Total Environment, 146, 485-491.

Zaman, A. U. and Bergstrom, D. J. (2014). Implementation of two-fluid model for dilute gas-solid flow in pipes with rough walls. Journal of Fluids Engineering, 136, 031301.

Zhang, L. (2009). 3D numerical modeling of hydrodynamic flow, sediment deposition and transport in stormwater ponds and alluvial channels. Old Dominion University, Norfolk, VA, United States.

Zeng, J., Constantinescu, G., Blanckaert, K., and Weber, L. (2008). Flow and bathymetry in sharp open-channel bends: Experiments and predictions. Water Resources Research, 44(9).

Zhong, D., Wang, G. and Sun, Q. (2011). Transport equation for suspended sediment based on two-fluid model of solid/liquid two-phase flows. Journal of Hydraulic Engineering, 137(5), 530-542.